Imperial College London
Department of Mathematics

Impurities in ultracold quantum gases: From polaron formation to mediated interactions

Jonas Hugo Jager

May 2022

Supervised by: Dr Ryan Barnett

Submitted in part fulfilment of the requirements for the degree of Doctor of Philosophy in Mathematics of Imperial College London and the Diploma of Imperial College London

Declaration of Originality

I declare that all of the research presented here is my own and original work, unless otherwise stated. This thesis, is in large part, a collection of research work, that has been carried out as joint work with collaborators most of it is either published in peer-reviewed journals or currently undergoing peer-review. Where appropriate, I clearly state at the beginning of each chapter whether content has been taken from a published paper or a pre-print. For each publication/pre-print included in this thesis I am the first author and additionally I clearly demarcate and specify my personal contributions. Academic citations are in accordance with standard practice.

London, 12.05.2022

Jonas Jager

Acknowledgement

First and foremost, I would like to express my deepest gratitude to my supervisor Ryan Barnett for taking me on as his student. It has been a great experience working with him. I deeply value the trust he has shown in me, and his support for my academic and personal development has helped me to become a better researcher. I have learned a lot from him, especially developing a deeper understanding of physics and developing strategies to tackle complex academic problems.

I am forever indebted to Michael Fleischhauer, who first sparked my interest in polarons as an undergraduate student and for the many exciting discussions and collaborations ever since, which have taught me a lot. His encouragement and guidance have been invaluable in developing my skills, competence and scientific temper. They will always remain a solid platform in all my future work.

I would also like to take this opportunity to thank the whole Fleischhauer group for always welcoming me and for the fun hikes. Also, thanks to Martin for stimulating discussions.

Many thanks to Benjamin Walter for many interesting discussions and teaching me a thing or two about field theory, and also for helping me with the improvement of the last chapter.

Thanks should also go to David, Parth and Peter for proofreading this thesis and being good friends, especially during somewhat stressful weeks.

I owe a deep debt of gratitude to my parents, Ulrike and Martin, for their unstinting emotional, moral and financial support all these years, particularly during the PhD.

Lastly, I would like to thank my family and all my friends for always supporting me. Special thanks to Enzi, Iraklis and Vatsal for their emotional support whenever it was needed the most.

Abstract

In this thesis, we investigate the properties of Bose polarons in various settings. The overarching theme of this work is that, in contrast to many existing treatments of the Bose polaron, we apply semi-classical methods from first principles. Most of this thesis is based on [JJ1,JJ2,JJ3,JJ4].

Our first result addresses the Bose polaron in one dimension. We develop a primarily analytical treatment of the one-dimensional Bose polaron, which takes the impurity condensate interaction into account already on the mean-field level. Additionally, we show how to include first-order quantum corrections. Our results show excellent agreement with quasi-exact Quantum Monte Carlo simulations.

Motivated by the success of using semi-classical methods, we develop a truncated Wigner like approximation to address out of equilibrium settings. Using the Keldysh path integral formalism, we arrive at a set of differential equations with stochastic initial conditions. This enables us to incorporate quantum fluctuations up to first order and study the impurity dynamics and polaron formation after a sudden quench of the impurity-boson interaction.

Subsequently, we turn our attention to a three-dimensional system and again rely on semi-classical approximations to study the condensate mediated interaction between two impurities. The two impurities can form a bound state called the bipolaron for sufficiently large mediated interactions. We discuss how standard methods lead to inadequate results and show how these limitations can be remedied by correctly accounting for boson-boson interaction. We calculate the shape of the mediated interaction potential and the ground state of the two impurities, thus characterising the bipolaron formation.

Thereafter, we point out the similarities between the semi-classical approximations of the polaron problem considered so far and colloids interacting with a fluctuating field. We develop a general framework that perturbatively treats a broad class of field theories and arrive at an effective action only depending on the impurity degrees of freedom. We apply this approach to model A and find good agreement with simulations of the full system in the perturbative regime.

Contents

List of publications

Peer-reviewed

[JJ1] **Jonas Jager**, Ryan Barnett, Martin Will, and Michael Fleischhauer, *Strong-coupling Bose polarons in one dimension: Condensate deformation and modified Bogoliubov phonons*, Phys. Rev. Res. **2**, 033142 (2020)

This publication is a collaboration with Ryan Barnett, Martin Will and Michael Fleischhauer. The calculations for including quantum corrections were performed by myself and I made major contributions to finding the correct analytical solutions. All authors contributed to clarifying the subtleties involving the effective mass, interpreting and deriving the analytical expressions and the writing of the manuscript.

[JJ2] **Jonas Jager**, Ryan Barnett, *Stochastic-field approach to the quench dynamics of the one-dimensional Bose polaron*, Phys. Rev. Research **3**, 033212 (2021)

This work was supervised by Ryan Barnett. I derived the effective equations and their validity, implemented and ran the numerical simulations. I also wrote the initial draft of the paper. Both authors contributed to the data interpretation and the improvement of the manuscript.

Pre-prints (currently under peer-review)

[JJ3] **Jonas Jager**, Ryan Barnett, *The effect of boson-boson interaction on the bipolaron formation*, arXiv:2111.07957

This work was supervised by Ryan Barnett. I implemented and ran the numerical simulations. Both authors contributed to conceptualising the problem and identifying the challenges arising when using an effective zero-range scattering potential. Both authors contributed to the data interpretation and the writing of the manuscript.

In preparation

[JJ4] **Jonas Jager**, Benjamin Walter, *Effective action approach to the non-equilibrium dynamics of a Newtonian impurity coupled to a fluctuating field*,

This is joint work with Benjamin Walter (currently at SISSA). I have implemented and ran the numerical simulations. We both contributed to the analytical results and the conceptualisation of the problem. All results presented are preliminary.

CHAPTER 1

Introduction

The interaction of impurities with their surrounding environment is a perennial problem in physics. It has been studied in many areas ranging from high energy quantum phenomena such as quark-gluon interactions [1] to low energy phenomena such as polarons which have been observed in a variety of different settings, e.g., crystals and ultracold quantum gases [2–5]. One of the earliest accounts of polarons and their physical significance was reported by Landau and Pekar, when they studied the interaction of an impurity electron with a crystal [2, 3, 6]. They discovered that the local polarisation deforms the crystal structure and that this deformation travels together with the impurity electron. The compound object which is formed through the polarisation is termed the polaron. As later noted by Fröhlich [7] the electron-crystal interaction can be understood through an effective Hamiltonian, where the lattice vibrations are mapped to phonons, and the polarisation is described by the interaction of the electron with the phonons. In this model, the impurity excites a phonon cloud which travels together with it. This effective description serves as a starting point for many modern descriptions of the polaron [2, 3, 8–10]. Notably, the polaron problem in a crystal was also one of the earliest applications of the Feynman path integral [11]. Additionally, it has been found that the polaron concept has numerous applications across condensed matter physics; for example, in understanding the electric conductivity of polymers [12, 13], and it has been hypothesised that polarons play a role in explaining high-T_c superconductivity [14, 15].

Due to the experimental advances in laser cooling [16] over the last decades and the first realisation of a Bose-Einstein condensate [17], ultracold atoms have been established as a clean and controllable experimental platform [18, 19] for studying microscopic quantum phenomena. This

permits for the probing of exotic phases of quantum matter and also enables quantum simulations to be conducted [20]. This opens the pathway to isolate and study individual phenomena that are typically not directly observable in conventional condensed matter systems [20]. In contrast to the archetypal solid-state setting, experiments relying on ultracold gases offer much greater experimental control [20, 21]. For example, the inter-atomic interactions can be tuned via Feshbach resonances [21], and the dimensionality of the system can be engineered [22]. Thus ultracold quantum gases also form an experimentally accessible testing ground for studying polarons with high precision. When considering polarons in ultracold gases, differentiating between Fermi and Bose polarons is essential. The Fermi polaron, which refers to an impurity in a degenerate Fermi gas, has been observed in several experiments [4, 23–29]. The Bose polaron is realised by immersing impurities into an ultracold Bose gas. It is experimentally less understood, than the Fermi polaron, but has recently been observed in numerous experiments [5, 22, 30–32]. Many of the phenomena which are observed experimentally, especially in low dimensional systems, are not adequately described by the standard methods. This thesis will focus on developing novel approaches to the Bose polaron.

Specifically, many theoretical descriptions for the Bose polaron are still based on the (extended) Fröhlich model, which is obtained by linearising the condensate around a homogeneous background solution and then describing the interaction of the impurity with the gas as a coupling to Bogoliubov phonons. The methods applied to the Bose polaron span a wide variety of different techniques [33–39], including variational [38, 40–42], field-theoretical [33, 43–45], renormalisation group (RG) [37, 46, 47] and open-system approaches [48], as well as quantum Monte-Carlo simulations [37, 49–51]. Contrary to the degenerate Fermi gas, a Bose gas is compressible, and the deformation of the Bose gas itself can become sizable; thus the boson-boson interaction plays an essential role in the strong coupling regime. The (extended) Fröhlich model, does not include phonon-phonon interactions and is therefore incapable of correctly accounting for boson-boson interaction, which is substantial when the impurity-boson coupling becomes large. This work addresses the aforementioned shortcomings for some prominent Bose polaron problems. The structure of the thesis is as follows.

In the second chapter, a brief derivation of the (extended) Fröhlich Hamiltonian is shown and a simple variational approach to find an approximate solution for the ground state is presented. This serves as a base case for more complete treatments. Additionally, some important concepts from scattering theory are introduced. To conclude this chapter, some common techniques which aid in the description of out of equilibrium dynamics and are important for the main part of this work are discussed.

The third chapter focuses on the equilibrium properties of a single quantum impurity interacting with a degenerate one-dimensional ultracold Bose gas. In contrast to the three-dimensional setting, where the polaron is accurately modeled over a wide range of parameters by the extended Fröhlich Hamiltonian, in one dimension methods relying on linearising the bosonic field operators can be quite inaccurate, even for relatively weak coupling. This is owing to the backaction of the impurity on the condensate, leading to a self-bound mean-field polaron for arbitrarily weak impurity-boson interactions. A model that takes this backaction into account on the mean-field level is presented. This model further includes higher-order corrections to the impurity-condensate interaction as a coupling to phonon like excitations of the full mean-field solution. A comparison of the polaron energy and mass to quantum diffusion Monte-Carlo simulations shows excellent agreement already on the level of analytical mean-field solutions and is further improved after accounting for quantum fluctuations.

Motivated by the success of the semi-classical methods for the equilibrium case, a semi-classical description of the dynamics of the impurity after a sudden interaction quench is developed in the fourth chapter. To address the impurity dynamics, the Keldysh path integral is employed to derive a truncated Wigner-like approach. This strategy, similar to that in the previous chapter, takes the effects of the impurity on the condensate into account on the mean-field level itself. It also permits further incorporation of thermal and quantum effects up to one-loop accuracy by averaging over stochastic initial conditions, and is therefore numerically tractable. This framework enables us to not only calculate the real space trajectory of the impurity but also the absorption spectrum.

The fifth chapter focuses on the interaction between two impurities in a three-dimensional system, instead of the previously considered one-dimensional system. The density deformation

caused by the two impurities results in an exchange interaction mediated by density fluctuations. Through the mediated interaction two impurities that are sufficiently close to each other, can form a bound state, which is commonly referred to as a bipolaron. We start by postulating that similar to the case discussed in the third chapter, standard methods based on linearising the condensate yield results only valid in the weak coupling regime and for sufficiently large impurity separations. It is shown how attempts to build on the Fröhlich model by utilising the extended Fröhlich model can lead to physically meaningless results. This is followed by a demonstration on how those shortcomings can be remedied within the Born-Oppenheimer approximation by accounting for boson-boson interactions on the mean-field level. The mediated interaction potential and typical bipolaron binding energies are then calculated and compared to the initial predictions made by the Fröhlich model.

The penultimate chapter points out the connection between the polaron problem in the semi-classical limit and colloids interacting with a fluctuating field, which is a prominent problem within statistical field theory. We develop an effective action description only containing the impurity degrees of freedom, which is applicable to a broad class of field theories. Here, we distinguish between the symmetric case (vanishing expectation of the order parameter) and the degenerate case (finite expectation of the order parameter). The developed method is perturbative, and we proceed by applying it to model A and assess its accuracy by comparing it to numerical simulations of the full theory. Here we find good agreement in the perturbative limit.

The final chapter gives a conclusive summary of the results and discusses their implications. We also point out possible future directions of this work.

Throughout this thesis we use $\hbar = 1$ and $k_{\mathrm{B}} = 1$.

CHAPTER 2

Fundamental concepts

2.1 Polarons in an ultracold quantum gas

This section aims to provide an overview of standard approaches to address impurities immersed into an ultracold Bose gas and, more specifically, discuss the Bose polaron. Though the material presented here is tailored towards the main results of this thesis, necessary references have been provided to explore the field further and gain a fundamental understanding of the topic.

We begin by stating and briefly explaining the Bose gas impurity Hamiltonian, which will be the fundamental building block for all treatments introduced throughout this thesis. Subsequently, some essential concepts from scattering theory are summarised; these are useful when relating the model parameters to experimentally observable quantities. From there, we outline the derivation of the (extended) Fröhlich Hamiltonian, which is of great importance not, only historically but also for ongoing efforts to understand the Bose polaron and is routinely used to derive baseline results. We conclude the section by introducing fundamental concepts like the effective mass and conceptual tools like the Lee-Low-Pines (LLP) transformation.

Hamiltonian for impurities in an ultracold Bose gas

Throughout this work, we consider a d-dimensional gas of bosons (B), which interacts with impurity atoms (I). The bosons are described by the field operators $\hat{\varphi}(\mathbf{r})$ and carry the mass m. In contrast, the impurity atoms will be treated in first quantisation, and we denote their position (momentum) by $\hat{\mathbf{X}}_i$ ($\hat{\mathbf{P}}_i$) and mass by M. While we keep the number of impurities as general as possible in

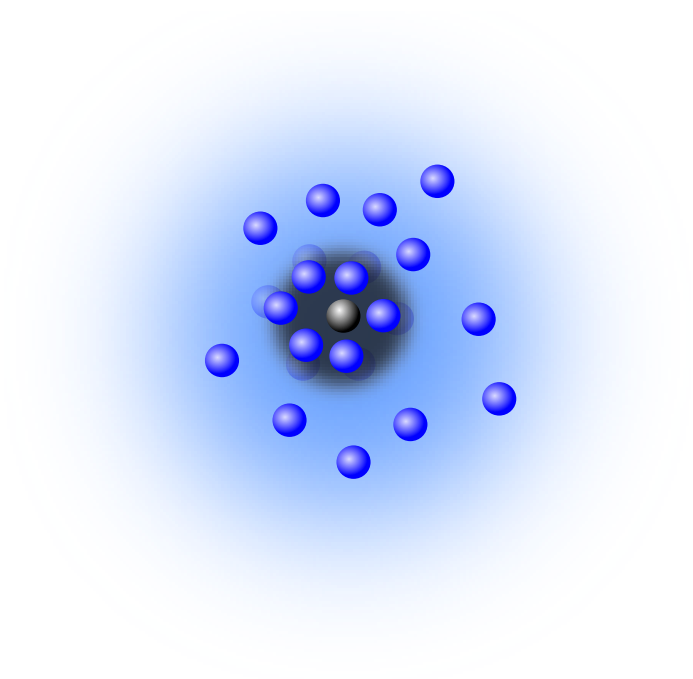

Figure 2.1: An impurity immersed into an ultracold bosonic gas. It interacts with the surrounding quantum gas and as a result, perturbs the condensate. The perturbation now travels with the impurity. The compound object can be described by a quasiparticle, commonly referred to as the polaron.

the introductory chapter, we already note here that we will focus on at most two impurities at a time in all later treatments. Focusing on at most two impurities is generally justified since in most experiments the impurity concentration is sufficiently low [5, 22, 30, 31]. For a brief discussion on the experimental realisation and the corresponding parameters we refer to Appendix A. The (often harmonic) trap, usually confining the Bose gas and the impurity, is neglected. Instead, we consider a box of finite volume L^d with periodic boundary conditions and take the thermodynamic limit, where appropriate. When considering bosonic low energy scattering processes, it is justified to replace the microscopic interaction potential by a contact potential[1] and therefore the pseudo contact potential given by $V_{\mathrm{int}}(\mathbf{r}-\mathbf{r}') = g_{\mathrm{BB}}\delta^d(\mathbf{r}-\mathbf{r}')$ is used to model the boson-boson interaction. The impurity-boson interaction potential will be left unspecified for now and in fact, using a contact potential for boson-boson and impurity-boson interaction simultaneously in more than one dimension is only valid when also linearising the bosonic fields [52, 53]. For the full Hamiltonian, a microscopic finite range potential has to be employed for at least one interaction potential. The finite range

[1] i.e. focusing on s-wave scattering, for a detailed discussion see [18].

potential is often chosen as a Gaussian or Heaviside potential, but any simple effective potential can be employed without altering the observed physics, as long as the scattering length is adjusted accordingly. In chapter 5 we discuss some of the problems arising from using a contact interaction for more than one impurity in greater detail. The full (grand canonical) Hamiltonian takes the form

$$\hat{\mathcal{H}} = \sum_i \frac{\hat{\mathbf{P}}_i^2}{2M} + \int \mathrm{d}^d\mathbf{r}\, \hat{\varphi}^\dagger(\mathbf{r}) \left(\frac{-\Delta}{2m} - \mu + \frac{g_{\mathrm{BB}}}{2}\hat{\varphi}^\dagger(\mathbf{r})\hat{\varphi}(\mathbf{r}) + \sum_i V\left(\mathbf{r} - \hat{\mathbf{X}}_i\right) \right) \hat{\varphi}(\mathbf{r})\,, \tag{2.1}$$

where μ denotes the chemical potential of the Bose gas and determines the number of bosons in the gas. The part of the Hamiltonian purely relating to the Bose gas will be referred to as $\hat{\mathcal{H}}_{\mathrm{B}}$ throughout the thesis.

An interlude on scattering theory

Before proceeding with deriving the (extended) Fröhlich Hamiltonian, we want to present a short discussion of some important scattering theory results. Most importantly, we introduce the Lippmann-Schwinger equation, which allows us to relate the interaction strength g of a contact potential $g\delta(\mathbf{r})$ with the experimentally measurable scattering length a. It is important to note that the model parameter g is never directly observable and that the use of a contact potential or simple Gaussian interaction potential is always a simplification compared to the often unknown and complicated real microscopic potential. However, such simplifications are justified in the low energy regime where s-wave scattering dominates the behavior, and the exact microscopic shape of the potential is irrelevant [18, 19]. Additionally, we will later see that the Lippmann-Schwinger equation can also be used to regularise the contact interaction in the (extended) Fröhlich model. The presented results are based on [54] and are not exhaustive, rather the goal of this subsection is to provide an overview of the essential scattering theory results used throughout this work. A more detailed discussion on scattering theory in the context of ultracold gases, can be found in [18, 21, 54].

We consider two particles of mass m and M interacting via the spherically symmetric scattering potential $\hat{V}$. For the scattering problem itself, we are only interested in the relative coordinates of the particles interacting with each other. Thus, it is convenient to move into the centre of mass

frame. In the centre of mass frame we find that the relative wave function is determined by the stationary Schrödinger equation

$$\left[\frac{\hat{\mathbf{P}}^2}{2m_\mathrm{r}} + \hat{V}\right] |\psi\rangle = E\,|\psi\rangle \ , \tag{2.2}$$

where the reduced mass is given by $m_\mathrm{r} = mM/(m+M)$. For large separations between the two particles, the interaction potential can be neglected and thus the eigenenergy of the stationary Schrödinger equation is given by $E_k = k^2/(2m_\mathrm{r})$. Combining this observation with the fact that for elastic scattering the energy is conserved allows us to set to set $E = E_k$. After defining

$$\hat{H}_0 = \hat{P}^2/(2m_\mathrm{r}) \tag{2.3}$$

and realising that a free momentum state lies in the kernel of $E_k - \hat{H}_0$, we can write down the formal solution to (2.2)

$$|\psi_\mathbf{k}\rangle = |\mathbf{k}\rangle + \frac{1}{E_k - \hat{H}_0 + i\epsilon}\hat{V}\,|\psi_\mathbf{k}\rangle \ , \tag{2.4}$$

where the $+i\epsilon$ term is needed to deal with the singularity in the denominator of the second term and render the solution well defined. In fact, the sign of ϵ determines the pole structure of the solution, a positive sign corresponds to an incoming plane wave and outgoing spherical wave. Hence it describes a scattering process. A negative sign corresponds to the reverse process and can be interpreted as an advanced solution. After developing the formal solution, it is instructive to derive an explicit expression for the wave function in position space. Multiplying (2.4) with $\langle\mathbf{r}|$ from the left and inserting a position space and a momentum space identity into the second term of the right hand side results in

$$\langle\mathbf{r}|\psi_\mathbf{k}\rangle = \psi_\mathbf{k}(\mathbf{r}) = e^{i\mathbf{k}\cdot\mathbf{r}} + \int \mathrm{d}\mathbf{r}'\mathrm{d}\mathbf{k}'\frac{e^{i\mathbf{k}'\cdot(\mathbf{r}-\mathbf{r}')}}{E_k - E_{k'} + i\epsilon}\,\langle\mathbf{r}'|\,\hat{V}\,|\psi_\mathbf{k}\rangle \ . \tag{2.5}$$

The momentum integral now depends on the dimension of the system. Henceforth in this subsection, we focus on the three-dimensional case and refer to [54, 55] for a more detailed discussion of lower-dimensional systems. When using a short ranged potential and considering large distances

compared to the potential's range, we can use

$$|\mathbf{r} - \mathbf{r}'| \approx r - \frac{\mathbf{r}}{r} \cdot \mathbf{r}' \,, \tag{2.6}$$

to approximate $r \gg r'$. After a short calculation (see [54] for more details) we find

$$\langle \mathbf{r}|\psi_{\mathbf{k}}\rangle = \psi_{\mathbf{k}}(\mathbf{r}) = e^{i\mathbf{k}\cdot\mathbf{r}} + f(\mathbf{k}', \mathbf{k})\frac{e^{ikr}}{r} \,, \tag{2.7}$$

where we have introduced $\mathbf{k}' = k\mathbf{r}/r$ and the scattering amplitude $f(\mathbf{k}', \mathbf{k}) = -\frac{m_\mathrm{r}}{2\pi} \langle \mathbf{k}'| \hat{V} |\psi_{\mathbf{k}}\rangle$.

To make the connection to the experimentally observable scattering length, we now introduce the two-body transition matrix

$$\hat{T}^{2\mathrm{B}} |\mathbf{k}\rangle = \hat{V} |\psi_{\mathbf{k}}\rangle \,, \tag{2.8}$$

which is especially useful when considering scattering processes in a medium. The transition matrix is related to the scattering amplitude through

$$f(\mathbf{k}', \mathbf{k}) = -\frac{m_\mathrm{r}}{2\pi} \langle \mathbf{k}'| \hat{T}^{2\mathrm{B}} |\mathbf{k}\rangle \,. \tag{2.9}$$

Therefore, it contains the same information as the wave function but is easier to work with in many cases. Introducing the well-known Lippmann-Schwinger equation in operator form is now possible, by multiplying (2.4) with $\hat{V}$ and we find

$$\hat{T}^{2\mathrm{B}} = \hat{V} + \hat{V}\frac{1}{E_k - \hat{H}_0 + i\epsilon}\hat{T}^{2\mathrm{B}} \,. \tag{2.10}$$

Since the scattering potential is assumed to be spherically symmetric, we can proceed by performing a partial-wave expansion of $|\psi_{\mathbf{k}}\rangle$ to define the s-wave (zero angular momentum), scattering length a, and the effective range of the potential r_eff. Those quantities are related to the two-body scattering matrix $\langle \mathbf{k}| \hat{T}^{2\mathrm{B}} |\mathbf{k}\rangle$ through

$$T^{2\mathrm{B}}(k) \approx \frac{2\pi a}{m_\mathrm{r}} \frac{1}{1 - a r_\mathrm{eff} k^2 + iak} \,. \tag{2.11}$$

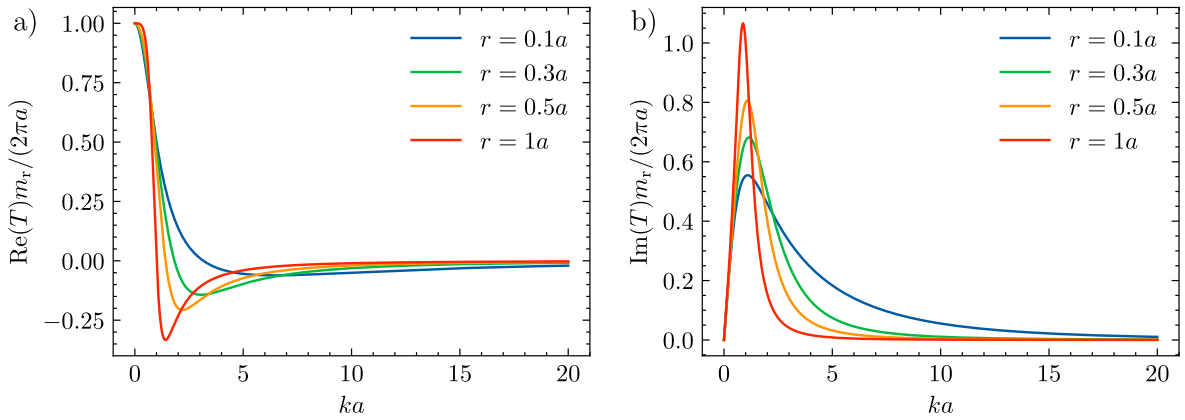

Figure 2.2: The a) real and b) imaginary part of the scattering matrix $T^{\mathrm{2B}}(k)$ for a short ranged spherically symmetric potential and different r_{eff} as a function of ka.

This expression allows us to connect the two-body scattering matrix $T^{\mathrm{2B}}(k)$ of any sufficiently local spherical potential to the experimentally accessible s-wave scattering length a. We depict the imaginary and real part of the scattering matrix in Figure 2.2.

To conclude this subsection we want to use the relationship defined by the Lippmann-Schwinger equation to describe the connection between a contact interaction $g\delta^d(\mathbf{r})$ and the scattering length a. After multiplying (2.10) with $\langle\mathbf{k}|$ from the left and $|\mathbf{k}\rangle$ from the right; rearranging and evaluating at $k = 0$ we find

$$\frac{1}{T^{\mathrm{2B}}(0)} = \frac{m_\mathrm{r}}{2\pi a} = \frac{1}{g} + \frac{1}{(2\pi)^3}\int^{\Lambda} \mathrm{d}^3\mathbf{k}\frac{2m_\mathrm{r}}{k^2}\,, \tag{2.12}$$

where we have introduced the sharp momentum cutoff Λ to ensure that the result is finite. The arising divergence here is associated with the use of a contact interaction. A more realistic interaction potential would decay faster in Fourier space rendering the results finite. We also note that this unphysical behaviour is usually not a problem since in ultracold gases we are mainly interested in the long wavelength behaviour and in most cases standard regularisation techniques are sufficient to recover finite results [55].

The (extended) Fröhlich model

After introducing the microscopic Hamiltonian and discussing some key results from scattering theory, we proceed by deriving an approximate effective Hamiltonian. The treatment relies on linearising the bosonic field operators and treating the effects of the impurity as an interaction

with the elementary excitations of the homogeneous Bose gas. The resulting (extended) Fröhlich model serves as an important starting point for addressing the Bose polaron. The derivation of the (extended) Fröhlich Hamiltonian is straightforward, and while the effective treatment possesses significant shortcomings [JJ1], [56–60] it highlights some crucial features of the polaron in an intuitive manner. The Fröhlich Hamiltonian does not only describe Bose polarons but also a much more comprehensive range of polarons (see for example [10, 61]). It was, in fact, first introduced by Fröhlich [7] in the 1950s to describe the interaction of an impurity electron with the lattice vibrations of a crystal. This is why the Fröhlich Hamiltonian can only describe weakly interacting Bose polarons; a crystal is rigid, while a superfluid can flow freely and thus its deformation can become more substantial. Additionally, the phonons interact with each other in a Bose gas and for strong deformations the phonon density is high enough that such interactions become sizable. The key idea for deriving the (extended) Fröhlich model is to first develop an effective theory of the Bose gas without impurities[2] and then include the interaction of the impurities with the excitations of the superfluid [7, 35, 38]. This seems intuitively sensible as long as the impurity density remains dilute and the impurity-boson interaction stays sufficiently weak; we refer to [46] for an elaborate discussion on the validity of the Fröhlich model. We begin by expanding the bosonic field operators

$$\hat{\varphi}(\mathbf{r}) = \sqrt{n_0} + \hat{\xi}(\mathbf{r}) \,, \tag{2.13}$$

around the density of a homogeneous condensate $n_0 = \mu/g_{\mathrm{BB}}$, here $\hat{\xi}(\mathbf{r})$ can be interpreted as the deviation of $\hat{\varphi}(\mathbf{r})$ from its mean-field value $\sqrt{n_0}$. We note, that this expansion is nothing but a canonical transformation and therefore exact; the approximation is only introduced when higher-order terms are dropped. Inserting the expansion into the purely bosonic part of (2.1) we find

$$\hat{\mathcal{H}}_{\mathrm{B}} = \int \mathrm{d}^d\mathbf{r} \left\{ \hat{\xi}^\dagger(\mathbf{r}) \left(\frac{-\Delta}{2m} - \mu + 2n_0 g_{\mathrm{BB}} \right) \hat{\xi}(\mathbf{r}) + \frac{g_{\mathrm{BB}}}{2} n_0 \left(\hat{\xi}(\mathbf{r})^2 + \mathrm{h.c.} \right) \right\} + \mathcal{O}(\hat{\xi}(\mathbf{r})^3) \,. \tag{2.14}$$

[2] See [18, 62] for a discussion on when an effective treatment for the Bose gas itself is admissible.

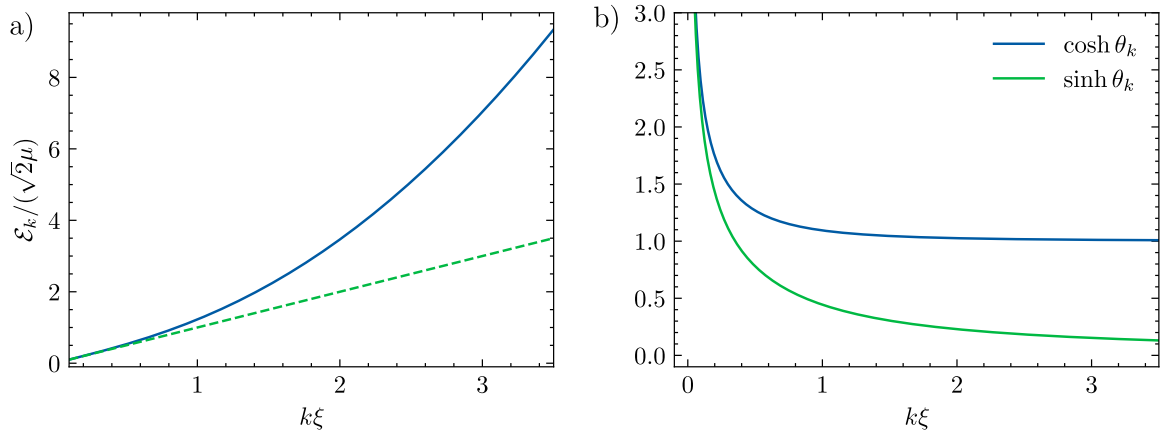

Figure 2.3: a) The dispersion relation $\mathcal{E}_k$ of the Bogoliubov phonons. The dotted line shows the purely linear part. The crossover from a linear massless dispersion to a quadratic dispersion (associated with a massive particle) is clearly visible. b) The amplitudes of the elementary excitations u_k and v_k.

Assuming that we are dealing with a dilute and weakly interacting Bose gas, we can truncate all terms of order $\hat{\xi}(\mathbf{r})^3$, and higher [18, 19]. Subsequently, the remaining quadratic part can be diagonalised by performing a Bogoliubov transformation. In the following discussion, we only present the idea and refer to [18] and [19] for a detailed discussion on the technicalities and the validity of the Bogoliubov treatment of a Bose gas. Meanwhile, section 3.5 provides a general technical discussion of the transformation. The essential step of the Bogoliubov transformation is to decompose $\hat{\xi}(\mathbf{r})$ into the elementary excitations of the system

$$\hat{\xi}(\mathbf{r}) = \frac{1}{L^{d/2}} \sum_n \left[u_n(\mathbf{r}) \hat{a}_n + v_n^*(\mathbf{r}) \hat{a}_n^\dagger \right] , \tag{2.15}$$

and choose the amplitudes in such a way that the Hamiltonian is diagonalised. In the case of a homogeneous gas we can use the translational invariance of the system to decompose $\hat{\xi}$ into its Fourier modes. After inserting the decomposition into (2.14) and choosing the amplitudes such that all off-diagonal elements vanish we find [18, 19]

$$u_{\mathbf{k}}(\mathbf{r}) = \cosh\theta_k e^{i\mathbf{k}\cdot\mathbf{r}} , \quad v_{\mathbf{k}}(\mathbf{r}) = -\sinh\theta_k e^{i\mathbf{k}\cdot\mathbf{r}} , \tag{2.16}$$

$$\begin{matrix}\cosh\theta_k \\ \sinh\theta_k\end{matrix} = \frac{1}{\sqrt{2}} \left(\frac{\frac{k^2}{2m} + g_{\mathrm{BB}} n_0}{\mathcal{E}_k} \pm 1 \right)^{1/2} , \tag{2.17}$$

with the gapless excitation spectrum $\mathcal{E}_k = ck\sqrt{1+\frac{1}{2}k^2\xi^2}$ which is shown as a function of $\frac{k}{\xi}$ in Figure 2.3. This illustrates that for small momenta, the excitations disperse linearly and behave like massless particles and for large momenta, this crosses over to a quadratic dispersion, usually associated with a massive particle. The healing length determines the characteristic length scale of the Bose gas and is given by $\xi = \frac{1}{\sqrt{2mn_0g_{\mathrm{BB}}}}$. Moreover, we have also defined the speed of sound $c = \sqrt{g_{\mathrm{BB}}n_0/m}$, which determines the critical velocity of the condensate [18]. Within the Bogoliubov approximation we find the chemical potential to be $\mu = g_{\mathrm{BB}}n_0$. It is a convention to refer to the elementary excitation represented by $\hat{a}_{\mathbf{k}}$ as Bogoliubov phonons and use k instead of n as a summation index to indicate that we sum Fourier modes in the homogeneous case. The resulting diagonalised Hamiltonian takes the form

$$\hat{\mathcal{H}}_{\mathrm{B}} = \sum_{\mathbf{k}} \mathcal{E}_k \hat{a}^\dagger_{\mathbf{k}}\hat{a}_{\mathbf{k}} \,. \tag{2.18}$$

With the effective description of a weakly interacting Bose gas in mind, the impurity-Bose gas interaction can be addressed by inserting the expansion

$$\hat{\varphi}(\mathbf{r}) = \sqrt{n_0} + \frac{1}{L^{d/2}}\sum_{\mathbf{k}}\left[u_{\mathbf{k}}(\mathbf{r})\hat{a}_{\mathbf{k}} + v^*_{\mathbf{k}}(\mathbf{r})\hat{a}^\dagger_{\mathbf{k}}\right] , \tag{2.19}$$

into (2.1). After neglecting constant terms and terms of order $\hat{\xi}^3$ and higher we arrive at the extended Fröhlich Hamiltonian [37, 38, 63]

$$\begin{aligned}\hat{\mathcal{H}}_{\mathrm{eF}} = \hat{\mathcal{H}}_{\mathrm{F}} + \hat{\mathcal{H}}_{\mathrm{2ph}} = \sum_{\mathbf{k}}\mathcal{E}_k\hat{a}^\dagger_{\mathbf{k}}\hat{a}_{\mathbf{k}} + \sum_i \frac{\hat{\mathbf{P}}_i^2}{2M} + g_{\mathrm{IB}}\sqrt{\frac{n_0}{L^d}}\sum_{\mathbf{k}\neq 0,i} W_k e^{-i\mathbf{k}\cdot\hat{\mathbf{X}}_i}\left(\hat{a}^\dagger_{\mathbf{k}} + \hat{a}_{-\mathbf{k}}\right) \\ g_{\mathrm{IB}}n_0 + \frac{g_{\mathrm{IB}}}{2L^d}\sum_{\mathbf{k},\mathbf{k}'\neq 0,i} e^{i(\mathbf{k}'-\mathbf{k})\cdot\hat{\mathbf{X}}_i}\Big[\left(W_kW_{k'} + W_k^{-1}W_{k'}^{-1}\right)\hat{a}^\dagger_{\mathbf{k}}\hat{a}'_{\mathbf{k}} \\ + \frac{1}{2}\left(W_kW_{k'} - W_k^{-1}W_{k'}^{-1}\right)\left(\hat{a}^\dagger_{\mathbf{k}}\hat{a}^\dagger_{-\mathbf{k}'} + \hat{a}_{-\mathbf{k}}\hat{a}_{\mathbf{k}'}\right)\Big] ,\end{aligned} \tag{2.20}$$

where the scattering amplitude is given by

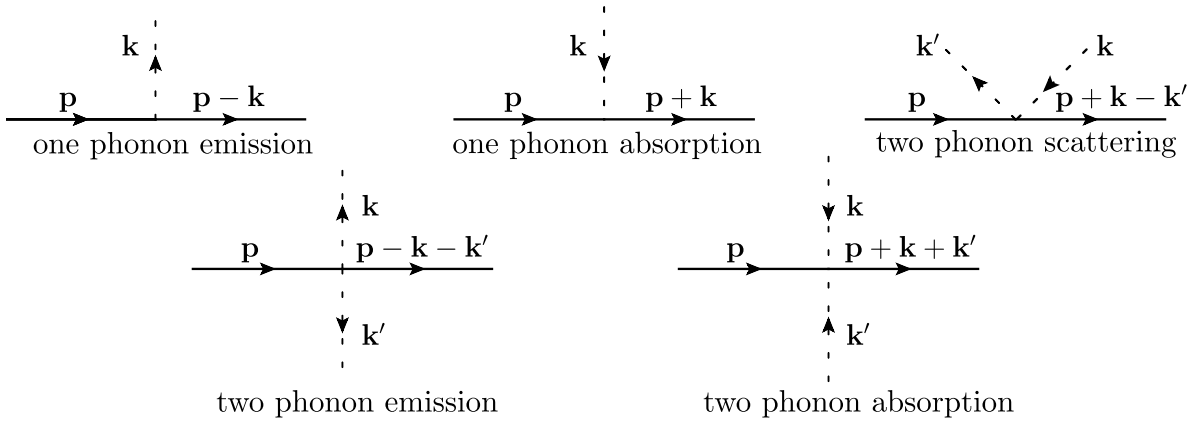

Figure 2.4: The different scattering processes described by the extended Fröhlich Hamiltonian. All processes are momentum conserving and we can distinguish between one phonon scattering processes (which are already included in the traditional Fröhlich model) and two-phonon processes (which are only included in the extended Fröhlich model). The illustration was taken from [64].

$$W_k = \left(\frac{\xi^2 k^2}{2 + \xi^2 k^2} \right)^{1/4} = \cosh \theta_k - \sinh \theta_k \, . \tag{2.21}$$

Here, $\hat{\mathcal{H}}_{\mathrm{F}}$ denotes the Fröhlich Hamiltonian, which only includes impurity scattering terms involving a single phonon. In contrast $\hat{\mathcal{H}}_{2\mathrm{ph}}$ additionally includes the two phonon impurity scattering terms. All scattering terms conserve momentum and are depicted in Figure 2.4.

Including two phonon scattering terms can improve the accuracy of the model. However, at strong coupling, when the condensate deformation becomes large, corresponding to a large phonon cloud in the Fröhlich model, phonon-phonon interactions are no longer negligible. Thus in this regime even the extended Fröhlich model loses its validity and the predictions become inaccurate. Further discussion in the subsequent sections will show that there are resonances occurring in the extended Fröhlich model, which are offset by the boson-boson interaction in a realistic setting.

A significant part of this thesis will address those shortcomings and showcase methods that are suitable for addressing the strong coupling regime. For the remainder of this section we assume that we are well within the validity region of the extended Fröhlich Hamiltonian and use it to demonstrate two key concepts, extending beyond the Fröhlich paradigm, namely the Lee-Low-Pines (LLP) transformation and the effective mass.

The Lee-Low-Pines transformation

This subsection, focuses on a single impurity and introduces the LLP transformation in the context of the (extended) Fröhlich model. We will later see that the LLP transformation is, in fact, more general and can be extended to the full Hamiltonian. The LLP transformation is a unitary transformation which moves the impurity into the origin of the coordinate system. Since the system is translationally invariant, total momentum is conserved. The LLP transformation makes this conservation law explicit and ultimately eliminates the impurity degrees of freedom from the problem. The LLP transformation is given by [8]

$$\hat{U}_{\mathrm{LLP}} = \exp\Big\{-i\hat{\mathbf{X}}\cdot\hat{\mathbf{P}}_{\mathrm{ph}}\Big\}\,, \tag{2.22}$$

where we introduced the total phonon momentum

$$\hat{\mathbf{P}}_{\mathrm{ph}} = \sum_{\mathbf{k}} \mathbf{k}\hat{a}^{\dagger}_{\mathbf{k}}\hat{a}_{\mathbf{k}}\,. \tag{2.23}$$

It is now straightforward to verify the following relationships:

$$\hat{U}^{\dagger}_{\mathrm{LLP}}\hat{a}^{\dagger}_{\mathbf{k}}\hat{U}_{\mathrm{LLP}} = \hat{a}^{\dagger}_{\mathbf{k}}e^{i\mathbf{k}\cdot\hat{\mathbf{X}}}, \quad \hat{U}^{\dagger}_{\mathrm{LLP}}\hat{\mathbf{P}}\hat{U}_{\mathrm{LLP}} = \hat{\mathbf{P}} - \hat{\mathbf{P}}_{\mathrm{ph}}\,. \tag{2.24}$$

Using (2.24) we find the transformed extended Fröhlich Hamiltonian

$$\begin{aligned}\hat{\mathcal{H}}_{\mathrm{LLP}} = \sum_{\mathbf{k}}\mathcal{E}_k\hat{a}^{\dagger}_{\mathbf{k}}\hat{a}_{\mathbf{k}} + \frac{\Big(\mathbf{p}-\hat{\mathbf{P}}_{\mathrm{ph}}\Big)^2}{2M} + g_{\mathrm{IB}}\sqrt{\frac{n_0}{L^d}}\sum_{\mathbf{k}\neq 0}W_k\big(\hat{a}^{\dagger}_{\mathbf{k}}+\hat{a}_{-\mathbf{k}}\big) + \frac{g_{\mathrm{IB}}}{2L^d}\sum_{\mathbf{k},\mathbf{k}'\neq 0}\Big[\big(W_kW_{k'}\\ +W_k^{-1}W_{k'}^{-1}\big)\hat{a}^{\dagger}_{\mathbf{k}}\hat{a}'_{\mathbf{k}} + \frac{1}{2}\big(W_kW_{k'}-W_k^{-1}W_{k'}^{-1}\big)\Big(\hat{a}^{\dagger}_{\mathbf{k}}\hat{a}^{\dagger}_{-\mathbf{k}'}+\hat{a}_{-\mathbf{k}}\hat{a}_{\mathbf{k}'}\Big)\Big] + g_{\mathrm{IB}}n_0\,,\end{aligned} \tag{2.25}$$

here $\hat{\mathbf{P}}$ is replaced by the c-number $\mathbf{p}$ since after the transformation, it represents the total momentum which is conserved. Thus, we have eliminated the impurity from the problem at the expense of the additional non-linear term $(\mathbf{p}-\hat{\mathbf{P}}_{\mathrm{ph}})^2$.

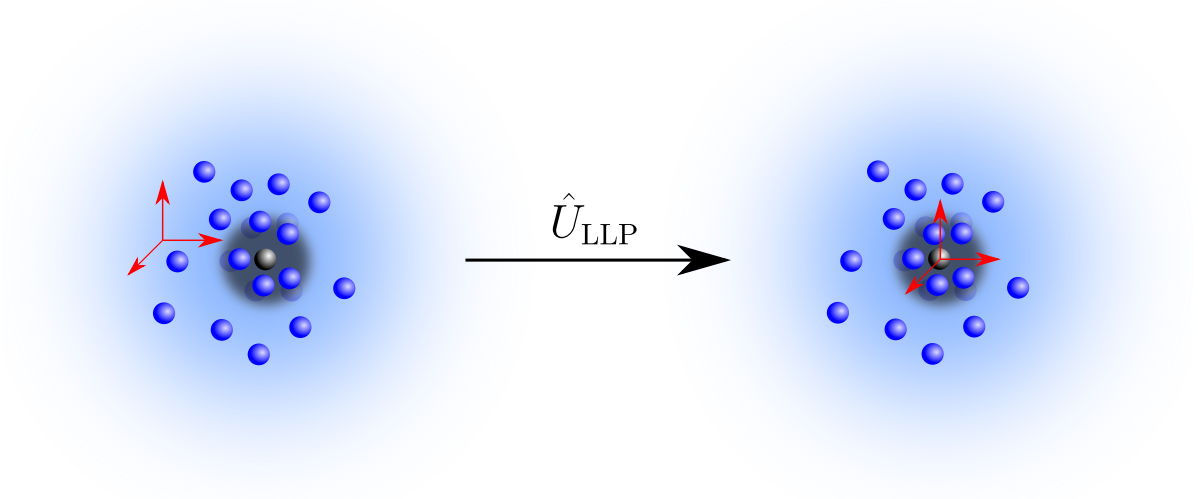

Figure 2.5: Schematic of the LLP-transformation. By leveraging the translational invariance of the problem, the impurity is moved into the origin of the coordinate system and thus eliminated from the problem. While this comes at the expense of an additional non-local term, it allows for taking full entanglement between impurity and Bose gas into account in a straightforward manner.

Variational mean-field theory

Having eliminated the impurity from the problem we can now apply an effective variational mean-field [38, 46] treatment to (2.25). It is imperative to note that because of the LLP-transformation, we only have to choose an ansatz for the phonons. This will take the full entanglement between impurity and phonons into account. Ultimately, an upper bound for the ground state energy can be calculated, which can be used to obtain an approximation for the effective polaron mass.

In the following, we will briefly summarise the variational ansatz from [37, 38] and also briefly discuss the arising divergences. The goal of any variational ansatz is to minimise the energy functional

$$E(\theta) = \langle \psi(\theta) | \, \hat{\mathcal{H}} \, | \psi(\theta) \rangle \ , \tag{2.26}$$

over a given set of parameters θ [65]. The choice of a suitable trial function depends on the exact structure of the problem; limiting cases can often provide some insights into what trial wave functions are suitable and provide good estimates. Upon inspection of (2.25) it can be seen that when neglecting two phonon terms and in the limit of $M \to \infty$ the model can be solved exactly by a simple coherent state ansatz [46]. Guided by this insight we will employ a variational ansatz,

where the trial function is a product of coherent states

$$|\psi^{\mathrm{var}}\rangle = \hat{U}_{\mathrm{coh}}|0\rangle \,, \tag{2.27}$$

with $|0\rangle$ being the phonon vacuum, which is also the ground state for $g_{\mathrm{IB}} = 0$. $\hat{U}_{\mathrm{coh}}$ is the unitary shift operator

$$\hat{U}_{\mathrm{coh}} = \exp\left(\sum_{\mathbf{k}} \alpha_{\mathbf{k}} \hat{a}_{\mathbf{k}} + \mathrm{h.c.}\right) \,, \tag{2.28}$$

which transforms the phonon operators as

$$\hat{U}_{\mathrm{coh}}^{\dagger} \hat{a}_{\mathbf{k}} \hat{U}_{\mathrm{coh}} = \hat{a}_{\mathbf{k}} + \alpha_{\mathbf{k}} \,. \tag{2.29}$$

In this case, the amplitudes $\alpha_{\mathbf{k}}$ are the variational parameters over which the energy functional

$$\begin{aligned} E[\{\alpha_{\mathbf{k}}\}, \mathbf{p}] = &\sum_{\mathbf{k}} \mathcal{E}_{\mathbf{k}} \alpha_{\mathbf{k}}^{*} \alpha_{\mathbf{k}} + \frac{(\mathbf{p} - \mathbf{P}_{\mathrm{ph}})^2 + \mathbf{P}_{\mathrm{ph}}^2}{2M} + g_{\mathrm{IB}} n_0 \\ &+ g_{\mathrm{IB}} \sqrt{\frac{n_0}{L^d}} \sum_{\mathbf{k} \neq 0} W_{\mathbf{k}} \left(\alpha_{\mathbf{k}} + \mathrm{c.c.}\right) + \frac{g_{\mathrm{IB}}}{2L} \sum_{\mathbf{k}, \mathbf{k}' \neq 0} \Big[\big(W_{\mathbf{k}} W_{\mathbf{k}'} + \\ &W_{\mathbf{k}}^{-1} W_{\mathbf{k}'}^{-1} \big) \alpha_{\mathbf{k}}^{*} \alpha_{\mathbf{k}'} + \frac{1}{2} \big(W_{\mathbf{k}} W_{\mathbf{k}'} - W_{\mathbf{k}}^{-1} W_{\mathbf{k}'}^{-1} \big) \big(\alpha_{\mathbf{k}}^{*} \alpha_{-\mathbf{k}'}^{*} + \mathrm{c.c.} \big) \Big] \end{aligned} \tag{2.30}$$

is minimised. Here, we have also defined the variational phonon momentum $\mathbf{P}_{\mathrm{ph}} = \sum_{\mathbf{k}} \mathbf{k} \alpha_{\mathbf{k}}^{*} \alpha_{\mathbf{k}}$. To determine the amplitudes that minimise (2.30) the saddle point equation

$$0 = \frac{\delta E[\{\alpha_{\mathbf{k}}\}, \mathbf{p}]}{\delta \alpha_{\mathbf{k}}^{*}} = g_{\mathrm{IB}} \frac{n_0}{L^d} W_{\mathbf{k}} + \Omega_{\mathbf{k}} \alpha_{\mathbf{k}} + \frac{g_{\mathrm{IB}}}{L} W_{\mathbf{k}} \sum_{\mathbf{k}' \neq 0} [W_{\mathbf{k}'} \operatorname{Re} \alpha_{\mathbf{k}} + i W_{\mathbf{k}'}^{-1} \operatorname{Im} \alpha_{\mathbf{k}}] \tag{2.31}$$

can be used, where $\Omega_{\mathbf{k}} = \mathcal{E}_{\mathbf{k}} + \frac{\mathbf{k}^2}{2M} - \frac{\mathbf{k}}{M} \cdot (\mathbf{p} - \mathbf{P}_{\mathrm{ph}})$. After separating the equation into its real and imaginary part we find

$$\operatorname{Re} \alpha_{\mathbf{k}} = -g_{\mathrm{IB}} W_{\mathbf{k}} \frac{\sqrt{n_0 L^{-d}} + L^{-d} \sum_{\mathbf{k}'} W_{\mathbf{k}'} \operatorname{Re} \alpha_{\mathbf{k}'}}{\Omega_{\mathbf{k}}} \,, \tag{2.32}$$

$$\operatorname{Im} \alpha_{\mathbf{k}} = g_{\mathrm{IB}} W_{\mathbf{k}}^{-1} \frac{L^{-d} \sum_{\mathbf{k}'} W_{\mathbf{k}'}^{-1} \operatorname{Im} \alpha_{\mathbf{k}'}}{\Omega_{\mathbf{k}}} \,. \tag{2.33}$$

Equation (2.33) can be trivially solved by setting $\mathrm{Im}\,\alpha_{\mathbf{k}} = 0$. The real part (2.32), is a self consistent equation, which can be resummed as a geometric series and we find

$$\mathrm{Re}\,\alpha_{\mathbf{k}} = -g_{\mathrm{IB}}\frac{n_0}{L^d}\frac{W_{\mathbf{k}}}{\Omega_{\mathbf{k}}}\frac{1}{1+\frac{g_{\mathrm{IB}}}{L^d}\sum_{\mathbf{k}'}\frac{W_{\mathbf{k}'}^2}{\Omega_{\mathbf{k}'}}} = -g_{\mathrm{IB}}\sqrt{\frac{n_0}{L^d}}\frac{W_{\mathbf{k}}}{\Omega_{\mathbf{k}}}\beta\,. \tag{2.34}$$

We note that for the Fröhlich model[3] the amplitude is given by $\mathrm{Re}\,\alpha_{\mathbf{k}} = -g_{\mathrm{IB}}\sqrt{\frac{n_0}{L^d}}\frac{W_{\mathbf{k}}}{\Omega_{\mathbf{k}}}$ [46]. Using the solution for the α_k we find that the phonon momentum is determined by

$$\mathbf{P}_{\mathrm{ph}} = \beta^2 g_{\mathrm{IB}}\frac{n_0}{L^d}\sum_{\mathbf{k}}\mathbf{k}\frac{W_{\mathbf{k}}^2}{\Omega_{\mathbf{k}}^2} \tag{2.35}$$

and the polaron energy takes the following form

$$E^{\mathrm{pol}}(\mathbf{p}) = \frac{p^2 - P_{\mathrm{ph}}^2}{2M} + g_{\mathrm{IB}}n_0\beta\,. \tag{2.36}$$

This enables the calculation of the effective mass. In fact, if one considers the full Hamiltonian (2.1) the situation becomes more subtle and will be discussed in the next subsection. However, for the (extended) Fröhlich model, it is straightforward to extract the effective mass from the dispersion relation $E(\mathbf{p}) = E(0) + \frac{p^2}{2m^*}$ in the $p \to 0$ limit. At this point one would usually take the thermodynamic limit, i.e. $N, L \to \infty$, s.t. $n_0 = \frac{N}{L^d} = cst.$ and $\frac{1}{L^d}\sum_{\mathbf{k}} \to \frac{1}{(2\pi)^d}\int \mathrm{d}^d\mathbf{k}$. However, the ground state energy and the phonon momentum as they stand are ill defined in the thermodynamic limit. The arising divergences depend on the dimension of the system and are of different origin. In the following, we will discuss the causes and remedies within the variational ansatz for one and three dimensional systems; for more involved renormalisation group treatments, we refer to [37, 46, 67]. The two dimensional case, is not considered in this work but can be found in [68].

We start with the one-dimensional case and note that the expressions for polaron energy and momentum are finite and well defined. In fact, there are some subtitles involved with regularising terms originating from normal ordering that were neglected in the derivation here, and we refer to

[3] i.e. when neglecting two phonon scattering terms

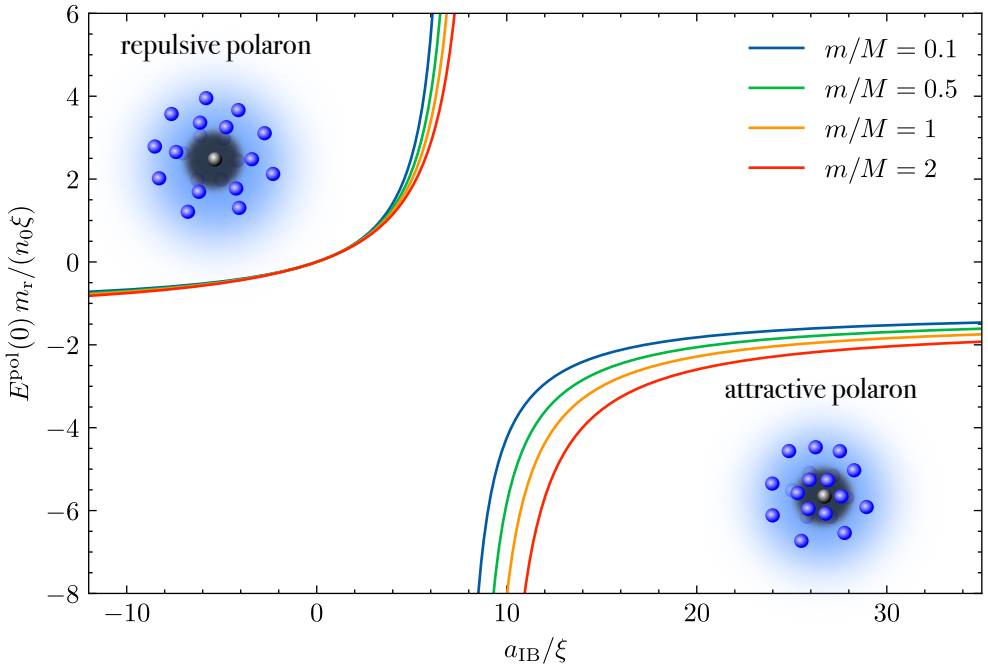

Figure 2.6: The polaronic ground state energy in 3D for different mass ratios and zero total momentum. All curves have been regularised using the Lippmann-Schwinger equation (2.12). There is a resonance within the energy spectrum, which is associated with a crossover from attractive to repulsive polaron [38, 66]. The sharp divergence is a result of neglecting boson-boson interaction within the (extended) Fröhlich model. In a physical system, one would not expect a divergence but instead a smooth crossover due to boson-boson interaction preventing a diverging number of phonons around the impurity [59].

[37, 69] for an in depth discussion.

For the three dimensional case the term $\int \mathrm{d}^3\mathbf{k} \frac{W_{\mathbf{k}}^2}{\Omega_{\mathbf{k}}}$ is ultraviolet (UV) divergent, which is caused by the usage of a contact interaction for the impurity-boson interaction. The Fourier modes of a delta function do not decay fast enough (in fact, they are constant) in three dimensions to render the results finite. A straightforward and ad-hoc way to deal with this divergence is to introduce the UV-cutoff Λ. The result can then be made independent of the cutoff by utilising the Lippmann-Schwinger equation for a delta potential (2.12). In its discrete form the equation is given by

$$\frac{1}{g_{\mathrm{IB}}} = \frac{m_{\mathrm{r}}}{2\pi a_{\mathrm{IB}}} - \frac{1}{L^d} \sum_{\mathbf{k}\neq 0}^{\Lambda} \frac{2m_{\mathrm{r}}}{\mathbf{k}^2}\,, \tag{2.37}$$

and relates the microscopic interaction strength g_{IB} with the experimentally accessible scattering length a_{IB}. Using this substitution, all results become finite and independent of the system size in the thermodynamic limit. In Figure 2.6, we show the energy for zero total momentum as a function

of the impurity-boson scattering length. This shows how the polaron crosses over from a purely repulsive polaron to an attractive polaron. The divergence would not occur in a real physical system since it is caused by a diverging number of phonons. Such divergences are balanced by boson-boson interaction in an interacting Bose gas.

The effective mass

The previous subsection, has demonstrated how the effective mass is calculated by using the ground state dispersion relation of the (extended) Fröhlich Hamiltonian. This subsection emphasise some fundamental differences between the ground state of the effective (extended) Fröhlich model and the full Hamiltonian (2.1) for the special case of a single impurity atom. The following expands on our previous discussions of the effective mass presented in [JJ1] and [64]. As outlined in the previous subsection, using the variational ansatz, the approximate ground state of the system for fixed total momentum is the polaronic solution, i.e., the total momentum of the system is carried by the polaron. For the linearised theory, this is not limited to the employed ansatz and holds true more generally [8, 10, 37, 38].

However, for the full Hamiltonian (2.1) the situation is significantly different and the ground state for finite momentum is in fact not the polaronic state but the uniformly boosted system. To show this we introduce the potential

$$\hat{\Omega} = \hat{\mathcal{H}} - \mathbf{v} \cdot \hat{\mathbf{P}}_{\mathrm{tot}} \,, \tag{2.38}$$

with the total momentum $\hat{\mathbf{P}}_{\mathrm{tot}} = \hat{\mathbf{P}} + \hat{\mathbf{P}}_{\mathrm{B}}$, where

$$\hat{\mathbf{P}}_{\mathrm{B}} = -i \int \mathrm{d}^d\mathbf{r}\, \hat{\varphi}^\dagger(\mathbf{r}) \nabla \hat{\varphi}(\mathbf{r}) \tag{2.39}$$

is the momentum of the Bose gas. Finding the ground state of (2.38) for fixed $\mathbf{v}$ is now equivalent to finding the ground state with fixed finite total momentum of (2.1). This relationship becomes apparent when one views $\mathbf{v}$ as a Lagrange multiplier fixing the total momentum. We now introduce

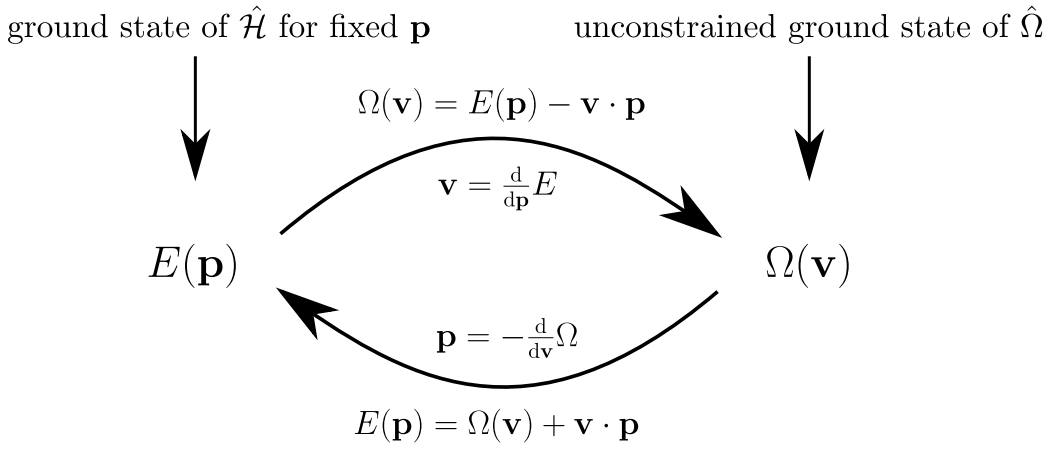

Figure 2.7: Illustrating the relationship between the different ways of calculating the effective mass. The two potentials are connected via a Legendre transformation and one can then deduce that both methods lead indeed to the same effective mass. The figure is based on [64].

the unitary transformation

$$\hat{U}_{\mathrm{cm}} = \exp\Big\{\Big(-iM_{\mathrm{tot}}\hat{\mathbf{R}}_{\mathrm{cm}}\cdot\mathbf{v}\Big)\Big\}\,, \tag{2.40}$$

where $M_{\mathrm{tot}} = Nm + M$ and $\hat{\mathbf{R}}_{\mathrm{cm}} = \frac{1}{M_{\mathrm{tot}}}\Big(m\int \mathrm{d}^d\mathbf{r}\,\mathbf{r}\hat{\varphi}^\dagger(\mathbf{r})\hat{\varphi}(\mathbf{r}) + M\hat{\mathbf{X}}\Big)$ to boost into the centre of mass frame. It can be easily verified that

$$\hat{\Omega} = \hat{U}_{\mathrm{cm}}^\dagger\hat{\mathcal{H}}\hat{U}_{\mathrm{cm}} - \frac{1}{2}M_{\mathrm{tot}}v^2\,, \tag{2.41}$$

holds. This relationship enables us to relate the eigenstates of $\hat{\mathcal{H}}$ with those of $\hat{\Omega}$. Precisely, the ground state value of $\hat{\Omega}$ for fixed $\mathbf{v}$ is given by

$$E_0 - \frac{1}{2}M_{\mathrm{tot}}v^2\,, \tag{2.42}$$

where E_0 is the ground state energy of $\hat{\mathcal{H}}$ for zero total momentum. This indeed shows that the ground state for finite momentum (corresponding to finite v) is the boosted global ground state of $\hat{\mathcal{H}}$. We conclude that by naively applying the standard definition; the effective mass evaluates to the total mass of the system. The boosted state is not admissible in the (extended) Fröhlich model. We will later see that enforcing locality is sufficient to find the right polaronic solution at finite momentum. We have used two different ways of finding the effective mass so far; namely on the

one hand we fix the total momentum, then find the constrained ground state of $\hat{\mathcal{H}}$ and read off the effective mass from the dispersion of $E(p)$. On the other hand we introduce a Lagrange multiplier, determining the un-constrained ground state of Ω and subsequently focus on $\Omega(v)$. In fact those two quantities are related by a simple Legendre transformation

$$\Omega(\mathbf{v}) = E(\mathbf{p}) - \mathbf{v}\cdot\mathbf{p} = E(\mathbf{p}) - \partial_{\mathbf{p}}E\cdot\mathbf{p}\,, \tag{2.43}$$

where $\Omega(\mathbf{v})$ ($E(\mathbf{p})$) is the functional obtained by minimising $\hat{\Omega}$ ($\hat{\mathcal{H}}$) for fixed $\mathbf{v}$ ($\mathbf{p}$). Here, we note that when minimising $\hat{\mathcal{H}}$ for fixed p one has to find the constrained ground state, which can be challenging from a technical point of view. Thus $\hat{\Omega}$ can sometimes be useful for purely technical reasons. The relationship is schematically depicted in Figure 2.7. We can now use the basic properties of a Legendre transformation to arrive at

$$\partial^2_{\mathbf{v}}\Omega(\mathbf{v}) = \left(\partial^2_{\mathbf{p}}E(\mathbf{p})\right)^{-1}\,. \tag{2.44}$$

This shows that the two definitions indeed lead to the same effective mass. Lastly, we want to discuss yet another commonly used method to obtain the effective mass. For this method the momentum of the Bose gas is used to obtain the effective mass; the arguments given here follow [46]. In the polaronic state the total momentum of the system is carried by the polaron and hence the polaron velocity is determined by $v_{\mathrm{p}} = p/m^*$. Noting that the impurity velocity coincides with the polaron velocity at all times in equilibrium we can write $v_{\mathrm{p}} = v_{\mathrm{I}} = P_{\mathrm{I}}/M$, where P_{I} is the impurity velocity. Utilising momentum conservation $p = P_{\mathrm{I}} + P_{\mathrm{B}}$ we find

$$\frac{p - P_{\mathrm{B}}}{M} = \frac{p}{m^*}\,, \tag{2.45}$$

which determines the effective mass in terms of the phonon momentum. This relation can also easily be derived from the dispersion relation by using

$$v_{\mathrm{p}} = \frac{\mathrm{d}E}{\mathrm{d}p} = \frac{p - P_{\mathrm{B}}}{M}\,, \tag{2.46}$$

which once again yields (2.44). This demonstrates that using the momentum of the superfluid to determine the effective mass is equivalent to using the dispersion relation.

2.2 The Keldysh path integral and semi-classical approximations

This section introduces techniques, based on the Keldysh path integral formalism, which are repeatedly used in the main text and put these into a broader context. The structure of this section is as follows; we start by introducing the Keldysh path integral formalism and present a brief derivation. The content of this part is mainly based on [70–72]. Using these results, we show how a one-loop approximation leads to the semi-classical truncated Wigner approximation (TWA). From there, we discuss, how by assuming deterministic initial conditions, the famous Gross-Pitaevskii equation is recovered and introduce the split-step Fourier algorithm, which is a numerical scheme to evolve the Gross-Pitaevskii equation in time. We conclude the section by discussing how the split-step Fourier algorithm can be used in imaginary time to find the system's ground state.

The Keldysh path integral

In this subsection, we present a derivation of the Keldysh path integral. Throughout the derivation of the path integral, we have the Hamiltonian (2.1) for a single impurity in mind while simultaneously trying to keep things as general as possible without much loss of clarity. It should then be straightforward to see how the derivation can be adopted to more general settings. For notational convenience, we drop the $\mathbf{r}$ dependence of the field $\hat{\varphi}$ and implicitly assume an integral over space where necessary. Furthermore, we assume that the initial configuration of the system is given by the density matrix $\hat{\rho}_0$. Here, we note that for the situations we have in mind, the system's evolution starting from a specific state is of interest, and thus the exact initial conditions are of crucial importance. This is in contrast to applications of the Keldysh formalism for steady-state situations,[4] where a non-equilibrium configuration is achieved by continuously driving the system

[4] see for example [73, 74]

and thus the initial conditions are irrelevant. More precisely, the goal is to calculate the expectation value of an observable of the form $\hat{\Omega}(\hat{\varphi}^{(\dagger)}, \hat{\mathbf{X}}, \hat{\mathbf{P}}, t)$. From standard quantum mechanics [65] we know that this expectation value can be expressed as

$$\langle \hat{\Omega}(\hat{\varphi}^{(\dagger)}, \hat{\mathbf{X}}, \hat{\mathbf{P}}, t)\rangle = \mathrm{Tr}\Big\{\hat{\rho}_0 T_\tau e^{i\int_0^t \hat{\mathcal{H}}(\tau)\mathrm{d}\tau}\hat{\Omega}(\hat{\varphi}^{(\dagger)}, \hat{\mathbf{X}}, \hat{\mathbf{P}}, t)e^{-i\int_0^t \hat{\mathcal{H}}(\tau)\mathrm{d}\tau}\Big\}\,, \tag{2.47}$$

where T_τ denotes the Keldysh time ordering. The Keldysh time ordering orders the operators along the contour going from times 0 to t and then back to 0 (see Figure 2.8). In other words, later times always appear closer to $\hat{\Omega}$. We proceed by first discretising the temporal evolution

$$T_\tau e^{i\int_0^t \hat{\mathcal{H}}(\tau)\mathrm{d}\tau} = \lim_{N\to\infty}\prod_{n=1}^{N} e^{i\hat{\mathcal{H}}(\tau_n)\Delta\tau} \tag{2.48}$$

and then inserting the identity

$$\mathrm{id} = \int \mathrm{d}p_i\mathrm{d}x_i\mathrm{d}\varphi_i^{(*)}\frac{e^{-|\varphi_i|^2}}{\pi}\left|x_i\right\rangle\left\langle p_i\right|\left\langle x_i|p_i\right\rangle\left|\varphi_i\right\rangle\left\langle\varphi_i\right|\,, \tag{2.49}$$

between any discrete time slice. Since the momentum (position) and the field operators commute we can view (2.49) as the tensor product of two identities acting on the appropriate sub-spaces. Evidently, we may generalise this identity to an arbitrary number of particles and fields. After inserting the identity for the forward contour we can use the general fact that for two non commuting operators A, B with associated eigenstates $|a_i\rangle$, $|b_i\rangle$ [71] the relation

$$\begin{aligned} e^{i\hat{\mathcal{H}}(\tau_i)\Delta\tau} &= \int \mathrm{d}a_i\mathrm{d}b_i\left|a_i\right\rangle\left\langle a_i\right|\left(1+\Delta\tau\sum_{n,m}\hat{A}^n(\tau_i)\hat{B}^m(\tau_i)+\mathcal{O}(\Delta\tau^2)\right)\left|b_i\right\rangle\left\langle b_i\right| \\ &= \int \mathrm{d}a_i\mathrm{d}b_i\left|a_i\right\rangle\left\langle b_i\right|\left\langle a_i|b_i\right\rangle e^{i\Delta\tau\mathcal{H}(\tau_i,a_i,b_i)}+\mathcal{O}(\Delta\tau^2) \end{aligned} \tag{2.50}$$

holds, to compute the effect of inserting a momentum-position identity. We note that the backwards contour can be dealt with in the same way, with the only difference that we now use the complex conjugate. For the field operators, the procedure only involves one set of states and therefore no overlap at equal times. Nevertheless, owing to the overcompleteness of the coherent state basis an

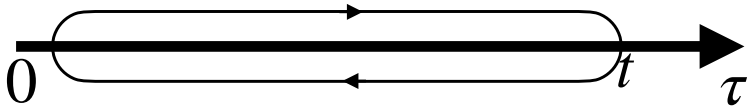

Figure 2.8: Illustration of the Keldysh-time-contour. The forward (backward) path is associated with the time propagation to the left (right) of the observable. Operators on the upper (lower) part of the contour are commonly denoted with the subscript $+$ $(-)$, which indicates the sign of the time evolution. In contrast to equilibrium settings or the time evolution of pure states, the degrees of freedom are doubled by the presence of the two contours.

additional normalisation factor has to be accounted for. Lastly, we need to keep in mind that after every identity there will be an overlap of two mismatched eigenstates with index i and $i+1$. This gives the extra terms

$$\langle x_i | p_{i+1} \rangle = \exp\{i p_{i+1} x_i\}\,, \tag{2.51}$$

$$\langle \varphi_i | \varphi_{i+1} \rangle = \exp\left\{ \frac{1}{2} \left(-|\varphi_i|^2 - |\varphi_i|^2 + 2\varphi_i^* \varphi_{i+1} \right) \right\}. \tag{2.52}$$

Combining it all, we find the discretised exponent for the forward (backward) contour

$$\exp\left\{ \pm i \Delta\tau \sum_{i=1}^{N} \left\{ -\mathcal{H}(\varphi_{i,\pm}^*, p_{i,\pm}, x_{i,\pm}) + p_{i+1,\pm} \frac{x_{i+1,\pm} - x_{i,\pm}}{\Delta\tau} + i\varphi_{i+1,\pm}^* \frac{\varphi_{i+1,\pm} - \varphi_{i,\pm}}{\Delta\tau} \right\} \right\}. \tag{2.53}$$

For the impurity the time derivative stems from combining the mismatched overlap terms as well as the overlap of the form $\langle x_i | p_i \rangle$. For the fields the time derivative arises from combining the mismatched overlap terms with the additional normalisation factor of the coherent state expansion. Additionally, there are two boundary terms and a bulk term[5] of the form

$$\exp\{-i a_{N,+} b_{N,+} + i a_{N,+} b_{N,-} - i a_{0,-} b_{0,-}\}\,, \tag{2.54}$$

[5]These terms can be attributed to the overlap of the identity between forward and backward contour.

where $a = p\left(\varphi^*\right)$ and $b = p\left(-i\varphi\right)$. It is now possible to take the continuum limit by letting $\Delta\tau \to 0$ and $N \to \infty$. Leaving us with the expression

$$\langle\hat{\Omega}(\hat{\varphi}^{(\dagger)}, \hat{\mathbf{X}}, \hat{\mathbf{P}}, t)\rangle = \int \mathcal{D}\left[\varphi_{\pm}^*, x_{\pm}, p_{\pm}\right] \langle\varphi_+(0), x_+(0)|\,\hat{\rho}\,|\varphi_-(0), x_-(0)\rangle\, \Omega\left(\varphi_+, \varphi_-^*, \mathbf{P}_+, \mathbf{X}_-\right) \tag{2.55}$$

$$\times e^{iS} e^{-|\varphi_+(t)|^2 - |\varphi_-(0)|^2 + \varphi_+^*(t)\varphi_-(t) - i(p_+(t)x_-(t)p_+(t)x_-(t) + p_-(0)x_-(0))},$$

where we have defined the action

$$S = \int_0^t \mathrm{d}\tau\, \left\{\varphi_+^* i\partial_\tau\varphi_+ - \varphi_-^* i\partial_\tau\varphi_- + p_+\partial_\tau x_+ - p_-\partial_\tau x_- + \mathcal{H}_+ - \mathcal{H}_-\right\}, \tag{2.56}$$

and $\mathcal{H}_\pm$ denotes the classical Hamiltonian evaluated on the forward (backward) contour.

Truncated Wigner approximation

In the previous subsection, we have seen how to express the expectation value of an arbitrary observable as a path integral. We also discussed how the Keldysh path integral is suitable for addressing out of equilibrium settings. This flexibility came at the expense of doubling the degrees of freedom. In particular, the representation used in (2.55) splits the integration variables into forward and backward contour. While this representation is useful for deriving a closed-form expression, it is not the most convenient representation for performing semi-classical approximations. From the Feynman path integral for quantum mechanics, it is well known that the saddle point approximation of the path integral recovers the classical equations of motion [65]. Inspired by this result, the question arises whether a transformation of variables can make such a relation explicit for the Keldysh path integral. Indeed, one can split the integration variables into quantum and classical parts. This representation lends itself for performing calculations and will turn out to be crucial for deriving the truncated Wigner approximation. The decomposition into quantum and classical fields

is done in the following way

$$\varphi_{\pm}^{(*)} = \varphi_c^{(*)} \pm \varphi_q^{(*)}/2\,, \tag{2.57}$$

$$x_{\pm} = x_c \pm x_q/2\,, \tag{2.58}$$

$$p_{\pm} = p_c \pm p_q/2\,. \tag{2.59}$$

We will later see that the classical field is called as such since its evolution coincides with the classical counterpart of the quantum mechanical system. After performing the redefinition the expectation value of an arbitrary observable can be expressed as

$$\begin{aligned}\langle\hat{\Omega}(\hat{\varphi}^{(\dagger)}, \hat{\mathbf{X}}, \hat{\mathbf{P}}, t)\rangle = \int \mathrm{d}p_0\mathrm{d}x_0\mathrm{d}\varphi_0^{(*)}\, W\left(x_0, p_0, \varphi_0^{(*)}\right) \int \mathcal{D}\left[\varphi_{c/q}^{(x)}, x_{c/q}, p_{c/q}\right] \\ \Omega\left(x_c(t), p_c(t), \varphi^{(*)}(t)\right) \exp\left\{ i \int_0^t \mathrm{d}\tau \left[x_q\partial_\tau p_c - p_q\partial_\tau x_c - [i\varphi_c^*\partial_\tau\varphi_q + \text{c.c.}] \right.\right. \\ \left.\left. + \mathcal{H}\left(p_c + p_q/2, x_c + x_q/2, \varphi_c^{(*)} + \varphi_q^{(*)}/2\right) - \mathcal{H}\left(p_c - p_q/2, x_c - x_q/2, \varphi_c^{(*)} - \varphi_q^{(*)}/2\right) \right] \right\}.\end{aligned} \tag{2.60}$$

It is important to note here that we have already integrated out the boundary terms at t, which is equivalent to writing Ω in its symmetrically ordered form. The initial conditions are now encoded in the Wigner function

$$W\left(x_0, p_0, \varphi_0^{(*)}\right) = \int \mathrm{d}\xi\mathrm{d}\eta^{(*)} \left\langle x_0 - \frac{\xi}{2}, \varphi_0 - \frac{\eta}{2} \middle| \hat{\rho}_0 \middle| x_0 + \frac{\xi}{2}, \varphi_0 + \frac{\eta}{2} \right\rangle$$
$$e^{ip_0\xi - |\varphi_0|^2 - \frac{1}{4}|\eta|^2 + \frac{[\eta^*\varphi_0 + \eta\varphi_0^*]}{2}}\,.$$

Expanding the term $\mathcal{H}_+ - \mathcal{H}_-$ in the quantum fields, one finds that there are only terms linear in the quantum fields and of order three and higher (corresponding to second order and higher in $\hbar$). Hence in a one loop approximation[6] the quantum fields will only contribute linearly, which leads to

[6]The one loop approximation corresponds to neglecting terms of order two and higher in $\hbar$.

an action of the form

$$S = \int \mathrm{d}t \left\{ x_q \partial_\tau p_c - p_q \partial_\tau x_c - [i\varphi_c^* \partial_\tau \varphi_q + \mathrm{c.c.}] + x_q \frac{\delta \mathcal{H}}{\delta x_c} + p_q \frac{\delta \mathcal{H}}{\delta p_c} + \left[\varphi_q \frac{\delta \mathcal{H}}{\delta \varphi_c^*} + \mathrm{c.c.} \right] \right\} . \tag{2.61}$$

Here, we implicitly assume that the partial derivatives of the Hamiltonian are evaluated with all quantum variables set to 0. Through this approximation it is now possible to integrate out the quantum fields and we find that this integration yields functional δ-distributions, which simply enforce the classical equations of motion

$$\partial_\tau p_c = -\frac{\delta H}{\delta x_c} , \quad \partial_\tau x_c = \frac{\delta H}{\delta p_c} , \tag{2.62}$$

$$i\partial_\tau \varphi_c = \frac{\delta H}{\delta \varphi_c^*} . \tag{2.63}$$

Given one solves the classical equations of motion, the only step that remains is to integrate over the initial conditions weighted by the Wigner function. In practice, there are several ways this can be achieved if there is no closed form solution. The Wigner function is, in general, a quasi-probability distribution and the integral over the initial conditions can be solved using Monte Carlo methods. In many cases the Wigner function tuns out to be a true probability distribution and it is possible to sample directly from it, significantly simplifying the procedure. If the accuracy achieved by the truncated Wigner approximation is insufficient, it is possible to further improve the approximation by keeping higher orders in the quantum fields. This will result in additional quantum jump terms. The scope of this work is confined to the truncated Wigner approximation, but further details are available in [70].

Gross-Pitaevskii equation

The Gross-Pitaevskii equation (GPE) is a semi-classical mean-field equation often used as a first approximation to understand the behaviour and the ground state of an ultracold bosonic gas [18, 19]. Generally speaking, the GPE is applicable to weakly interacting Bose gases, where most particles

are in the same state. For a more detailed discussion on its validity and some worked examples, we refer to [18, 19].

This subsection aims to show that the GPE can in fact be seen as a special case of the TWA with deterministic initial conditions. For simplicity, we discuss the GPE for a Bose gas without impurity, where the general Hamiltonian is given by

$$\hat{\mathcal{H}}_\varphi = \int \mathrm{d}^d\mathbf{r}\, \hat{\varphi}^\dagger(\mathbf{r}) \left(\frac{-\Delta}{2m} - \mu + \frac{g_{\mathrm{BB}}}{2}\hat{\varphi}^\dagger(\mathbf{r})\hat{\varphi}(\mathbf{r}) + V(\mathbf{r}) \right) \hat{\varphi}(\mathbf{r}) \tag{2.64}$$

and note that a detailed discussion of the case with impurity is given in chapter 4. For deterministic initial conditions the Wigner function takes the simple form

$$W(\varphi, \varphi^*) = \delta\left[\varphi(\mathbf{r}, 0) - \varphi_0(\mathbf{r})\right] \,, \tag{2.65}$$

where again the delta function is to be understood in a functional sense. Together with the results from the previous subsection we can now write down the time dependent GPE

$$i\partial_t\varphi(\mathbf{r}, t) = \left(\frac{-\Delta}{2m} - \mu + g_{\mathrm{BB}}|\varphi(\mathbf{r}, t)|^2 + V(\mathbf{r}) \right) \varphi(\mathbf{r}, t) \,, \tag{2.66}$$

which describes the time evolution of a (trapped) Bose gas starting at $t = 0$ in the state $\varphi_0(\mathbf{r})$. Setting $\partial_t\varphi(\mathbf{r}, t) = 0$ recovers the time independent GPE which can be used to find an approximate ground state of the system. The meaning of the GPE in terms of quantum mechanical states can be easily seen from the derivation of the path integral. Namely, the GPE can also directly be found from the Hamiltonian by limiting the time evolution of the system to the sub-manifold of coherent states and then minimising the arising energy functional [18].

The split step Fourier method

The split-step Fourier method is an efficient pseudospectral method for solving partial differential equations [75]. In this subsection, we introduce the split-step Fourier method to solve the GPE and show how it can be combined with the imaginary time evolution to find the ground state

wave function of the system. We start by introducing the split-step Fourier method for the single component GPE (2.66). From there, it is straightforward to see how it can be generalised to two-component GPEs or combined with the time propagation of an impurity in position-momentum representation.

The GPE can be solved formally for infinitesimal dt by writing

$$\varphi(\mathbf{r}, t + dt) = e^{-iHdt}\varphi(\mathbf{r}, t) \,, \tag{2.67}$$

where $H = T + V = \frac{-\Delta}{2m} + (g_{\mathrm{BB}}|\varphi(\mathbf{r}, t)|^2 + V(\mathbf{r}))$. This propagates the wave function from t to $t + dt$. By using the Zassenhaus formula [76] the operator exponential can be written as

$$e^{i(T+V)dt} = e^{iTdt}e^{iVdt}e^{i[T,V]dt^2} + \mathcal{O}(dt^3) = e^{iTdt}e^{iVdt} + \mathcal{O}(dt^2) \,, \tag{2.68}$$

where by $[\cdot\,,\cdot]$ we denote the commutator between two operators. For sufficiently small dt we can therefore use this relationship to propagate the wave function in time with local error of at most dt^2. For the special case, where T is a derivative operator,[7] we note that this operator is diagonal in Fourier space, which makes evaluating the exponential in Fourier space simpler and computationally efficient. Denoting the (inverse) Fourier by $\mathcal{F}$ ($\mathcal{F}^{-1}$) we can therefore write the time propagation as

$$\varphi(\mathbf{r}, t + dt) = \mathcal{F}^{-1}\left\{e^{-idt\frac{k^2}{2m}}\mathcal{F}\left[e^{-idt\left(V(\mathbf{r})+g_{\mathrm{BB}}|\varphi(\mathbf{r},t)|^2\right)}\right]\varphi(\mathbf{r}, t)\right\} \,, \tag{2.69}$$

where we stress that all exponentials are taken of scalars and no operator (matrix) exponentials have to be evaluated. By iteratively applying this relationship we can now propagate the wave function in time.

The local error can be improved upon by using more sophisticated operator splittings [75]. One of the most well-known and widely applied methods is the symmetric split-step Fourier method [77], which has a local error of $\mathcal{O}(dt^3)$. For most results in this work where a split-step Fourier method was used, symmetric splitting was applied. Here, instead of doing a full time step for the non-linear

[7] In particular, here T is the Laplacian.

part, one starts by only performing half a time step for the non-linear part. Subsequently, the entire momentum space step is carried out. Then, the wave function is propagated by the remaining half time step of the non-linear part (where the non-linear part is evaluated at the updated wave function). As mentioned, this has the advantage of a smaller error while also only having to perform the Fourier transform once.

Besides real-time propagation, another important application of the split-step Fourier algorithm is its use to perform an imaginary-time evolution. Performing the evolution in imaginary time permits the discovery of the ground state of a given system. Here, one starts with a random wave function $\varphi(\mathbf{r})$, where it is assumed that the overlap between the ground state and $\varphi(\mathbf{r})$ is non zero. After performing a Wick-rotation, i.e. $idt \to \tau$ (2.69) is repeatedly applied. After each step, the wave function needs to be normalised again, since the algorithm is not norm preserving in imaginary time. To see that this method indeed converges to the ground state of the system, we write the time propagation in terms of its spectral decomposition

$$\varphi(\mathbf{r}, \tau + d\tau) = \sum_n a_n \varphi_n(\mathbf{r}) e^{-\epsilon_n \tau} \,, \tag{2.70}$$

where ϵ_n are the eigenenergies. At each time step, we observe that every mode gets damped exponentially with higher energies decreasing faster and the ground state amplitude decays the slowest. Normalising the wave function after every step ensures that the wave function does not decay below numerical precision and that only the ground state mode survives after a sufficiently long time. It is important to note that this method's applicability relies on the energy spectrum of the system being gapped.

CHAPTER 3

Strong-coupling Bose polarons in 1D: Condensate deformation and modified Bogoliubov phonons

This chapter is based on [JJ1] with some verbatim textual overlap.

3.1 Polarons in lineland

In the following two chapters, we address the polaron in and out of equilibrium in one dimension. One-dimensional systems have proven to behave quite differently from their higher dimensional counterparts [78]. A lot of somewhat specialised tools ranging from the famous Bethe-ansatz [79] to more modern approaches borrowing ideas from conformal field theory [80] have been developed to address one-dimensional systems. While all those methods answer interesting questions in their

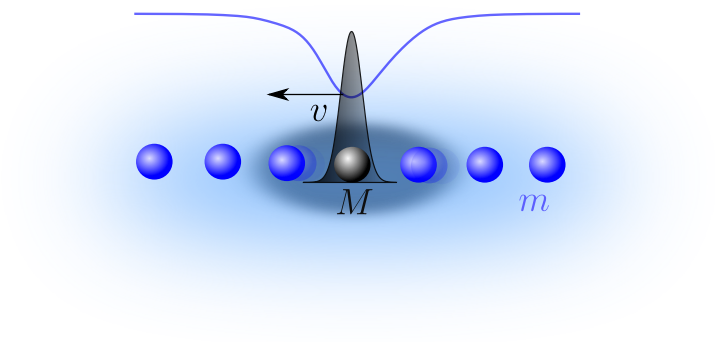

Figure 3.1: In this chapter, we consider an impurity in a one-dimensional ultracold Bose gas. In equilibrium, the impurity perturbs the surrounding gas, and a Bose polaron is formed.

own right, in the present work we take a different approach. The following two chapters aim to apply general methods applicable in d-dimensions to the one-dimensional problem. Most of these methods have not been established in the context of Bose polarons yet, and are therefore novel. The motivation to focus on one-dimensional systems is, on one hand, out of convenience to establish a proof of concept and, on the other hand, to uncover effects otherwise suppressed in higher dimensions. Additionally, the Bose polaron in one dimension has been realised experimentally [22], see Appendix A for a brief discussion of the experiment and a comparison with the theory developed in this chapter.

Analytical solutions to a wide range of problems are available in one dimension. As per the discussion to follow, this is also the case for the stationary mean-field equations of the Bose polaron in one dimension [56, 58]. We will build on these findings and use the analytical solutions to construct a quantum description by expanding around the mean-field solution and then including quantum fluctuations up to second order. Doing so, we find remarkable agreement with quasi-exact diffusion Monte Carlo (DMC) simulations. The success of this seemingly simple approach is explained by observing that we already take the condensate deformation and the associated boson-boson interaction into account on the mean-field level. We also touch upon the subtleties of using the standard definition of the effective mass for the full Hamiltonian discussed in section 2.1 and show that those can be addressed by choosing adequate boundary conditions. We then point out some crucial differences between our approach and those taken by other authors [57, 58]. To conclude this chapter, we present a detailed discussion on how one can include quantum fluctuations on top of the mean-field solution and demonstrate how to deal with the divergences typically arising for such treatments.

Introduction

This chapter considers the equilibrium properties of the one-dimensional Bose polaron. Many theoretical works considering the Bose polaron in equilibrium focus on the (extended) Fröhlich model or other linearised effective models, where the impurity couples to the excitations of a uniform superfluid (see section 2.1) [33–38, 45]. To study the equilibrium properties of the linearised model,

sophisticated methods have been developed including variational [38, 40, 41], field-theoretical [33, 43–45], renormalisation group (RG) [37, 46] and open-system approaches [48], as well as Quantum Monte-Carlo simulations [37, 49, 50]. Despite the use of highly accurate methods to solve the extended Fröhlich model in one dimension, their comparison with results obtained from quasi-exact diffusion Monte-Carlo (DMC) calculations show that the extended Fröhlich model is only valid in the weak coupling regime. The limited applicability of the (extended) Fröhlich model is because the condensate deformation becomes substantial, when the impurity-boson interaction is large. This deformation can act as an effective potential for the impurity, leading to a self-bound state. This state is not accounted for correctly within the (extended) Fröhlich model, which is in contrast to the 3D case, where the normalised impurity-Bose interaction needs to exceed a threshold, determined by the inverse gas parameter [81, 82], for a self-bound state to occur. For a typical condensate, the gas parameter is very small, and the (extended) Fröhlich model remains valid over a wide range of coupling strengths. To address the shortcomings of the (extended) Fröhlich model, we expand the bosonic field operators about the exact mean-field solution in the presence of a mobile impurity in the LLP-frame [8]. This approach has two significant advantages; it incorporates the backaction of the impurity already on the mean-field level as previously done in [81–83], while at the same time retaining the full entanglement between the impurity and the bosonic field by working in the LLP-frame. The remainder of this chapter is structured as follows: A derivation of the analytical expressions for the mean-field polaron wavefunction is initially shown, from which previous approximations for the polaronic mass and energy are reproduced. Subsequently, we solve the corresponding Bogoliubov-de Gennes equations in a self-consistent approach to include quantum corrections. Our results are benchmarked against quasi exact DMC results [37], where we find excellent agreement in all regimes for repulsive interactions. This validates the hypothesis that expanding around the non-uniform condensate is an excellent starting point. We also present results for attractive interactions. Here too, we find good agreement with DMC results for the energy of the polaron but poorer agreement for the polaron mass. We attribute this discrepancy to the existence of many-particle bound states in the attractive regime [37, 49]. Before delving into the details of the calculations, a few remarks are in order. Strictly speaking, there is no BEC in a

homogeneous 1D system [84]. In addition, the quasi-particle concept is believed to break down [63, 85] due to a diverging number of low energy excitations emitted by the impurity. Thus, special care must be taken during the calculating of quantum effects. While other treatments of the 1D polaron in the LLP frame exist which account for the deformation of the condensate [56–58, 86], the scope of extending them to incorporate quantum fluctuations is limited. Lastly, we note that our approach naturally carries over to higher dimensions, with the only difference being that the mean-field equations lack analytical solutions here.

3.2 The model

Our starting point is a single impurity atom coupled to an ultracold Bose gas in one dimension, described by the one-dimensional version of (2.1)

$$\hat{\mathcal{H}} = \int \mathrm{d}x\, \hat{\varphi}^\dagger(x)\Big(-\frac{1}{2m}\partial_x^2 + \frac{g_{\mathrm{BB}}}{2}\hat{\varphi}^\dagger(x)\hat{\varphi}(x) - \mu + g_{\mathrm{IB}}\delta(x-\hat{X})\Big)\hat{\varphi}(x) + \frac{\hat{P}^2}{2M}\,. \tag{3.1}$$

The relative interaction strength is denoted by $\eta = g_{\mathrm{IB}}/g_{\mathrm{BB}}$. The healing length $\xi = 1/\sqrt{2m\mu}$ and the speed of sound $c = \sqrt{\mu/m}$ have already been defined in section 2.1. As discussed in section 2.1, expanding the bosonic field operator in (3.1) around a homogeneous condensate as $\hat{\varphi}(x) = \sqrt{n_0} + \hat{\xi}(x)$ with $n_0 = N/L$ leads to the (extended) Fröhlich Hamiltonian (see section 2.1). In this work, we choose a different starting point and consider the effects of the impurity at the condensate level itself.

We proceed as in the case of the Fröhlich model and eliminate the impurity position operator from (3.1) by a Lee-Low-Pines (LLP) [8] type transformation

$$\hat{U}_{\mathrm{LLP}} = \exp\Big(-i\hat{X}\hat{P}_{\mathrm{B}}\Big)\,. \tag{3.2}$$

Here, in contrast, the *total* momentum of the bosons $\hat{P}_{\mathrm{B}}$ enters. As discussed in section 2.1 $\hat{U}_{\mathrm{LLP}}$ transforms to a co-moving frame, where the impurity sits at the origin of the coordinate system, and its momentum is transformed to the total conserved momentum of the system and thus can

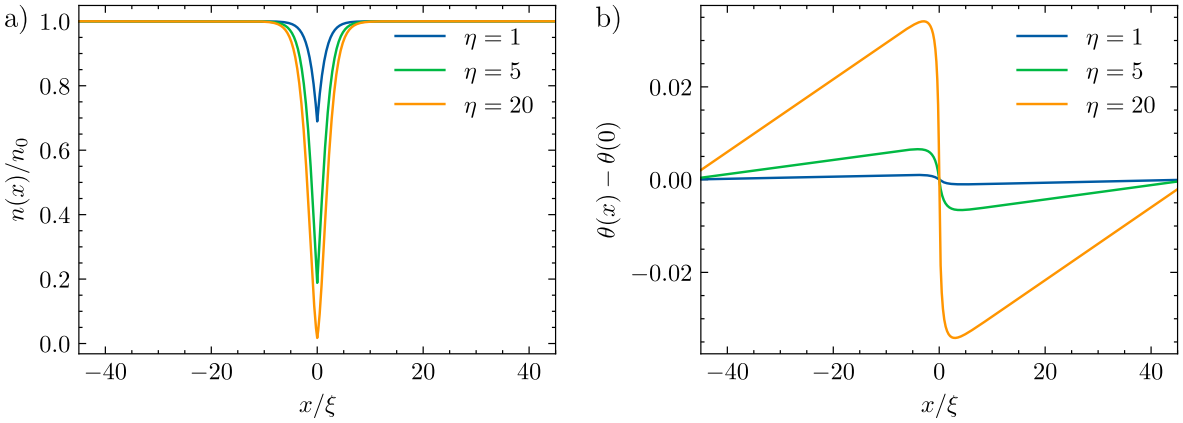

Figure 3.2: Mean-field a) density and b) phase for various repulsive couplings. All other parameters are as in [22], i.e. $M/m = 0.47$, the peak density $n_0 = 7/\mu\mathrm{m}$ and $g_{\mathrm{BB}} = 2.36 \times 10^{-37}\mathrm{Jm}$. For the phase we fixed $u = 0.01c$, which determines the total momentum on the mean-field level.

be treated as a c-number, denoted by p. By eliminating the impurity from the problem through an exact transformation, the entanglement between the impurity and the condensate is already included on the mean-field level. Thus, we do not have to assume a factorised wave function, as, for example, done in [82, 83]. At the same time an impurity-mediated interaction between the bosons $\sim \int \mathrm{d}x \left(p - \hat{P}_{\mathrm{B}}\right)^2 / 2M$ appears in the transformed Hamiltonian. To treat this, it will prove helpful to introduce a Hubbard-Stratonovich field $\hat{u}$, resulting in

$$\hat{\mathcal{H}}^{\mathrm{S}}_{\mathrm{LLP}} = \int \mathrm{d}x\, \hat{\varphi}^\dagger(x) \Bigg(-\frac{1}{2m_{\mathrm{r}}}\partial_x^2 + \frac{g_{\mathrm{BB}}}{2}\hat{\varphi}^\dagger(x)\hat{\varphi}(x) - \mu + g_{\mathrm{IB}}\delta(x) \Bigg) \hat{\varphi}(x) + \hat{u}\left(p - \hat{P}_{\mathrm{B}}\right) - \frac{1}{2}M\hat{u}^2\,, \tag{3.3}$$

where $\hat{u}$ satisfies $M\hat{u} = p - \hat{P}_{\mathrm{B}}$, and can thus be viewed as the impurity velocity. When working in the LLP frame it will prove useful to introduce the re-scaled healing length $\tilde{\xi} = \sqrt{m/m_{\mathrm{r}}}\xi$ and speed of sound $\tilde{c} = \sqrt{m/m_{\mathrm{r}}}c$.

3.3 Mean-field equations in the presence of the impurity

In this section we present the mean-field solutions of (3.3) for finite momentum. We now expand the operators around their mean-field solutions $\hat{\varphi}(x) = \varphi(x) + \hat{\xi}(x)$ and $\hat{u} = u + \delta\hat{u}$ where $\varphi(x)$

and u are chosen to solve the mean-field equations of (3.3), given by

$$\left(-\tfrac{1}{2m_\mathrm{r}}\partial_x^2 + g_\mathrm{BB}|\varphi(x)|^2 - \mu + iu\partial_x \right)\varphi(x) = 0\,, \tag{3.4}$$

$$\partial_x\varphi(x)\Big|_{0^-}^{0^+} = 2m_\mathrm{r}g_\mathrm{IB}\varphi(0)\,, \tag{3.5}$$

$$\varphi(\tfrac{L}{2}) = \varphi(-\tfrac{L}{2})\,, \tag{3.6}$$

subject to the additional boundary condition $|\varphi(\pm L/2)|^2 = n_0 + \mathcal{O}(1/L)$. We also require the mean-field velocity to satisfy

$$Mu = p - P_\mathrm{B}\,, \tag{3.7}$$

which is essentially momentum conservation. In practice, it is convenient to find the solution for a fixed u and then calculate the corresponding total momentum p using the above relationship. To remedy the problem of the uniformly boosted system being the ground state, we require that the polaron is a local quantity. Thus the condensate must be stationary far away from the impurity up to $1/L$ corrections, i.e. $\partial_x\theta(x) \sim 1/L$ for large $|x|$. Solutions to the mean-field equations of the form $\sqrt{n(x)}e^{i\theta_0(x)}$ exist in the literature where the phase is not periodic [86, 87] and have been applied to the 1D polaron before [56–58]. The non-periodic phase corresponds to unphysical sources at the boundary and leads to incorrect predictions, such as a negative kinematic polaron mass. To correct for this flaw, we make the ansatz $\varphi(x) = \tilde{\varphi}(x)e^{i\theta_1(x)}$, where θ_1 will correct the boundary conditions. As shown later, θ_1 will be of order x/L and therefore satisfies the condition of the condensate being approximately stationary at the boundary. After inserting this ansatz into (3.6) we find

$$\begin{aligned}
&\left(-\frac{1}{2m_\mathrm{red}}\partial_x^2 + g_\mathrm{BB}|\tilde{\varphi}(x)|^2 - \tilde{\mu} + i\tilde{u}\partial_x \right)\tilde{\varphi}(x) = 0\,,\\
&\partial_x\tilde{\varphi}(x)\Big|_{0-}^{0+} = 2m_\mathrm{red}g_\mathrm{IB}\tilde{\varphi}(0)\,,\\
&e^{i\theta_1 L}\tilde{\varphi}(L/2) = \tilde{\varphi}(-L/2)\,,
\end{aligned} \tag{3.8}$$

where we introduced the following definitions: $\tilde{\mu} = \mu + (\partial_x\theta_1)u/M + \mathcal{O}(1/L^2)$ and $\tilde{u} = u - (\partial_x\theta_1)/(m_\mathrm{r})$. Both additional terms are again of order $1/L$. The solution to those equations can be

found by inserting the ansatz into the mean-field equations and then first solving the arising second order differential equation for $\sqrt{n(x)}$. Using this result the phase can be determined, see [86, 87] for more details. The result is as follows; for the density we find

$$n(x) = \frac{\mu}{g_{\mathrm{BB}}}\Big(1 - \beta\,\mathrm{sech}^2\big(\sqrt{\beta/2}(|x| + x_0)/\tilde{\xi}\big)\Big)\,,$$

with $\beta = 1 - \frac{u^2}{\tilde{c}^2} + \mathcal{O}(1/L^2)$ and $\mu = g_{\mathrm{BB}} n_0^{\mathrm{MF}} - (\partial_x\theta_1)u + \mathcal{O}(1/L^2)$; where $\mathcal{O}(1/L^2)$ contributions will have no effect on any observables considered in this chapter. The phase is subsequently determined to be

$$\theta_0(x) = \begin{cases} f(x) & x > 0 \\ 2f(0) - f(-x) & x < 0 \end{cases}\,,$$
$$f(x) = \arctan\big(\frac{\sqrt{4u^2\beta/\tilde{c}^2}}{e^{\sqrt{2\beta}(x+x_0)/\tilde{\xi}} - 2\beta + 1}\big)\,, \tag{3.9}$$

If we consider the mean-field solution alone we determine the mean-field density to be

$$n_0^{\mathrm{MF}} = n_0(1 + 2\sqrt{2\beta}\tilde{\xi}/L(1 - \tanh\Big(\sqrt{\beta/2}x_0/\tilde{\xi}\Big))) + \mathcal{O}(1/L^2)\,, \tag{3.10}$$

where $n_0 = N/L$ is the average boson density. When considering quantum fluctuations later on, the mean-field density needs to be adjusted. The jump condition determines x_0 through a third order polynomial in $\alpha = \tanh\Big(\sqrt{\beta/2}x_0/\tilde{\xi}\Big)$

$$-\beta^{3/2}\alpha^3 - \frac{\beta\eta}{\sqrt{2}n_0\xi}\alpha^2 + \beta^{3/2}\alpha = \frac{\eta\beta}{\sqrt{2}n_0\tilde{\xi}}\,. \tag{3.11}$$

This equation has up to three solutions but only one solution is stable. In general, a solution only exists if the impurity velocity does not exceed a critical value. The critical value can be extracted

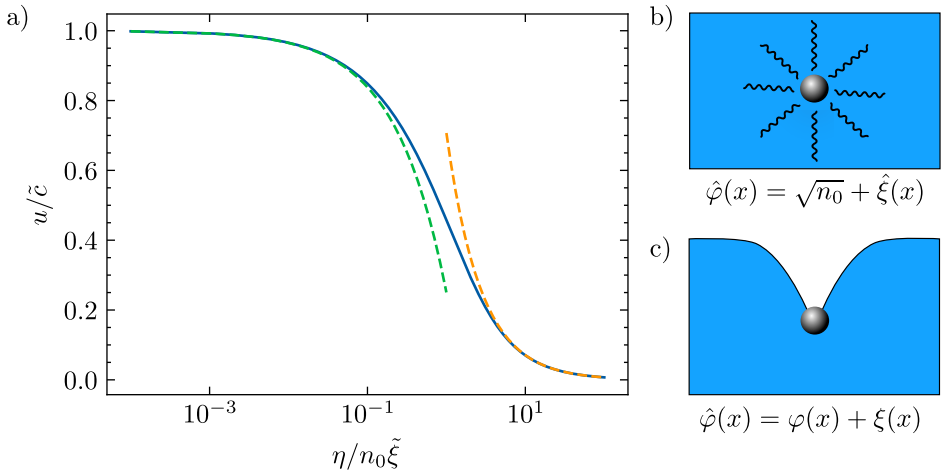

Figure 3.3: a) The critical velocity as a function of $\frac{\eta}{n_0\tilde{\xi}}$. The approximations are shown as dotted lines. It is clear that for weak and strong coupling, the approximations are in good agreement with the exact solution. b) In the (extended) Fröhlich model, one expands around the uniform condensate, and many phonons are excited in the strong coupling limit; thus, one has to take phonon-phonon interaction into account. c) When expanding around the deformed condensate, the influence of the phonons remains small, even for strong couplings. Figures b) and c) are based on [88].

from the jump condition [86] and is determined implicitly by

$$\frac{\eta}{n_0\tilde{\xi}} = 4(1-4(u/\tilde{c})^2)\frac{\left(\sqrt{1+8(u/\tilde{c})^2}-(1+2(u/\tilde{c})^2)\right)^{1/2}}{4(u/\tilde{c})^2-1+\sqrt{1+8(u/\tilde{c})^2}}\,. \tag{3.12}$$

For weak and strong coupling we can derive the approximations

$$u_c = \tilde{c}\begin{cases} 1-\frac{3}{4}\left(\frac{\eta}{n_0\tilde{\xi}}\right) & \eta \ll 1 \\ \frac{n_0\tilde{\xi}}{\sqrt{2}\eta} & \eta \gg 1 \end{cases}. \tag{3.13}$$

In Figure 3.3 we show the critical velocity as a function of the scaled coupling and the quality of the analytical approximation. Here we can see that for the limit $\eta \to 0$, the Fröhlich result for the critical velocity is recovered, with the only difference that c is replaced by $\tilde{c}$. This is a result of the LLP transformation. For strong couplings, the situation is vastly different. The critical velocity approaches 0, which can be explained by realising that in 1D, the condensate is entirely depleted around the impurity and is effectively split. The critical velocity approaching zero also shows that the polaron always becomes unstable at finite velocity for sufficiently large interactions in one

dimension, which is not observed in the (extended) Fröhlich model.

For finite momentum, the condition for x_0 has to be solved numerically but in the limit $u \to 0$ we find for $g_{\mathrm{IB}} > 0$: $x_0 = \frac{\tilde{\xi}}{\sqrt{2}} \log(y)$, with $y = \sqrt{1 + 8\frac{n_0^2\tilde{\xi}^2}{\eta^2}} + 2\frac{\sqrt{2}n_0\tilde{\xi}}{\eta}$. Lastly, we fix $\theta_1(x)$ to ensure the periodicity of the phase by

$$\theta_1(x) = 2\left[f(0) - f(L/2)\right]\frac{x}{L}\,. \tag{3.14}$$

The $1/L$ corrections are indeed important when calculating physical quantities. This can be seen by considering the boson momentum

$$P_{\mathrm{B}} = \int n(x)\partial_x\theta(x)\,\mathrm{d}x = \int n(x)\partial_x\theta_0(x)\,\mathrm{d}x + n_0\left[2(f(0) - f(L/2)\right]\,. \tag{3.15}$$

Interestingly, one can use the same solutions on the attractive side ($g_{\mathrm{IB}} < 0$). Here, we find $x_0 \to x_0^{\mathrm{a}} = x_0 + i\pi/2\tilde{\xi}(2/\beta)^{1/2}$. It is instructive to insert the attractive solution x_0^{a} into (3.9) and obtain the density profile for the attractive side explicitly

$$n^a(x) = \frac{\mu}{g_{\mathrm{BB}}}\Big(1 + \beta\,\mathrm{csch}^2\big(\sqrt{\beta/2}(|x| + x_0)/\tilde{\xi}\big)\Big)\,. \tag{3.16}$$

It becomes apparent that the density far away from the impurity is now lowered instead of increased, and is given by $n_0^{\mathrm{MFa}} = n_0(1 - 2\sqrt{2\beta}\tilde{\xi}/L(\coth\Big(\sqrt{\beta/2}x_0/\tilde{\xi}\Big) - 1)) + \mathcal{O}(1/L^2)$. This seemingly small correction can have a profound impact for $|\eta| \gg 1$. In this limiting case $\coth\Big(\sqrt{\beta/2}x_0/\tilde{\xi}\Big)$ diverges and a microscopically large amount of the bosons aggregates around the impurity. For a finite system, this signals a collapse of the condensate onto the impurity. This violates the assumption of a dilute gas around the impurity, which is required to ensure the validity of the mean-field treatment. Due to those effects, we restrict our analysis of the attractive side to moderate values of $|g_{\mathrm{IB}}|$.

In Figure 3.2 and Figure 3.4, mean-field predictions for condensate density and phase are shown for different repulsive and attractive values of the interaction strength and a slowly moving impurity. From the analytical solution, we can derive a parameter characterising the relative condensate

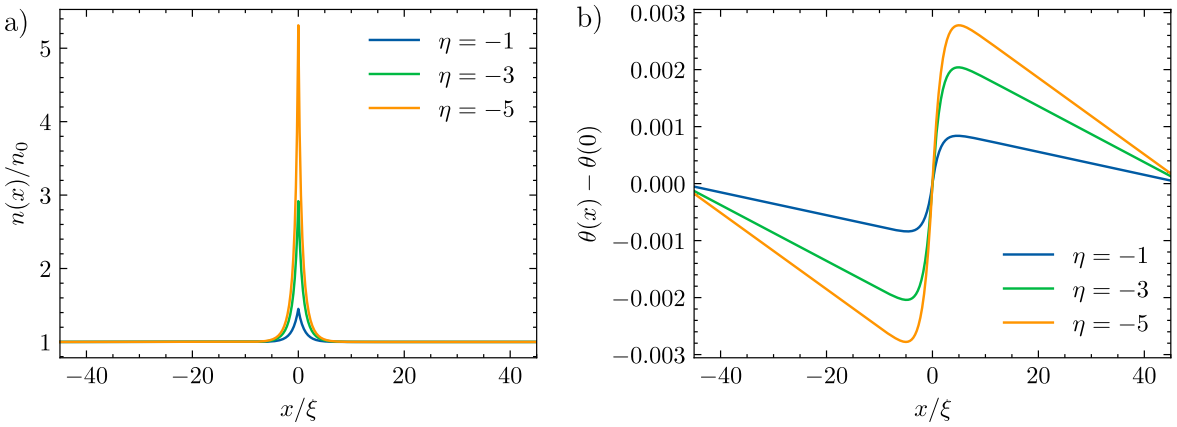

Figure 3.4: Mean-field a) density and b) phase for various attractive couplings. All other parameters are as in [22], i.e. $M/m = 0.47$, the peak density $n_0 = 7/\mu\mathrm{m}$ and $g_{\mathrm{BB}} = 2.36 \times 10^{-37}\mathrm{Jm}$. For the phase we fixed $u = 0.01c$, which fixes the total momentum on the mean-field level.

deformation

$$\eta/n_0\overline{\xi} = \eta\sqrt{2\overline{\gamma}}, \tag{3.17}$$

with $\overline{\gamma} = \gamma m_r/m$. Here,

$$\gamma = 1/(2n_0^2\xi^2)\,, \tag{3.18}$$

is the Tonks parameter of the 1D Bose gas [79, 89], which should be less than unity for the Bogoliubov approximation to hold. The deformation becomes sizable if $\eta/n_0\overline{\xi} \sim 1$.

Energy and effective mass on the mean-field level

With the analytical expressions for the condensate density and phase we can calculate the polaron energy from

$$E_{\mathrm{p}} = E(g_{\mathrm{IB}}) - E(g_{\mathrm{IB}} = 0)\,, \tag{3.19}$$

and the effective mass m^* of the polaron using (2.45)

$$M/m^* = \lim_{p\to 0}\left(1 - \frac{P_{\mathrm{B}}}{p}\right)\,, \tag{3.20}$$

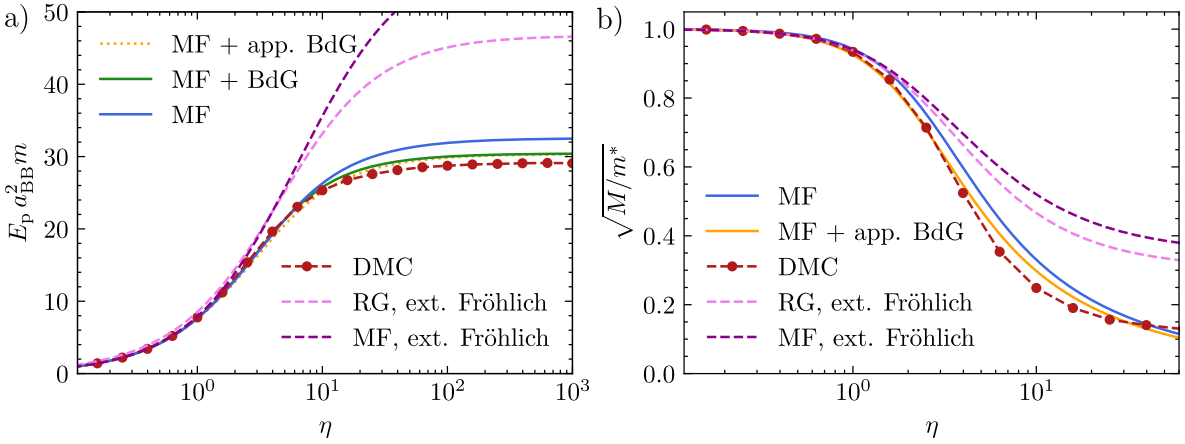

Figure 3.5: Polaron a) energy and b) effective mass for the repulsive polaron. The curves are obtained using different theoretical methods; all parameters are as in [22], where $\gamma \approx 0.438$. The DMC, RG and MF (both based on the extended Fröhlich model) curves were calculated in [37]. We find exceptional agreement with the DMC results for the energy and the effective mass when expanding around the right mean-field solutions and including quantum fluctuations. Only for the very strong coupling regime, we do not predict a saturation of the effective mass. We explain this deviation from DMC results by noting that the DMC curves are obtained for a finite number of bosons. Therefore the total mass of the system is finite and possesses an upper bound for the effective mass. The condensate deformation becomes relevant for $\eta/n_0\bar{\xi} > 1$ (3.17), corresponding here to $\eta > 1.9$, where predictions from the ext. Fröhlich model start to deviate from the full model.

with P_B being the mean-field momentum of the condensate. This yields

$$E_p^{r,a} = g_{IB} n_0 \left(\frac{|y| \mp 1}{|y| \pm 1} \right)^2 + \frac{8}{3} n_0 \tilde{c} \left(\frac{3|y| \pm 1}{(|y| \pm 1)^3} \right), \tag{3.21}$$

for the energies of the repulsive ($E_p^{(r)}$, upper sign) and attractive ($E_p^{(a)}$, lower sign) polaron, and for the mass:

$$\frac{M}{m^*} = \frac{M(y^2-1)}{8 n_0 \tilde{\xi} m_r \sqrt{2} + M(y^2-1)}. \tag{3.22}$$

These expressions agree with previous findings in [56] and [58]. It is interesting that for $\eta \to \infty$, (3.21) approaches the energy of a dark soliton, and the effective mass m^* goes to infinity which is in contrast to results obtained from the extended Fröhlich Hamiltonian [37]. The explanation for this is quite intuitive; in one dimension, the impurity splits the condensate for $\eta \to \infty$, and thus the impurity has to push an infinite (in the thermodynamic limit) number of bosons away to move. The previously mentioned collapse of the condensate to a multi particle-bound state on the attractive side for $\eta \gg 1$, can also be seen by noting that $E_p^a \to -\infty$ for $\eta \to -\infty$.

3.4 Boundary conditions

This subsection addresses the importance of periodic boundary conditions for correctly calculating the effective mass. When imposing periodic boundary conditions, one finds a constant density far away from the impurity, as expected. Nevertheless, the phase is linearly changing at the order of $1/L$ and is, therefore, not constant. One might be tempted to use a solution where both density and phase are truly constant, far away from the impurity (up to exponentially small corrections). A solution with this different boundary condition would still be given by the mean-field solution stated above with $\theta_1(x) = 0$. The effective mass can then be deduced from the wave function in the same manner as was done for periodic boundary conditions. Calculating the effective mass this way, one finds that the effective mass decreases for increasing η, and it can even become negative. This unphysical result is in disagreement with DMC results. In addition, it also contains a phase jump at infinity, which introduces a nonsensical source term there. Addressing this issue from a more technical perspective, it becomes clear that, functional derivatives cannot be taken for constant-phase solutions. On a mean-field level, this can be alleviated by modifying the functional derivatives by exactly this source term, as has been done in the context of solitons [90, 91]. Another possible way to deal with the phase problem is to integrate the phase as done in prior work [58]. Upon considering quantum fluctuations in addition to the mean-field solution, none of the methods mentioned above allow a straightforward generalisation. We found expanding about a periodic mean-field solution to be indispensable for the Bogoliubov theory and note that this issue persists when extracting the mass from the total momentum dependence of the mean-field energy of the system. When enforcing the non-periodic phase and expanding the total mean-field energy to quadratic order in the total momentum as $E \approx E_0 + \frac{p^2}{2m^*}$, one obtains an incorrect result for the polaron mass m^*. On the other hand, when extracting the polaron mass from expanding in u as $E \approx E_0 + \frac{1}{2}m^*u^2$ one fortuitously obtains the correct result with both periodic and non-periodic [57] mean-field solutions. These difficulties can be attributed to the fact that the mean-field equations of motion do not form a Hamiltonian system, unless the phase correction is applied. For the full quantum system, one can

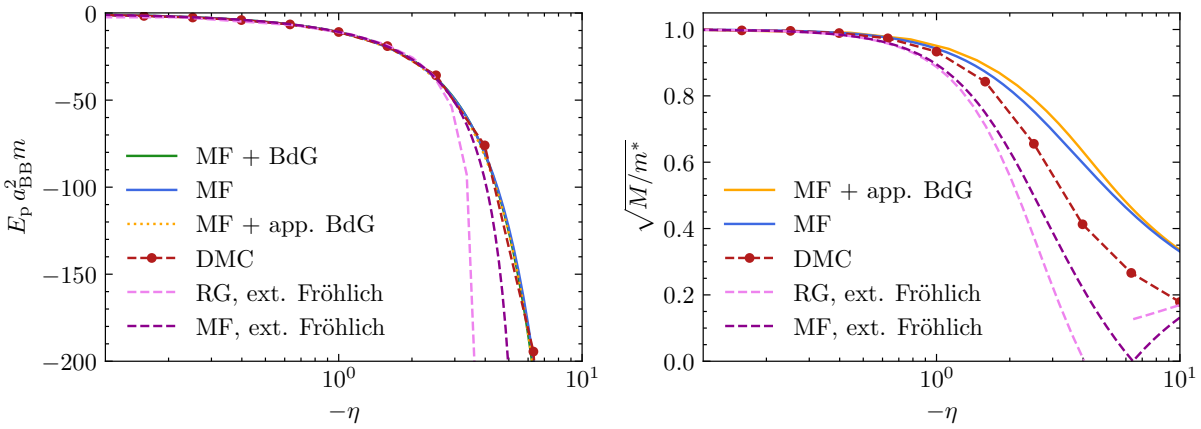

Figure 3.6: Polaron a) energy and mass b) calculated using different methods for attractive impurity couplings. All parameters are as in [22], and the RG, MF (based on the extended Fröhlich model), and DMC curves were calculated in [37]. A surprisingly good agreement is achieved with the DMC results for the polaron energy, while the agreement is less good for the mass. We explain this by the collapse of the solution to a multi-particle bound state, where we do not expect the mean-field solution to be a good approximation. Furthermore, we do not observe the transition from the attractive to the repulsive polaron observed in the Fröhlich model, signalled by the breakdown of the RG treatment. For more details on this transition, we refer to [37, 38].

deduce that the fundamental relation

$$\frac{dE}{dp} = u \tag{3.23}$$

holds exactly by the Feynman-Hellman theorem [92]. Incidentally, this relation can be used to obtain $M/m^* = \lim_{p\to 0}(1 - \frac{P_{\mathrm{B}}}{p})$ which, as described in section 2.1, is used, to compute the polaron mass. With periodic boundary conditions, one retains the exact relation (3.23) within the mean-field theory. On the other hand, when the non-periodic solution is used a short calculation gives the relation

$$\frac{dE_{\mathrm{np}}}{dp} = u - u\bar{n}\frac{d}{dp}\Delta\theta\ , \tag{3.24}$$

where E_{np} is the total mean-field energy of the non-periodic state, $\bar{n}$ is the average density, and $\Delta\theta$ is the phase change across the condensate.

3.5 Quantum fluctuations

The following paragraph will outline how one can calculate the first-order quantum corrections using a generalised Bogoliubov transformation. After expanding the fields in $\hat{\mathcal{H}}^{\mathrm{S}}_{\mathrm{LLP}}$ in the quantum fluctuations we find up to second order in $\hat{\xi}^\dagger(\mathbf{r})$ and $\delta\hat{u}$

$$\begin{aligned}\hat{\mathcal{H}}^{\mathrm{S}}_{\mathrm{LLP}} = \int \mathrm{d}x \Bigg[\hat{\xi}^\dagger(x)\Big(-\frac{1}{2m_{\mathrm{r}}}\partial_x^2 + 2g_{\mathrm{BB}}|\varphi(x)|^2 - \mu + g_{\mathrm{IB}}\delta(x) + iu\partial_x\Big)\hat{\xi}(x) \\ + \frac{g_{\mathrm{BB}}}{2}\Big(\varphi(x)^2\hat{\xi}^\dagger(x)^2 + \mathrm{h.c.}\Big)\Bigg] - i\delta\hat{u}\int \mathrm{d}x\Big(\hat{\xi}^\dagger(x)\partial_x\varphi(x) + \varphi^*(x)\partial_x\hat{\xi}(x)\Big) - \frac{1}{2}M\delta\hat{u}^2\,,\end{aligned} \tag{3.25}$$

where the correction to the impurity velocity is given by

$$M\delta\hat{u} = -i\int \left[\varphi^*(x)\partial_x\hat{\xi}(x) + \hat{\xi}^\dagger(x)\partial_x\varphi(x)\right]\mathrm{d}x + \mathcal{O}(\hat{\xi}(x)^2)\,. \tag{3.26}$$

The quadratic Hamiltonian (3.25) can be diagonalised by a Bogoliubov rotation to a generalised basis of phonons on a deformed background. For distances far from the impurity, i.e. $|x| \to \infty$, these phonons look like the ones of a homogeneous BEC. This allows us to extract the quantum depletion.[1] For the quantum-corrected density far away from the impurity, we find

$$n_0 = n_0^{\mathrm{MF}} + \frac{1}{\pi}\sqrt{m_{\mathrm{r}}g_{\mathrm{BB}}n_0^{\mathrm{MF}}}\,. \tag{3.27}$$

Thus we have to adjust the mean-field density accordingly. To diagonalise (3.25) we observe that all terms involving $\delta\hat{u}$ become non local and thus difficult to handle in general, except for the special case $p = 0$. This enables us to diagonalise (3.25) and to calculate the polaron energy for $p = 0$ without further approximations. For a moving impurity we introduce an approximation setting $\delta\hat{u} = 0$ and keep u as variational parameter in the mean-field equations. After diagonalising the remaining quadratic Hamiltonian (3.25) u is determined selfconsistently by

$$Mu \;=\; p - \langle\hat{P}_{\mathrm{B}}\rangle\,, \tag{3.28}$$

[1] See [55] for a detailed discussion on how to regularise the arising UV-divergences of the zero-point energy.

$$\langle \hat{P}_{\mathrm{B}} \rangle \;\; = \;\; -i \int \varphi^*(x) \partial_x \varphi(x) \, \mathrm{d}x - i \langle \int \hat{\xi}^\dagger(x) \partial_x \hat{\xi}(x) \, \mathrm{d}x \rangle \, ,$$

where the expectation value is taken with respect to the phonon vacuum.

Numerical details

We now discuss the numerical details of the method used to obtain the quantum corrections to the mean-field solutions. An extensive overview of the techniques used here can be found in [93]. We note that this is equivalent to solving the resulting Bogolibouv-de Gennes equations. We start by discretising $\hat{\mathcal{H}}^{\mathrm{S}}_{\mathrm{LLP}}$ after either making the approximation of treating u as a variational parameter or for $p = 0$ after integrating out the $\hat{u}$-field. For all numerical results presented here, the discretisation was done in real space and is therefore straightforward apart from the delta distribution, which was approximated by a Kronecker delta as $\delta(x) \to \delta_{i,0}/a$, where a is the discretisation spacing. Discretising in real space comes at the expense of not accounting correctly for the UV behaviour. The deviation from the continuum UV behavior is due to discretising the derivative operators. Nevertheless, for the observables we are interested in, the UV behaviour is not essential, and we found fast convergence; thus, the diagonalisation in real space is justified. For notational convenience, we omit the hats on all discretised operators. The discretised Hamiltonian can be written as

$$H^{\mathrm{S}}_{\mathrm{LLP}} = \sum_{ij} \left[A_{ij} \varphi_i^\dagger \varphi_j + \frac{1}{2} (B_{ij} \varphi_i^\dagger \varphi_j^\dagger + B^*_{ij} \varphi_i \varphi_j) \right] = \frac{1}{2} \mathbf{\Phi}^\dagger M \mathbf{\Phi} - \frac{1}{2} \mathrm{Tr}(A) \, , \tag{3.29}$$

where $\mathbf{\Phi}^\dagger = [\varphi_1^\dagger, \varphi_2^\dagger, ...\varphi_n^\dagger, \varphi_1, \varphi_2, ...\varphi_n]$ is the discrete version of $\hat{\xi}(x)$ and M is the semi positive definite matrix

$$M = \begin{bmatrix} A & B \\ B^* & A^* \end{bmatrix} \, . \tag{3.30}$$

We emphasise that the trace term is of fundamental importance in 1D since it renders results like the zero-point energy finite without performing additional regularisation. Following the steps outlined

in [93], we now diagonalise

$$\nu M = \begin{bmatrix} A & B \\ -B^* & -A^* \end{bmatrix}, \tag{3.31}$$

and thus find T such that

$$T^\dagger M T = \mathrm{diag}(\omega_1, \omega_2, ..., \omega_n, \omega_1, \omega_2, ..., \omega_n)\,, \tag{3.32}$$

while guaranteeing $T^\dagger \nu T = \nu$, which allows us to introduce new bosonic operators $\mathbf{\Psi}^\dagger = [b_1^\dagger, b_2^\dagger, ...b_n^\dagger, b_1, b_2, ...b_n]$ through

$$\mathbf{\Phi} = T\mathbf{\Psi}\,, \tag{3.33}$$

for which the Hamiltonian takes diagonal form. The new operators b_i can be interpreted as quasiparticle-like bosonic excitations with eigenenergy ω_i. For a stable polaron the energy of those excitations is minimised, i.e. the system is in its vacuum state $|0\rangle$ with respect to the b_i. From here it is then easy to verify that the quantum corrections to the expectation value of an observable of the form $O_\mathrm{Q} = \sum_{ij} O_{ij}\varphi_i^\dagger \varphi_j$ is given by

$$\langle O_\mathrm{Q}\rangle = \langle 0|\mathbf{\Psi}^\dagger T^\dagger \begin{bmatrix} O & 0 \\ 0 & 0 \end{bmatrix} T\mathbf{\Psi}|0\rangle = \langle 0|\mathbf{\Psi}^\dagger \begin{bmatrix} C & D \\ E & F \end{bmatrix} \mathbf{\Psi}|0\rangle = \mathrm{Tr}(F)\,. \tag{3.34}$$

To conclude this section, we will comment on the IR (infrared) divergences which are characteristic in 1D systems and how they are dealt with here. First, we note that quantities like the two-point function

$$\langle \varphi_i^\dagger \varphi_i\rangle = \langle 0|(\mathbf{\Psi}^\dagger T^\dagger)_i (T\mathbf{\Psi})_i|0\rangle \sim L\,, \tag{3.35}$$

are indeed IR divergent in our treatment. For the global quantities at zero total momentum, i.e. $p = 0$, this divergence can be regularised by considering the zero-point energy

$$E = \frac{1}{2}(\sum_i \omega_i - \mathrm{Tr}(A))\,, \tag{3.36}$$

which is UV and IR finite and then taking adequate derivatives.[2] When considering $\hat{\mathcal{H}}^{\mathrm{S}}_{\mathrm{LLP}}$ for $p \neq 0$ without any approximations, the phonon momentum seems to be IR divergent, and also for the polaron energy, we found a system size dependence. Lastly, we remark that the phonon momentum remains IR and UV finite in the approximate treatment, i.e., when viewing u as a variational parameter. Therefore, we conclude that all results presented are cutoff independent, and no divergences occur. It is then possible to calculate the effective mass, including quantum corrections from

$$M/m^* = Mu/p. \tag{3.37}$$

As can be seen in Figure 3.5, where the energies of the full and approximate solution of the BdG equations are shown, the approximate treatment of the Hubbard-Stratonovich field yields very good results.

3.6 Discussion & summary

Figure 3.5 shows that the mean-field solution significantly improves the agreement with DMC simulations for $g_{\mathrm{IB}} > 0$ as compared to the Fröhlich model. Including quantum fluctuations leads to an almost perfect agreement for the energy. We find however that the effective mass diverges for $g_{\mathrm{IB}} \to \infty$, even after including quantum fluctuations, which seems to be in contrast to the DMC results [37], but can be explained by noting that in the DMC calculation, the number of particles is limited and therefore the effective mass cannot exceed the total mass of the system. This divergence is a characteristic of the 1D geometry and is, for example, also observed in the Tonks limit [50]. One would naively expect this to happen since, for $\eta \gg 1$, the condensate is split into two halves by the impurity, preventing any transport of the condensate across it. The only possible contribution could come from tunnelling, which is highly suppressed for $\eta \gg 1$. The same reasoning addresses why the quantum correction to the effective mass is most significant for intermediate couplings. Here, the classical current is reduced by the substantial condensate deformation, but tunnelling

[2] E.g., with respect to the chemical potential for the depletion.

is still relevant. Note that these arguments rely on treating the system as one dimensional. For experimental systems in the one-dimensional regime, we expect that transverse modes may become influential for the limiting behaviour of M/m^*. This analysis has to be done on a case-by-case basis, and we want to stress that all our calculations are benchmarked against strict 1D numerical quantum Monte Carlo results. For a detailed discussion on the influence of the transverse mode and when it is permissible to treat the system investigated in [22] as strictly one-dimensional, we refer to [37]. Another quantity of experimental relevance [22] is the axial width of the polaron $\left(\langle \hat{X}^2 \rangle - \langle \hat{X} \rangle^2\right)^{1/2}$. In the present work, which is carried out in the LLP frame and requires translational invariance, such a quantity is infinite. Including a trapping potential for the impurity is beyond the scope of the present work but could be addressed by using a variational ansatz that is a superposition of ground states (of the infinite system) with different total momenta. On the other hand, studies that do not invoke the LLP transformation can lead to symmetry-broken mean-field states with finite values of the axial width [81, 82] even without a trap, but these typically neglect impurity-condensate entanglement.

In summary, we have shown that a non-perturbative description of the Bose polaron in 1D requires taking into account the boson-boson interaction on the condensate level itself, while keeping the impurity-condensate entanglement. Since the density of phonons defined on such a deformed background remains small, their intrinsic interactions can be neglected to good approximation. Our approach provides a quantitatively accurate and, to a large extent, analytical description of Bose polarons even for strong impurity-boson interactions as long as the Tonks parameter remains small. Those findings suggest that a similar method could be used to gain more insight into the polaron formation following a sudden quench. A possible way to address this will be presented in the next chapter. We expect that the adoption of the presented method will enable for an accurate description in 3D at and beyond the critical strength of the impurity-boson interaction for self-trapping.

CHAPTER 4

Stochastic-field approach to the quench dynamics of the one-dimensional Bose polaron

The following chapter is based on [JJ2] with some verbatim textual overlap.

Introduction

After achieving remarkable accuracy for the equilibrium treatment, it is natural to utilise an approach based on a mean-field treatment of the full system paired with first-order quantum corrections to study out of equilibrium settings and investigate the polaron formation. In the following chapter, we thus consider interaction quench dynamics involving the abrupt immersion of an impurity into a homogeneous, finite temperature Bose gas. The interaction quench is schematically depicted in Figure 4.1. Experimentally, such an interaction quench can be realised through a Feshbach resonant radio-frequency pulse [21] that switches on the impurity-superfluid interaction nearly instantaneously. Said quench dynamics have been extensively studied. But previous treatments largely focused either on zero temperature or still rely on the (extended) Fröhlich model (or very similar approximations) [38, 48, 53, 57, 66, 94–102]. In many of the equilibrium and some of the out of equilibrium treatments, the LLP transformation [8], which eliminates the impurity from the problem at the expense of adding an additional quartic vertex, has proven extremely useful [37, 53, 63, 69]. However, using the LLP transformation requires further approximations when considering finite temperature [66].

While the vast majority of the existing literature has focused on three-dimensional systems,

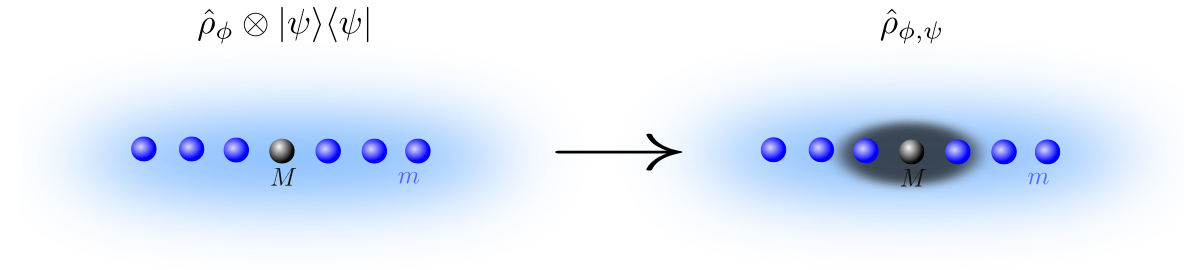

Figure 4.1: Illustration of the interaction quench. The system starts in a product state, where we assume that the impurity is in a pure state, and the density matrix of the Bose gas is given according to its thermal distribution. After the quench, the system becomes entangled and cannot be described by a product of density matrices anymore. In general, the time evolution of the full density matrix is out of reach. We will show how the time evolution (up to one loop accuracy) can be mapped to partial differential equations with stochastic initial conditions.

where the (extended) Fröhlich model is widely applicable, in 1D, the situation is different. In [37] it was shown that the applicability of Fröhlich-type approximations are somewhat limited in 1D and while the mass balanced case is integrable for the Fermi gas [103] no such limit exists in the case of a Bose gas. Instead, it is natural to incorporate the effects of the impurity on the condensate already at the mean-field level. The previous chapter outlined how this can be done efficiently for a single impurity at zero temperature. Still, this method does not extend to several impurities, and it can not be generalised to finite temperatures in a straightforward manner. Several approaches do not eliminate the impurity from the problem to circumvent those complications. Additionally, they can address finite temperature [11, 48], and for example, treat the impurity in a manner related to the coherent state representation of the impurity [82]. However, they rely on a product wavefunction and it has been shown in [JJ1], [57, 104] that a product wave function within the tree-level approximation yields inconsistent results compared with those obtained in the more accurate LLP-frame in 1D. Therefore, it is perhaps more appropriate to treat the impurity in a position-momentum path integral as it highlights the particle nature of the impurity. Using the coherent state path integral for the condensate has been shown to yield good results in 1D not only for the polaron but also for the bipolaron problem [57, 58, 88]. This is conceptually close to the approach developed initially by Feynman [11] and applied to the Bose polaron in [35, 45], with the main difference, that we do not expand the condensate around a homogeneous density, and our focus lies on out of equilibrium phenomena. In this section, we develop a conceptually

simple and numerically tractable approach to address quench dynamics at finite temperatures in a general manner. Ultimately, this is achieved by mapping the dynamics to a set of deterministic differential equations with stochastic initial conditions. By averaging the different trajectories, expectation values can be calculated with one-loop accuracy. We then use this methodology to study an impurity's temporal evolution after a sudden interaction quench into the bath. We find that the impurity delocalises quickly for weak impurity-bath couplings and that observables like the velocity of the impurity crucially depend on incorporating quantum and thermal effects. In the case of strong impurity-bath couplings, we observe self-trapping, while thermal effects and quantum corrections are considerably less pronounced.

This chapter is organised as follows. We start by discussing the truncated Wigner approximation for the problem at hand.[1] We also show how to obtain the absorption spectrum in the language of semi-classical dynamics. We proceed by specifying the initial Wigner function and show how to regularise the divergences that arise in the one-dimensional setting. After that, we briefly outline the numerical considerations and discuss the validity of the proposed method. To conclude, we discuss the results for an impurity at rest and finite initial momentum and outline further directions.

4.1 The Keldysh formalism for the Bose polaron

In this section, we discuss the equations of motion arising from applying the truncated Wigner approximation. We start by considering the one-dimensional version of (2.1) for a single impurity

$$\hat{\mathcal{H}} = \frac{\hat{P}^2}{2M} + \int_x \left\{ \hat{\varphi}^\dagger(x) \Big[\frac{-\partial_x^2}{2m} + \frac{g_{\mathrm{BB}}}{2} \hat{\varphi}^\dagger(x)\hat{\varphi}(x) + g_{\mathrm{IB}} V\left(x - \hat{X}\right) \Big] \hat{\varphi}(x) \right\}, \tag{4.1}$$

In contrast to the previous section, we have left the interaction potential between the impurity and the condensate general instead of directly assuming a contact potential. We will not employ a delta function here but a smoothed-out version for numerical reasons that will be discussed later. In the following, we are going to apply the Kedlysh formalism to (4.1). As discussed for a general setting

[1] For more details on the path integral, we refer to section 2.2.

in section 2.2 the expectation value of an arbitrary observable is given by

$$\langle\Omega(\hat{X},\hat{P},\hat{\varphi}^\dagger(x),\hat{\varphi}(x)),t)\rangle = \int_{X_0,P_0,\varphi_0(x),\varphi_0^*(x)} W(X_0,P_0,\varphi_0(x),\varphi_0^*(x)) \int \mathcal{D}[X_c(\tau),X_q(\tau), \tag{4.2}$$

$$P_c(\tau),P_q(\tau),\varphi_q(x,\tau),\varphi_c(x,\tau),\varphi_q^*(x,\tau),\varphi_c^*(x,\tau)]\exp\big(iS[X_c(\tau),X_q(\tau),P_q(\tau),P_c(\tau),$$
$$\varphi_q(x,\tau),\varphi_c(x,\tau),\varphi_q^*(x,\tau),\varphi_c^*(x,\tau)]\big)\,\Omega_W(X_c(t),P_c(t),\varphi_c^*(x,t),\varphi_c(x,t),t)\,,$$

where W is the Wigner function that depends on the initial density matrix and will be specified below. Here, $\Omega_W(X_c(t),P_c(t),\varphi_c^*(x,t),\varphi_c(x,t),t)$ is the Weyl ordered operator of the observable of interest.[2] The subscript c denotes the classical field and the subscript q the quantum field, which describes the quantum fluctuation around the classical saddle point solution. As discussed in section 2.2 those two fields arise when mixing forward and backward contour in the Keldysh formalism. The $\mathcal{D}$ denotes the integration over all field configurations in space and time. While the integration over the initial configuration of the fields is to be understood as an integration at every point in space. The integral over the initial momentum and space configuration of the impurity in (4.2) can be understood as normal integrals in X_0 and P_0.

As discussed in detail in section 2.2, the semi-classical approximation is to drop all terms of order two and higher in $\hbar$, corresponding to an expansion up to second order in the quantum fields. As is characteristic for the truncated Wigner approximation, we find that there are, in fact, only terms linear in the quantum fields, and the action is given by

$$\begin{aligned} S = \int_\tau \Bigg\{ \Big[-X_q(\tau)\frac{\mathrm{d}}{\mathrm{d}\tau}P_c(\tau) + P_q(\tau)\frac{\mathrm{d}}{\mathrm{d}\tau}X_c(\tau) - \frac{P_q(\tau)P_c(\tau)}{M}\Big] - \int_x \Big[(\varphi_c^*(x,\tau)\big[-i\partial_\tau \\ -\frac{\partial_x^2}{2m} + g_{\mathrm{BB}}|\varphi_c(x,\tau)|^2 + g_{\mathrm{IB}}V(X_c(\tau)-x)\big]\varphi_q(x,\tau) + \mathrm{c.c.}) \\ +g_{\mathrm{IB}}\frac{\mathrm{d}}{\mathrm{dx}}V(x-X_c(\tau))X_q(\tau)|\varphi_c(x,\tau)|^2\Big]\Bigg\}\,. \end{aligned} \tag{4.3}$$

In line with the derivation in section 2.2 it is now easy to see that all the quantum fields can be easily

[2] See [70] for more details on operator ordering.

integrated out and yield functional delta distributions enforcing the following classical equations of motion

$$\frac{\mathrm{d}}{\mathrm{d}\tau}X_c(\tau) = \frac{P_c(\tau)}{M}\,, \tag{4.4}$$

$$\frac{\mathrm{d}}{\mathrm{d}\tau}P_c(\tau) = g_{\mathrm{IB}}\int_x \frac{\mathrm{d}}{\mathrm{dx}}V(x - X_c(\tau))|\varphi_c(x,\tau)|^2\,, \tag{4.5}$$

$$i\partial_\tau\varphi_c(x,\tau) = \left(\frac{-\partial_x^2}{2m} + g_{\mathrm{BB}}|\varphi_c(x,\tau)|^2 + g_{\mathrm{IB}}V\left(X_c(\tau) - x\right)\right)\varphi_c(x,\tau)\,. \tag{4.6}$$

The only challenge remaining at this point is to integrate over the initial conditions weighted by the Wigner function. In the case considered here the Wigner function will turn out to be a probability distribution, Consequently, this can be achieved by sampling the initial conditions according to the Wigner function, solving the classical equations of motion and then averaging the desired observable over the calculated trajectories. Within the outlined framework it is now straightforward to calculate the impurity dynamics. Another quantity of great interest is the impurity Green's function [33, 38, 66, 103, 105], from which the absorption spectrum can be calculated by taking the Fourier transformation. The impurity Green's function is defined by

$$G(t) = \mathrm{Tr}\left\{\exp\left(i\hat{H}_0 t\right)\hat{\rho}\exp\left(-i\hat{H}t\right)\right\}\,, \tag{4.7}$$

where $\hat{H}_0$ stands for (4.1) with $V(x-\hat{X}) = 0$ and $\hat{\rho}$ is the initial density matrix. We now observe that this has the same structure as the trace that is considered to derive the Keldysh path integral, with the only difference, that the forward and backward contour differ by an extra interaction term. We can therefore proceed in a similar fashion to the derivation of (4.2). The only difference in S is the resulting impurity-boson interaction

$$S_{\mathrm{int}} = \int_{\tau,x}\Bigg[\left(\varphi_c^*(x,\tau)\big[\frac{1}{2}g_{\mathrm{IB}}V^{(n)}(\tilde{x})\big]\varphi_q(x,\tau) + \mathrm{c.c.}\right) + X_q(\tau)\frac{g_{\mathrm{IB}}}{2}V^{(1)}(\tilde{x})|\varphi_c(x,\tau)|^2 \tag{4.8}$$

$$X_q(\tau) + g_{\mathrm{IB}}V(\tilde{x})(|\varphi_c(x,\tau)|^2 + \frac{|\varphi_q(x,\tau)|^2}{4}) + \frac{g_{\mathrm{IB}}}{8}|\varphi_c(x,\tau)|^2V^{(2)}(\tilde{x})X_q(\tau)^2\Bigg]\,,$$

where we have introduced the shorthand notation $\frac{\mathrm{d^n}}{\mathrm{dx^n}}V(x - X_c(\tau)) = V^{(n)}(\tilde{x})$. Compared with

(4.4), a factor of $1/2$ changes the resulting magnitude of the interaction, and a new purely classical term arises. Lastly, we observe that there is also a quadratic term in $\varphi_q(x,\tau)$ and $X_q(\tau)$ now. This term has to be considered if we want to keep the accuracy up to one-loop order, which complicates matters. An ad hoc approximation is to drop this term altogether and therefore stay in a strictly semi-classical regime. To see when this approximation is justified, one can compare the arsing terms and their order of magnitude. We note, that the $|\varphi_q(x,\tau)|^2$ term directly competes with the $|\varphi_c(x,\tau)|^2$ term. As long as one is within the applicability region of a general c-field treatment, $|\varphi_q(x,\tau)|^2$ will be small compared to $|\varphi_c(x,\tau)|^2$ whenever the condensate deformation is not large. This corresponds to small and intermediate η. For the corrections in the impurity degrees of freedom one has to compare $\frac{g_{\mathrm{IB}}}{2}V^1(\tilde{x})|\varphi_c(x,\tau)|^2$ with $V^{(2)}(\tilde{x})X_q(\tau)^2|\varphi_c(x,\tau)|^2$. We note that the derivative terms can be brought onto the bosonic field variables through partial integration. One then realises that the second derivative of the fields will be small compared to the first derivative for weak coupling. Additionally, for large impurity masses M, the magnitude of X_q will stay small. Those two considerations show that one would expect the absorption spectrum to yield reliable results for weak to intermediate impurity-boson coupling and potentially a more comprehensive range of couplings if the impurity is sufficiently heavy. We refer to section 4.3 for more details on the validity of the approach presented here.

We also stress that this approximation is only made when calculating the absorption spectrum and the impurity Green's function, and all dynamical results do not rely on this approximation. Henceforth, the additional stochastic term will be dropped. This leaves us with the expression

$$G(t) = \langle \exp\left(i \int_{\tau,x} g_{\mathrm{IB}} V(X_c(\tau) - x)|\varphi_c(x,\tau)|^2 \right) \rangle_W \ , \tag{4.9}$$

where we denote the average with respect to the initial Wigner function as $\langle ... \rangle_W$. We are now in the position to calculate the real space trajectories of the impurities for finite temperature as well as the absorption spectrum.

Connection to the equilibrium case

Before proceeding we would like to make some remarks about the classical equations of motion and connect them to the equilibrium case, discussed in the previous chapter, to show that even without taking the first-order correction into account those equations give satisfactory results in the limiting case of heavy impurities. For the equilibrium case we assume the impurity to travel at constant velocity $\frac{\mathrm{d}}{\mathrm{d}\tau}X_c(\tau) = v$, implying $\frac{\mathrm{d}}{\mathrm{d}\tau}P_c(\tau) = 0$, which in turn tells us that $|\varphi_c(x,\tau)|^2$ is symmetric around the impurity position. Together with the equilibrium assumption this directly leads to the conclusion that the bosonic field takes the following form $\varphi_c(x,\tau) = \varphi_c(x - v\tau) = \varphi_c(x - X_c(\tau))$. In the equilibrium setting we consequently find $i\partial_\tau\varphi_c(x,\tau) = -iv\partial_x\varphi_c(x - X_c(\tau))$. Combining these observations and defining $\tilde{x} = x - X_c(\tau)$ we find the equilibrium equation

$$\left(\frac{-\partial_{\tilde{x}^2}}{2m} + g_{\mathrm{BB}}|\varphi_c(\tilde{x})|^2 + iv\partial_{\tilde{x}} + g_{\mathrm{IB}}V(\tilde{x})\right)\varphi_c(\tilde{x}) = 0\,. \tag{4.10}$$

We can now compare this equation with the one obtained by performing a Lee-Low-Pines transformation and find that it has, in fact, the same form as the one found in the previous chapter (3.6) and in [56–58], where it has been shown that quantities obtained from solving this equation, like the effective polaron mass or the polaron energy are in excellent agreement with results obtained by quasi-exact quantum Monte Carlo methods. The only difference is that instead of the reduced mass, the boson mass appears in front of ∂_x^2, which is explained by the fact that the effect of normal ordering is lost in this derivation. However, this effect is unimportant for heavy impurities. To summarise, we showed that the equation obtained by employing a coherent state ansatz for the bosonic field paired with a position momentum representation for the impurity reduces to the correct mean-field equations in the equilibrium case, if the impurity mass is large.

4.2 The quench protocol and the initial Wigner function

In the following we specify the quench protocol and the initial Wigner function. We start by introducing the initial state and then specify the Wigner function for a 1D quasi condensate. Here,

we will also discuss all the regularisation necessary to arrive at a divergence-free quasi condensate description. The quench protocol is the following: We start with a free impurity and an interacting superfluid at temperature T. At $t = 0$, the interaction between the superfluid and the impurity is turned on instantly. Experimentally this is realised through a Feshbach resonance [21]. We assume that the initial density matrix can be written as a direct product of the impurity state (which is assumed to be pure) and the thermal density matrix of the superfluid

$$\hat{\rho} = \hat{\rho}_{\varphi} \otimes |\psi\rangle\langle\psi| \, . \tag{4.11}$$

Consequently, the Wigner function also factorises, and we can sample the initial conditions independently. For the condensate, we employ a quasi condensate description; in 1D, this is best done by employing a density and phase representation. We note that this has been used before for a trapped gas in [106]. Since we want to focus on a homogeneous gas in the continuum, we need to regularise the non-condensed part. In this representation, the condensate field operator can be written as

$$\hat{\varphi}(x, 0) = \sqrt{n_0 + \delta\hat{\rho}(x)} \exp\Big(i\hat{\theta}(x)\Big). \tag{4.12}$$

The density operator and the phase operator can be expressed within the Bogoliubov approximation [19] as

$$\hat{\theta}(x) = \frac{-i}{2\sqrt{n_0}} \sum_k \Big[(u_k + v_k)e^{ikx}\hat{a}_k - \text{h.c.}\Big] \tag{4.13}$$

$$\delta\hat{\rho}(x) = \sqrt{n_0} \sum_k \Big[(u_k - v_k)e^{ikx}\hat{a}_k + \text{h.c.}\Big], \tag{4.14}$$

where u_k and v_k are the usual Bogoliubov modes. As discussed in the previous chapters for such treatments to be valid one has to be in the vicinity of a weakly interacting Bose gas, which is characterised by the Tonks parameter (3.18) being less than unity. We refer to section 4.3 for a detailed discussion of the validity of the presented approach. In the path integral this corresponds to a shift of variables meaning that instead of integrating over $\varphi_0^{(*)}(x)$, we integrate over $a_k^{(*)}$, corresponding to the operators $\hat{a}_k^\dagger$. In the standard way, we can now write down the thermal Wigner

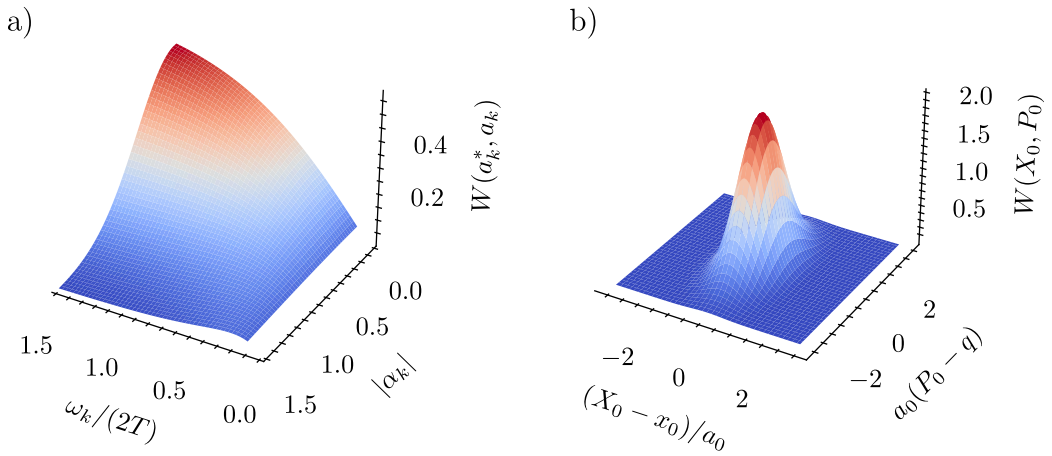

Figure 4.2: The initial Wigner function of the a) phonons and for b) the impurity.

function (within the coherent state representation) for the a_k [70]

$$W(a_k^*, a_k) = \frac{2}{\pi} \tanh\left(\frac{\omega_k}{2T}\right) \exp\left\{ -2|a_k|^2 \ \tanh\left(\frac{\omega_k}{2T}\right)\right\}, \tag{4.15}$$

with the Bogoliubov dispersion ω_k. It can be seen immediately, that the average condensate particle number is given by $N_0/L = n_0$. In order to account for the quantum and thermal depletion, we fix the total particle number N and then choose N_0 according to $N_0 = N - N_d$ (this is done for every realisation), where after proper regularisation (see [54, 55])

$$N_d = \sum_k \left[\frac{e_k - \omega_k}{2\omega_k} + \frac{\mu}{2e_k + 2\mu} + \frac{e_k}{\omega_k}\left(a_k^* a_k - \frac{1}{2}\right)\right], \tag{4.16}$$

with the single-particle dispersion $e_k = k^2/(2m)$. Here, a first-order T-matrix approximation was employed, and in line with the Bogoliubov theory up to one loop, μ is the chemical potential within the Bogoliubov approximation and hence is not temperature dependent. The $1/2$ is needed to cancel the extra factor from symmetric ordering. After averaging, this reproduces the expected result for a thermal quasi condensate in 1D. It should be noted that μ has to be chosen consistently with the total particle number, which can be done by fixing one reference point where the total particle number is known. Henceforth we assume a mean-field density at $T = 0$. This then fixes μ in the Bogoliubov approximation through $\mu = g_{\mathrm{BB}} n_0(T = 0)$. We can then use (4.16) to determine the total particle number, which remains fixed throughout the calculation. It is now possible to sample

individual realisations of the condensate, whose description is free of IR and UV divergences.

Upon closer inspection, one might realise that even though the mean of the phase and density corrections are zero, the variance scales up to linearly with the system size L. A direct result of this is that the computational time needed to achieve convergence also scales with the system size. This computational challenge can be tackled by gradually increasing the system size until the results are independent of the system size and then validating certain data points for larger system sizes. Furthermore, this restricts the discretisation of space, as outlined in [107], which will be discussed in the next section. Because the effect of the impurity is local, we find relatively low dependence on the system size already for small systems. Lastly, we assume that the impurity is not entangled with the condensate[3] at $t = 0$ and is localised in space around x_0 or equivalently in momentum space around q. It is therefore natural to choose a wave packet as the initial wave function

$$\langle x|\psi\rangle = \frac{1}{\pi^{1/4}\sqrt{a_0}} \exp\big(-(x-x_0)^2/(4a_0^2)\big)\,. \tag{4.17}$$

Here a_0 is an external parameter that determines how localised the initial state is. The Wigner function in this setting is well known to be [70]

$$W(X_0, P_0) = 2\exp\big(-2a_0^2(P_0-q)^2 - (X_0-x_0)^2/(2a_0^2)\big)\,. \tag{4.18}$$

We can now conclude that the product of the Wigner functions is a simple multivariate normal distribution, and it is, therefore, straightforward to sample from it. In the next section, we will outline the details of the numerical procedure employed.

4.3 Numerical considerations

This section shows that three quantities can describe the whole parameter space, and we will briefly outline the discretisation of space and all the subtleties involved. We now define the following

[3]The state can be represented as a product wave function.

scaled parameters

$$\tilde{\tau} = \tau/\tau_s\,, \quad \tilde{x} = x/x_s\,, \quad \tilde{\varphi}(\tilde{x}) = \sqrt{x_s}\varphi(x)\,, \quad \tilde{P} = Px_s\,, \quad \tilde{X} = X/x_s\,, \tag{4.19}$$

where we choose

$$\tau_s = \tilde{\xi}/c\,, \quad x_s = \sqrt{2}\xi = \tilde{\xi}\,. \tag{4.20}$$

Dropping the twiddle we then find the Hamiltonian

$$\hat{\mathcal{H}} = \alpha\hat{P}^2 + \int_x \Big\{\hat{\varphi}^\dagger(x)\big[\frac{-\partial_x^2}{2} + \frac{\sqrt{\gamma}}{2}\hat{\varphi}^\dagger(x)\hat{\varphi}(x) + \eta\sqrt{\gamma}V(x-\hat{X})\big]\hat{\varphi}(x)\Big\}\,, \tag{4.21}$$

where as in the previous chapter $\eta = \frac{g_{\mathrm{IB}}}{g_{\mathrm{BB}}}$ and $\alpha = \frac{m}{M}$ is the mass ratio. From here the equations of motion

$$\frac{\mathrm{d}}{\mathrm{d}\tau}X_c(\tau) = \alpha P_c(\tau)\,, \tag{4.22}$$

$$\frac{\mathrm{d}}{\mathrm{d}\tau}P_c(\tau) = \eta\sqrt{\gamma}\int_x \frac{\mathrm{d}}{\mathrm{dx}}V(x - X_c(\tau))|\varphi_c(x,\tau)|^2\,, \tag{4.23}$$

$$i\partial_\tau\varphi_c(x,\tau) = \Big(\frac{-\partial_x^2}{2} + \sqrt{\gamma}|\varphi_c(x,\tau)|^2 + \eta\sqrt{\gamma}V(X_c(\tau)-x)\Big)\varphi_c(x,\tau)\,, \tag{4.24}$$

can be obtained. In order to tame the extensive variance and ensure numerical stability, we have to choose the discretisation $l = L/N_{\mathrm{grid}}$ as outlined in [107]. Namely, l has to be large enough to satisfy $n_0 l \gg 1$, while at the same time ensuring that the energy cutoff introduced by l does not alter the physics. This translates to $l < \xi(\lambda)$, where ξ is the healing length that sets a natural length scale for our problem and λ is the thermal de Broglie wavelength. For all results presented in this chapter we averaged over $N_{\mathrm{s}} = 850 \times 10^3$ realisations and chose a system size of $L = 200\tilde{\xi}$, for a more detailed discussion on convergence we refer to Appendix B. Lastly, we note that we employ a soft interaction potential of the form

$$V(x) = \frac{1}{\sqrt{2\pi l^2}}e^{-x^2/(2l)}\,, \tag{4.25}$$

which converges to the delta distribution as $l \to 0$, but has the advantage of being smoother than δ_x/l, where δ_x denotes the Kronecker delta.

Validity of formalism

This subsection addresses the regime of validity of the formalism derived above. We start by giving some general arguments on the validity of the approach, followed by a term-by-term discussion of the higher-order corrections and their order of magnitude. While we have to restrict our considerations to weak or moderate impurity-boson couplings for the absorption spectrum, we would like to highlight that the result is strictly non-perturbative in g_{BB} and g_{IB} for all dynamical properties calculated (excluding the absorption spectrum). Hence we can safely say that the method presented is valid for $\gamma \leq 1$, which is equivalent to the validity of the Gross-Pitaevskii equation, which, as outlined in section 2.2 corresponds to the tree-level approximation of (4.1). The same reasoning applies to g_{IB}, leading to the conclusion that our results, at least for short times, are valid across the whole range from weak to strong impurity-boson couplings. For longer times, one has to consider the deformation of the condensate.

Another interesting point to consider is that if α is small (meaning the impurity is heavy), the accuracy of the presented approach will improve further since the impurity will behave more classically. Indeed α can be seen as a strict control parameter for the corrections arising due to higher-order terms in $X_q(\tau)$. Combining those considerations with the known fact that, in general, the truncated Wigner approximation is exact for short time scales [70], we can conclude that for short to intermediate time scales, our results are trustworthy for all values of boson-boson and impurity-boson coupling (given that $\gamma \leq 1$). For weak coupling, it is ab initio reasonable to assume that the presented results hold for more extended time scales since higher-order quantum corrections should accumulate slowly, if at all. However, no such universal statement can be made for strong couplings.

There are two contributions of order $\hbar^2$ or higher, which were neglected in our approach and would have to be added to (4.8) if one wanted to solve the problem exactly, the first one coming from the boson-boson interaction and the second one being due to the impurity-boson interaction.

The first one takes the form

$$\sqrt{\gamma}\left(|\varphi_q(x,\tau)|^2\varphi_q(x,\tau)\varphi_c^*(x,\tau)+\text{c.c.}\right). \tag{4.26}$$

This term is closely related to the standard Bogoliubov approximation, with the main difference being that the classical field here is taken to be the deformed field. We note that at no point of our simulations the expectation value of $\langle|\varphi_c(x,\tau)|^2\rangle$ falls below the value of $3\tilde{\xi}$, meaning that it is safe in the spirit of the well-established Bogoliubov approximation, to neglect higher-order terms in the quantum fields, which only scale linearly in φ_c and are of $\mathcal{O}(\varphi_c\varphi_q^3)$ which is certainly small compared to $\mathcal{O}(|\varphi_c|^3\varphi_q)$, as long as the density of the condensate stays larger than the healing length. Nevertheless, the argument given comes into question in the case of very low-density gases and strong impurity-boson coupling. It is a priori not clear whether the outlined method is reliable in this regime. However, this regime was not investigated in the present work. This argument is further underlined by the remarkable accuracy of pure c-field methods (which do not take first-order quantum corrections into account) for the equilibrium polaron, see section 3.1 and [53, 56, 88], where the c-field approximation was shown to also hold for low-density gases and strong coupling. The fact that the boson-boson interaction to all orders in g_{BB} and first-order in $\hbar$ is already taken into account in our calculations strengthens the trust in our results further. A somewhat more complicated expression is obtained when considering the impurity-boson interaction term. Here, one finds that already in (4.8) all orders of $X_q(\tau)$ are present and the higher order terms take the following form

$$\begin{aligned}\eta\sqrt{\gamma}\Bigg(&-\frac{|\varphi_q(x,\tau)|^2}{4}\sum_{n=0}^{\infty}V^{(2n+1)}(\tilde{x})\frac{X_q^{(2n+1)}}{4^n(2n+1)!}-|\varphi_c(x,\tau)|^2\sum_{n=1}^{\infty}V^{(2n+1)}(\tilde{x})\frac{X_q^{2n+1}}{4^n(2n+1)!}\\&+(\varphi_c^*(x,\tau)\varphi_q(x,\tau)+\text{c.c.})\sum_{n=1}^{\infty}V^{(2n)}(\tilde{x})\frac{X_q^{2n}}{4^{n-1}(2n)!}\Bigg).\end{aligned} \tag{4.27}$$

Again for approximating the impact of those terms, it is convenient to bring the derivative terms to the bosonic field operators. It becomes clear that all corrections can be understood as a gradient

expansion in the bosonic field operators, whose impact is undoubtedly small for short time scales, where the condensate deformation stays weak. This also holds true for prolonged time scales as long as the coupling stays moderate. Besides the gradient terms, each correction is accompanied by terms of increasing power in $X_q(\tau)$, which are small at short times and whose impact can be controlled by α. To summarise, while the validity of this approach for large couplings and long time scales can not be judged a priori, we note that for short time scales, the results here hold regardless of impurity-boson coupling strength and also note that α serves as a control parameter of the approximation in the impurity degrees of freedom.

4.4 Results

Post-quench density profile

In this subsection, we focus on the density of the condensate for repulsive and attractive impurity-bath couplings at different times after the quench and supplement those findings with the variance of the position $\sigma_X^2 = \langle(\hat{X} - \langle\hat{X}\rangle)^2\rangle$ and the variance of the velocity $\sigma_V^2 = \langle(\hat{P}/M - \langle\hat{P}/M\rangle)^2\rangle$. We find a dynamically distinct behaviour for weak and strong couplings on the repulsive and attractive side. In Figure 4.3, the condensate density at different times and the evolution of the variance of the position and the variance of the velocity for repulsive interactions are shown. Before discussing the results in more detail, we notice that even for $\eta = 30$, the minimum of the condensate density is still larger than $3\tilde{\xi}$, indicating that the approximations made later for the absorption spectrum are justified. We note that the impurity delocalises faster than a free impurity for weak coupling. For stronger couplings, the impurity stays localised much longer in time, indicating self-trapping, which is depicted in Figure 4.3 c). The velocity variance saturates after a finite time, and the time scale is inversely proportional to the impurity-boson coupling. We note that this can be explained by realising that two competing effects determine the dynamics. Namely, the impurity tends to distribute the repulsion equally throughout the condensate, causing the impurity to delocalise and the opposing effect of self-trapping, where the impurity deforms the condensate and then self-traps in the deformation. It is intuitively clear that self-trapping will not occur for weak couplings, which

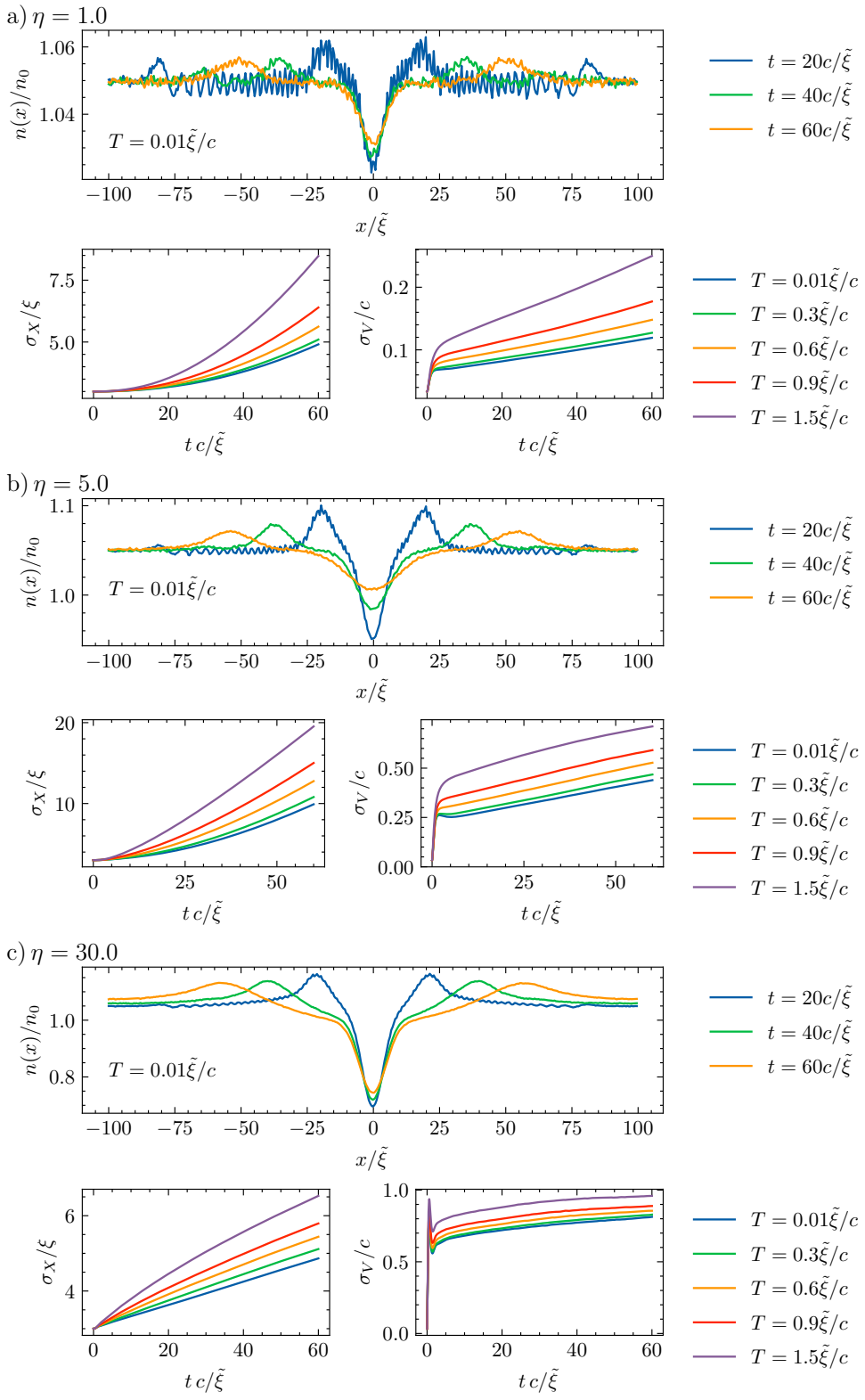

Figure 4.3: The superfluid density, the position variance and the variance of the velocity for different repulsive interactions and temperatures. In all plots the parameters are $\alpha = 0.2$, $\gamma = 0.04$, $n_0 = 5\tilde{\xi}$ and $a_0 = 3/\tilde{\xi}$. As expected, we can clearly see that the impurity deforms the condensate over time. It also becomes apparent that the impurity delocalises over time and that this effect is slowed down with increasing η.

explains the different behaviours seen in Figure 4.3. We have also observed that the variance of the impurity velocity can exceed the speed of sound, which is associated with the emission of non zero energy excitation, indicating an energy transfer from the impurity to the bath, which has also been observed in [108].

The temperature influences the value with which the position and velocity variance saturate; it does not significantly influence the timescale. For strong coupling, the temperature dependence becomes relatively weak, which can be explained by noting that the impurity-boson scattering length determines the relevant energy scale, which is much larger than the thermal length in this case. In Figure 4.4 the same situation for attractive couplings is shown. Here the difference between strongly attractive and moderate attractive couplings becomes obvious. We observe that in the case of moderately attractive couplings, the impurity not only diffuses but also forms a purely attractive polaron. In contrast, for strongly attractive couplings, an attractive polaron with repulsive interactions is observed, and the time scales of the polaron formation are prolonged. This difference is a dynamical effect and can be understood by noting that when the interaction is turned on, particles from the condensate start to accumulate around the impurity, which in turn depletes the condensate around the impurity. The superfluid is interacting with itself. Therefore, the depletion is filled by the particles around it, with the time scale being set by the boson-boson interaction and the mean field particle number. Meanwhile, the impurity-boson interaction strength determines the number of particles that can accumulate around the impurity before the boson-boson action prevents further accumulation. At the same time, the impurity delocalises, which prevents the formation of a well-defined peak around the impurity and the interaction can thus appear repulsive for a long time. Ultimately this is, of course, only a metastable state. This process continues for a longer time when the impurity-boson interaction is large, resulting in a polaron that looks repulsive, which can be observed in Figure 4.4 b).

Impurity velocity

Another quantity of great interest is the impurity velocity in the out of equilibrium case. It gives insight into the polaron formation and the time scales at work. It is also of great importance for the

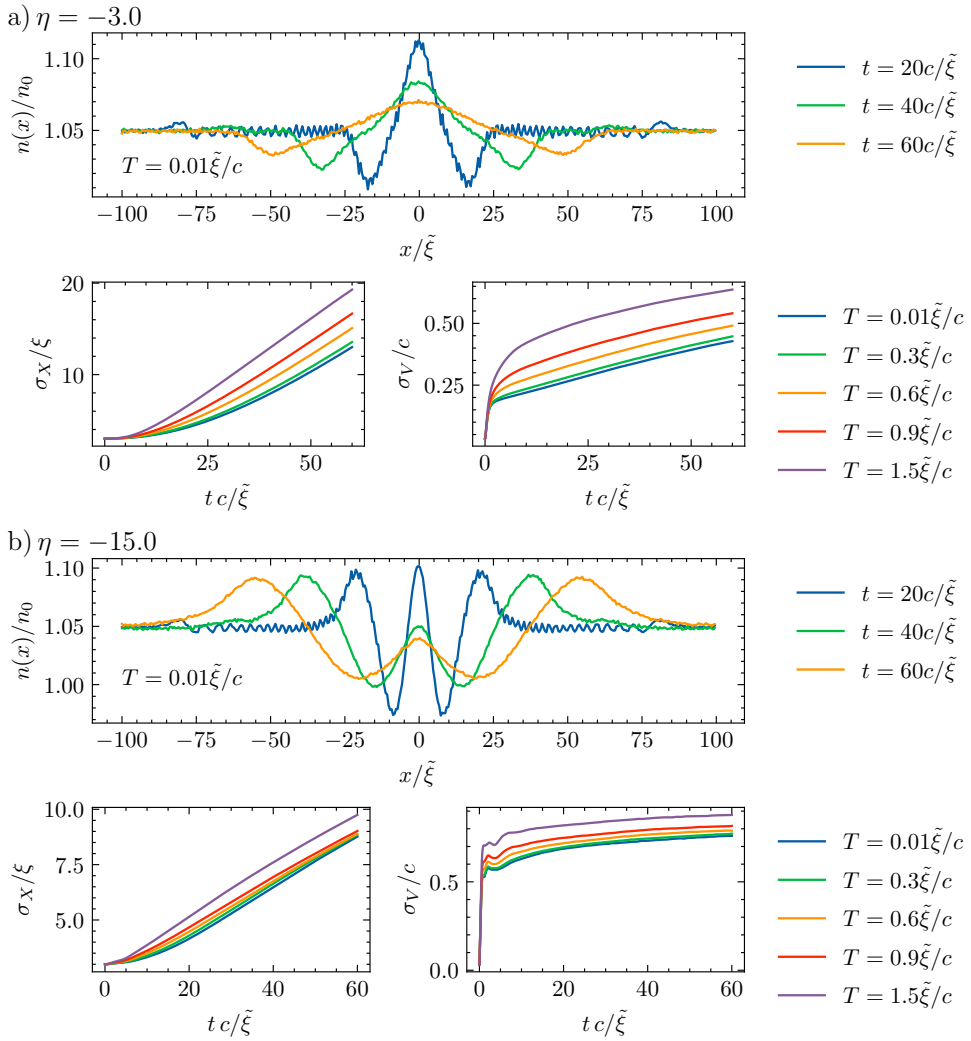

Figure 4.4: The superfluid density, position variance and velocity variance for different attractive interactions and temperatures. In all plots the parameters are as follows $\alpha = 0.2$, $\gamma = 0.04$, $n_0 = 5\tilde{\xi}$ and $a_0 = 3/\tilde{\xi}$. We can see that the impurity attracts surrounding particles, which in turn depletes the condensate. As can be seen in b), this appears as a repulsively interacting polaron.

equilibrium case since it can be used to calculate the effective mass of the polaron (2.45). Here, the impurity is not at rest when the quench occurs but instead carries some finite momentum. The sudden quench of the impurity-boson interaction leads to a momentum transfer from the impurity to the surrounding particles, and we expect a slowdown of the impurity. The time evolution for the velocity of the impurity is depicted in Figure 4.5. Here it becomes apparent that quantum corrections have a noticeable impact on the evolution of the velocity at weak to intermediate coupling. This can be understood by noting that the impurity is treated as a point particle on the mean-field level, and as observed in Figure 4.3, this is not a valid approximation for weak couplings. Additionally,

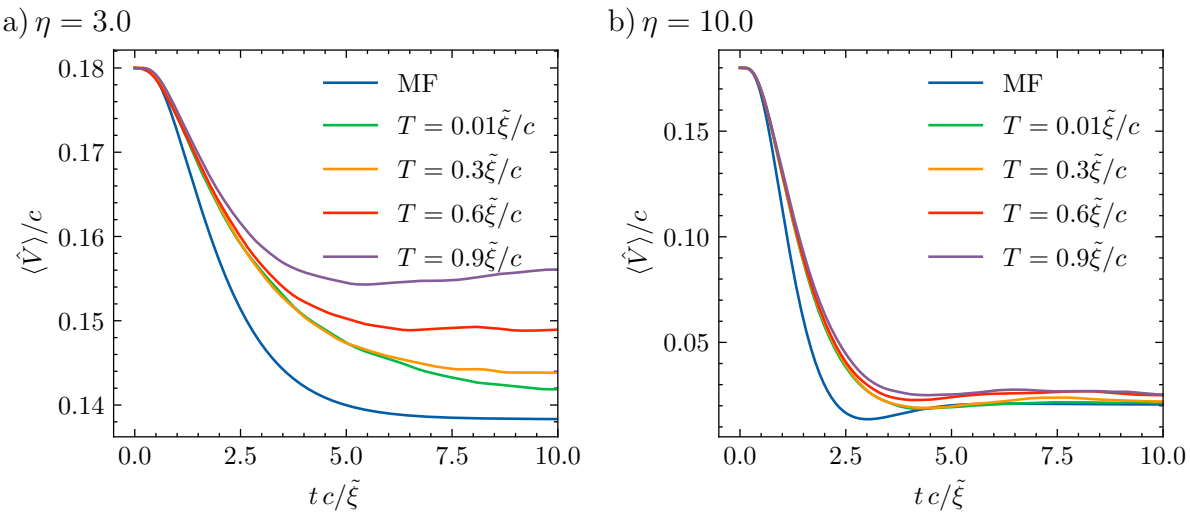

Figure 4.5: The impurity velocity over time for different temperatures. The parameters are $\alpha = 0.2$, $\gamma = 0.04$, $n_0 = 5\tilde{\xi}$ and $a_0 = 3/\tilde{\xi}$. The quantum corrections have a big influence for moderate impurity-bath interactions.

this also explains why the MF velocity is lower than the corrected solution. We also note that the steady-state velocity increases with the temperature. This is easily explained by realising that the surrounding gas has a higher average squared velocity for increasing temperature, and therefore the momentum transfer will be smaller. In contrast, for strong couplings, the impurity stays localised and approximating it as a point particle is less of a simplification. The same behaviour can be observed for the temperature dependence, which is more critical for weak and intermediate couplings, this is again unravelled by comparing the scattering length with the thermal length. We also observe that the impurity transfers some of its momentum to the Bose gas and relatively quickly reaches an equilibrium velocity for not too strong interactions. For stronger interactions, we observe a different behaviour. After an initial abrupt slow down of the impurity, the impurity acceleration changes sign before the velocity approaches its equilibrium value. This is a direct result of the back action from the condensate on the impurity. We note that a similar abrupt slowdown has been observed in the three dimensional setting in [67].

The absorption spectrum

Next, we turn our attention to the (injection) absorption spectrum

$$A(\omega) = 2\mathrm{Re}\int_0^\infty G(t)e^{i\omega t}\,\mathrm{d}t \tag{4.28}$$

[28, 29], which can be measured using Ramsey spectroscopy [5, 27, 28]. The absorption spectrum can be calculated by taking the Fourier transform of the impurity Green's function, which characterises the dephasing of the system and is closely related to the Lochschmidt echo [109]. The absorption spectrum gives essential information about the polaron formation and can be used to estimate the polaron energy and lifetime [10, 110]. At this point, we also want to stress that pure mean-field (MF) calculations in position momentum basis are not sufficient to calculate the impurity Green's function. This can be seen by noting that there is no averaging for a classical calculation, which means there is no dephasing between different trajectories. Therefore one always obtains $|G| = 1$ in purely classical calculations. Our results are depicted in Figure 4.6. It can be observed that the quasi-particle peak widens with increasing temperature, which is also reported in 3D [66]. However, in contrast to the 3D case, [38], where the extended Fröhlich model was considered, we do not find several peaks on the repulsive side. We also note that the overall amplitude decreases with η, and the quasi-particle peak gets washed out with increasing η, which is a direct consequence of the orthogonality catastrophe [52, 111, 112]. Hence, the emergence of a clear quasi-particle peak comes under question. Nevertheless, the absorption spectrum shows a functional dependence associated with quasi-particle behaviour, and we do not find an infrared dominated regime as observed in other one-dimensional systems [110]. Those findings are supplemented by the overlap $G(t)$. Here we can see another vastly different feature of the one-dimensional case compared to the three-dimensional one [38, 66], namely that $|G|$ approaches zero even for moderate couplings, signalling the onset of the orthogonality catastrophe. As expected, the dephasing becomes more rapid with increased temperature and increased g_{IB}.

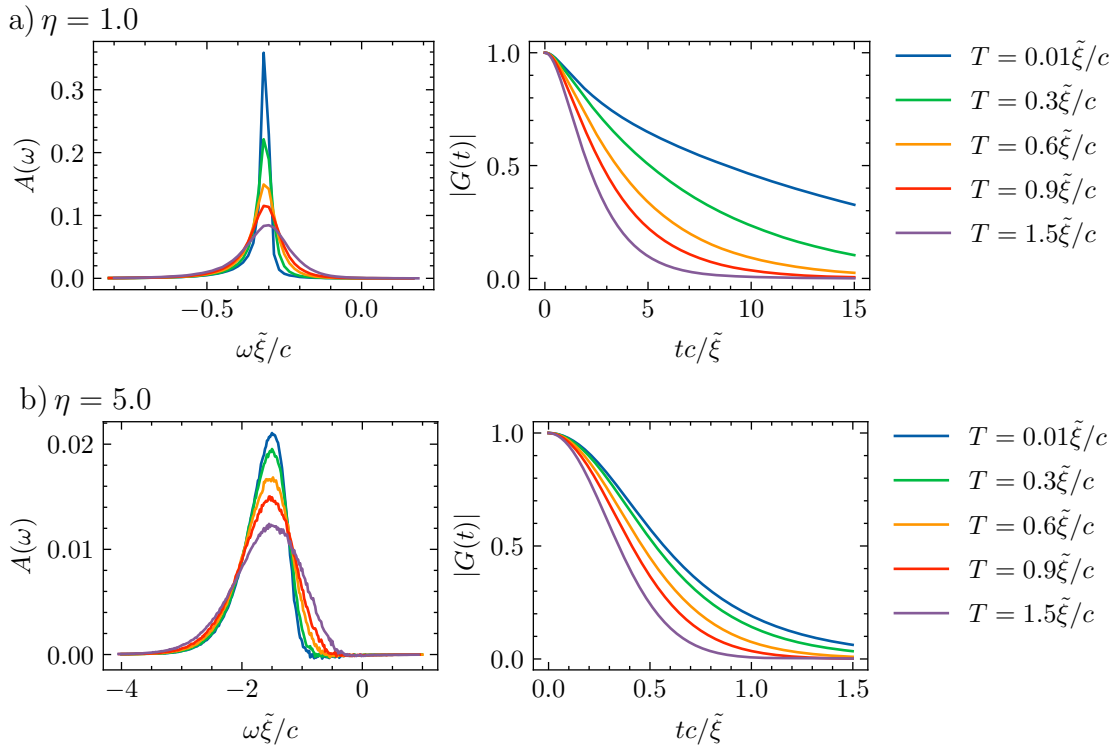

Figure 4.6: The absorption spectrum $A(\omega) = 2\mathrm{Re}\int_0^\infty G(t)e^{i\omega t}\,\mathrm{d}t$ for different temperatures T calculated using the truncated Wigner approximation for $\alpha = 0.2$, $\gamma = 0.04$, $n_0 = 5\tilde{\xi}$ and $a_0 = 3/\tilde{\xi}$.

4.5 Summary & outlook

In summary, by leveraging the Keldysh formalism, we derived a truncated Wigner approach to study dynamical properties of the Bose polaron in 1D. This allowed us to reduce the problem to simulating semi-classical equations of motion with stochastic initial conditions. We showed how to adequately account for temperature effects of the surrounding bath by sampling the phase and density of the condensate. We also discussed how to regularise the arising divergences that typically occur in such one-dimensional systems. The method presented here takes the deformation of the condensate into account and, therefore, adequately describes the condensate's back action on the impurity on the mean-field level already. It is, therefore, applicable from weak to strong impurity bath couplings.

We then used this framework to calculate the dynamics and the absorption spectrum of an impurity after sudden immersion in a surrounding bath. By considering the condensate density and the position/velocity variance, we showed that there is a distinct dynamical behaviour associated

with the strong and weak coupling regime, namely our results indicate self-trapping of the impurity for strongly repulsive interactions, and we also find a repulsive polaron on the attractive side. We also investigated the temperature dependence of the polaron formation and found a substantial influence of quantum corrections on dynamical properties like the velocity of the impurity, showing the necessity to go beyond pure mean-field considerations. Lastly, we studied the absorption spectrum and the impurity Green's function. Here, we observed a clear quasi-particle peak for weak to intermediate couplings. In contrast, we see that the quasi-particle peak is washed out for strong couplings and that temperature effects widen the quasi-particle peak. In contrast to the higher dimensional case, the impurity Green's function approaches zero even for weak couplings.

At this point, we want to stress that our approach is neither limited to 1D nor a single impurity. It could therefore serve as an exciting starting point to explore higher dimensional systems, as well as the interplay of several impurities. While the generalisation to several impurities is relatively straightforward, we want to stress that, as pointed out, for instance, in [68, 113, 114], the generalisation to higher dimensions is highly non-trivial in general. First, we note that in higher dimensions, it is not possible to use bare contact interactions for the boson-boson interaction and the impurity-boson interaction simultaneously when employing this approach. One has to resort to using more realistic interaction potentials for at least one of them as has, for example, been done in the three-dimensional context in [52, 53]. Another major challenge is a purely numerical one, as it becomes more costly to sample the Bose fields in higher dimensions. Nevertheless, we expect that the presented method may be paired with some small approximations, as, for example, the one that has been developed in [115] to address higher dimensional systems.

CHAPTER 5

The effect of boson-boson interaction on the bipolaron formation

The following chapter is based on [JJ3] with some verbatim textual overlap.

Introduction

So far, we have considered a single impurity, but when multiple impurities are present, exchange interactions mediated by the surrounding environment can lead to impurity-impurity bound states known as bipolarons. Such exchange-mediated interactions are ubiquitous in physical systems, being relevant for Cooper pairs in superconductors [116] as well as quark-gluon interactions [1]. In the solid-state context, lattice phonons are responsible for the mediated interactions. The resulting bipolarons may play a role in high-T_c superconductivity [14, 117] and are also a vital ingredient for understanding the electric conductivity of polymers [12, 13].

In ultracold gases, the interaction between two neutral impurities immersed in a Bose gas is crucial for understanding the interplay between several impurities and studying the properties of two mixed quantum gases, where one type is very dilute. Here, the Fröhlich model generically predicts an attractive Yukawa potential between two impurities in 3D [118, 119]. In [60], it was noted that the Yukawa potential is not entirely accurate, after all, and its validity is limited to weak couplings and sufficiently large impurity separation. Building on the single impurity case, one, therefore, might expect that the results obtained from the Fröhlich model for weak couplings can be improved upon in a direct way by including higher-order phonon impurity scattering terms. However, we will show that if one proceeds in a naive manner for two impurities, this can lead to unphysical divergences in the ground state energy. The divergence is attributed to the bound

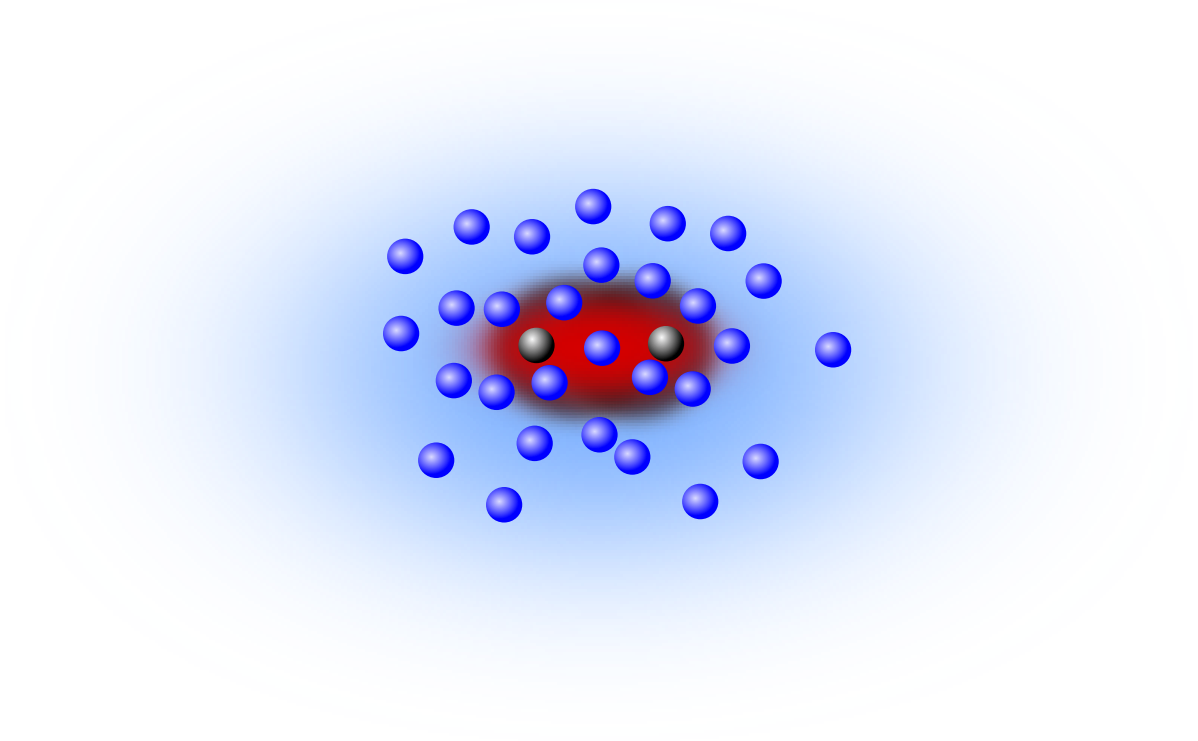

Figure 5.1: Caricature of two impurities forming a bipolaron through the interactions mediated by the condensate. The black (blue) spheres represent the impurities (bosons). The impurities deform the condensate. The deformation induces an exchange mediated interaction between the impurities. This can lead to the formation of a bound state between the two impurities called the bipolaron (indicated in red).

state formation between the two impurities and the excitations of the Bose gas, something that has also been observed in [120]. In contrast to the single impurity case, this occurs irrespective of the sign of the scattering length. The mechanisms leading to this bound state are similar to those responsible for the bound state formation between two localised potentials known from standard quantum mechanics [121], which can be used to gain physical insights into the breakdown of the extended Fröhlich model.

In this work, we present a physically intuitive model to address the bipolaron problem. This model constitutes a good starting point for more advanced treatments and also rectifies the shortcomings of the (extended) Fröhlich model. We start by introducing the full microscopic Hamiltonian. Next, we linearise the model and integrate out the phononic degrees of freedom, leading to the Yukawa potential. We then argue that the Yukawa potential is inaccurate for sufficiently strong coupling and outline why some of the standard methods used to go beyond the Fröhlich model in the

single impurity case do not generalise straightforwardly. Thereafter, we show how those problems can be remedied by accounting for boson-boson interaction at the mean-field level in line with the approaches presented in the previous chapters, treatments of bipolarons in 1D [88, 122] and numerous other treatments for single polarons [52, 53, 57, 59, 97, 123, 124]. This is done by moving to the centre of mass coordinates for the two impurities and applying the Lee-Low-Pines transformation [8] and thereby bringing the Hamiltonian into a form amenable to the Born-Oppenheimer (BO) approximation. The BO approximation is valid if the momentum scales decouple, and for this reason, the following treatment is, strictly speaking, only valid if the impurity atoms are sufficiently heavy. Next, we minimise the resulting Gross-Pitaevskii (GP) energy functional. This leaves us with an effective Schrödinger equation for the two impurities. From the effective Schrödinger equation, we can calculate the bipolaron binding energy and determine when a bound state occurs.

5.1 The model

In this section we introduce the model. Our starting point is the microscopic Hamiltonian (2.1) in three dimensions and adapted to the case of two impurities

$$\hat{\mathcal{H}} = \int \mathrm{d}^3\mathbf{r}\, \hat{\varphi}^\dagger(\mathbf{r})\Big(-\frac{\nabla^2}{2m} + \frac{g_{\mathrm{BB}}}{2}\hat{\varphi}^\dagger(\mathbf{r})\hat{\varphi}(\mathbf{r}) - \mu \\ +V(\mathbf{r}-\hat{\mathbf{X}}_1) + V(\mathbf{r}-\hat{\mathbf{X}}_2)\Big)\hat{\varphi}(\mathbf{r}) + \frac{\hat{P}_1^2+\hat{P}_2^2}{2M}\,. \tag{5.1}$$

The interaction between the impurities and the condensate is modelled by the interaction potential $V(\mathbf{r})$. As discussed in section 2.1 most linearised treatments rely on employing a contact potential of the form $g_{\mathrm{IB}}\delta(\mathbf{r})$ [60, 119]. As is known for such models, when keeping the full Hamiltonian and applying a contact interaction for the impurity-boson interaction and the boson-boson interaction simultaneously, the Hamiltonian only admits zero energy (bi)polaron solutions [52]. Thus, we employ a finite-range potential when working with the non-linearised model in the Born-Oppenheimer

approximation. We choose the widely-used Gaussian pseudopotential

$$V(\mathbf{r}) = -V_0 e^{-\frac{\mathbf{r}^2}{L^2}}\,, \tag{5.2}$$

with depth V_0 and range L. The connection to the s-wave scattering length can be made by numerically solving the two-body Schrödinger equation. For the three-dimensional setting, one finds [125]

$$a_{IB}^{3D} = \lim_{r\to\infty}\left(r - u(r)/u'(r)\right)\,, \tag{5.3}$$

where $u(r)$ satisfies the (radial) differential equation

$$\left(-\frac{1}{2m_{\mathrm{r}}}\frac{\mathrm{d}^2}{\mathrm{d}r^2} + V(r)\right)u(r) = 0\,, \tag{5.4}$$

m_{r} is the reduced mass and the boundary conditions are $u(0) = 0$ and $u'(0) = 1$. This relation can be used to make the connection to the experimentally observable scattering length and also to the contact potential used in the linearised case.

To conclude this section, we introduce relative coordinates and apply a unitary transformation to eliminate the centre of mass degrees of freedom. Starting with the Hamiltonian (5.1), we transform into the centre of mass frame and denote the relative position (momentum) of the impurities by $\hat{\mathbf{R}}$ ($\hat{\mathbf{P}}$) and the centre of mass position (momentum) by $\hat{\mathbf{r}}$ ($\hat{\mathbf{p}}$). Subsequently, we apply the Lee-Low-Pines transformation $\hat{U} = \exp\left(i\hat{\mathbf{r}}\cdot\hat{\mathbf{P}}_{\mathrm{B}}\right)$, where $\hat{\mathbf{P}}_{\mathrm{B}} = -i\int \mathrm{d}^d r\, \hat{\varphi}^\dagger(\mathbf{r})\nabla\hat{\varphi}(\mathbf{r})$ is the total momentum of the Bose gas. This eliminates the centre of mass coordinate [8, 88] and we arrive at the Hamiltonian

$$\begin{aligned}\hat{\mathcal{H}} = \frac{:\left(\mathbf{p}-\hat{\mathbf{P}}_{\mathrm{B}}\right)^2:}{4M} + \frac{\hat{P}^2}{M} + \int \mathrm{d}^3\mathbf{r}\,\hat{\varphi}^\dagger(\mathbf{r})\Bigg(\frac{-\nabla^2}{2m_{\mathrm{r}}} + \frac{g_{\mathrm{BB}}}{2}\hat{\varphi}^\dagger(\mathbf{r})\hat{\varphi}(\mathbf{r}) - \mu \\ + V(\mathbf{r}+\hat{\mathbf{R}}/2) + V(\mathbf{r}-\hat{\mathbf{R}}/2)\Bigg)\hat{\varphi}(\mathbf{r})\,.\end{aligned} \tag{5.5}$$

As before, $\mathbf{p}$ denotes the total momentum, which is, in full analogy to section 2.1, a conserved quantity and, therefore, can be replaced by a c-number. Throughout our calculations, we set $p = 0$

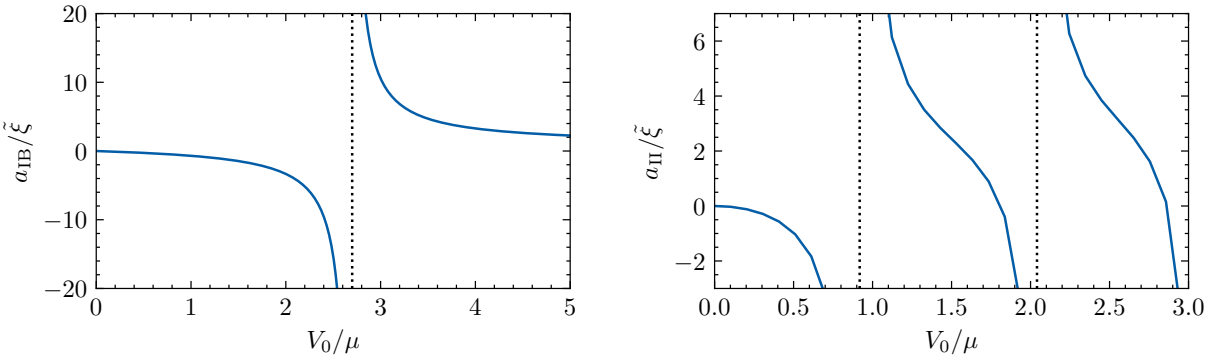

Figure 5.2: The dependence of a) the impurity-boson scattering length a_{IB} and b) the scattering length of the the mediated potential a_{II} on the microscopic amplitude of the potential V_0 for $L = \tilde{\xi}$. The dotted line indicates the scattering resonance, across which the sign of the scattering length changes.

and focus on systems at rest to obtain the mediated interaction. One might notice that we are neglecting direct impurity-impurity interactions in our considerations. This is strictly speaking only justified when the impurities are well separated. As will be further explained later in this chapter, the range of the bare impurity-impurity interaction will usually be much smaller than the range of the mediated potential. The standard procedure is to linearise the field operators and subsequently perform a Bogoliubov rotation, resulting in the (extended) Fröhlich model. The following section will briefly outline how to retrieve these results by linearising only the density and neglecting phase-density interactions.

5.2 Linearised theory

This section addresses the bipolaron problem using a path integral approach, expanded in density fluctuations. Though the resulting expressions can be obtained directly from the Fröhlich model, the path integral approach gives a clearer picture of how the interaction is mediated by the density fluctuations of the condensate. Furthermore, it demonstrates that the neglected boson-boson interaction is the root cause of the shortcomings in predicting the mediated interactions. We start by rewriting the field operators as

$$\hat{\varphi}(\mathbf{r}) = \sqrt{n_0 + \delta\hat{\rho}(\mathbf{r})}e^{i\hat{\theta}(\mathbf{r})}\,, \tag{5.6}$$

where $n_0 = \mu/g_{\mathrm{BB}}$. After performing this redefinition and dropping terms of order higher than quadratic in $\delta\rho$ and $\partial_i\theta$, we arrive at the imaginary-time action

$$S = \int \mathrm{d}\tau \Big\{ \int \mathrm{d}^3\mathbf{r} \Big[\delta\rho\partial_\tau\theta + \frac{n_0(\nabla\theta)^2}{2m_{\mathrm{r}}} + \frac{1}{2}\delta\rho\Big(\frac{-\nabla^2}{4m_{\mathrm{r}}n_0} + g_{\mathrm{BB}}\Big)\delta\rho \Big] + g_{\mathrm{IB}}\left(\delta\rho(\mathbf{R}/2) + \delta\rho(-\mathbf{R}/2)\right) + \frac{\mathbf{P}^2}{M} \Big\}.$$

It is now possible to first integrate out the density and, subsequently, the phase, which leaves us with an effective action for the impurities[1]

$$S = \sum_n \Big\{ \frac{\mathbf{P}^2}{M} - \frac{g_{\mathrm{IB}}^2}{(2\pi)^3} \int \mathrm{d}^3k \, \frac{n_0 e_k \cos\left(\mathbf{k}\cdot\mathbf{R}/2\right)}{\mathcal{E}_k^2 + \omega_n^2} \Big\}, \tag{5.7}$$

where ω_n are Matsubara frequencies, $e_k = k^2/2m_{\mathrm{r}}$ is the energy of a free boson modified by the effective mass and $\mathcal{E}_k = \sqrt{\frac{e_k}{2}(e_k + 2n_0 g_{\mathrm{BB}})}$ is the adjusted Bogoliubov dispersion (2.16). This leads to the mediated interaction

$$V_{\mathrm{eff}}(\omega_n, \mathbf{R}) = -\frac{g_{\mathrm{IB}}^2}{(2\pi)^3} \int \mathrm{d}^3k \, \frac{n_0 e_k \cos\left(\mathbf{k}\cdot\mathbf{R}/2\right)}{\mathcal{E}_k^2 + \omega_n^2}, \tag{5.8}$$

where by evaluating the momentum integral and applying the Born-Oppenheimer approximation, which allows us to take $\omega_n = 0$, one can obtain the mediated interaction in real space. Performing the integration is straightforward and yields the Yukawa potential

$$\tilde{V}_{\mathrm{BP}}^{\mathrm{Yuk}}(R) = -\frac{4n_0\pi a_{\mathrm{IB}}^2}{m_{\mathrm{r}}R} e^{-\sqrt{2}R/\tilde{\xi}}, \tag{5.9}$$

where we have used the usual relation $g_{\mathrm{IB}} = \frac{2\pi}{m_{\mathrm{r}}} a_{\mathrm{IB}}$ and as in the previous chapters $\tilde{\xi} = \frac{1}{\sqrt{2g_{\mathrm{BB}}n_0 m_{\mathrm{r}}}}$ is the reduced healing length. For heavy impurities and moderate couplings, one can find the ground state energy of the bipolaron by solving the resulting Schrödinger equation. In the case of heavy impurities, one can use the generalised parametric Nikiforov–Uvarov method to calculate

[1] See [35, 45] for similar calculations for the Bose polaron.

approximate eigenenergies for the Yukawa potential [126], which results in the ground state energy

$$E_{BP}^{\mathrm{Yuk}} = -4\pi^2 \frac{M n_0^2 a_{\mathrm{IB}}^4}{m_{\mathrm{r}}^2} \,. \tag{5.10}$$

We note that this bound state only exists when $|a_{\mathrm{IB}}| \geq \sqrt{\frac{m}{\sqrt{2} M n_0 \pi \tilde{\xi}}}$ [126]. At this point a major shortcoming of the approach becomes apparent, namely the bound state energy scales linearly in M and accordingly the bipolaron energy diverges for $M \to \infty$. This is unphysical. The diverging energy can be traced back to the fact that the Yukawa potential is unbounded from below, and for $M \to \infty$, the kinetic energy becomes irrelevant. Ergo, the ground-state energy becomes proportional to the minimum of the potential, which is $-\infty$ for the Yukawa potential. Additionally, this treatment predicts a divergence at the Feshbach resonance. We do not expect this to happen when accounting for boson-boson interactions.

In principle, one can improve upon these results by expanding the action perturbatively and resumming certain classes of diagrams. However, as shown in [59] for the case of a single impurity, this is strictly speaking beyond the validity of the model and can lead to unphysical results near the scattering resonance due to the breakdown of the model associated with the bound state formation. In the next section, we show, with the help of the extended Fröhlich model for two impurities, that not accurately accounting for the boson-boson interaction can be problematic and leads to divergences in the mediated potential. The idea is simple, in analogy with the case of a single particle interacting with two delta potentials (see [121] and Appendix C), a bound state can form between the excitations and the two impurities. This bound state is energetically favourable, and without phonon-phonon interaction preventing an accumulation in this state, the condensate breaks down. To alleviate those problems, one must incorporate boson-boson interaction[2] and employ an interaction potential with a finite range. In section 5.4, we describe how the boson-boson interaction can be accounted for on the mean-field level.

Before turning to the discussion on the inadequacies of the Fröhlich model, we repeat the

[2] which translates to phonon-phonon interaction in the Fröhlich picture.

calculation above for a Gaussian potential (instead of a contact potential) and find

$$V_{\mathrm{BP}}^{\mathrm{Gauss}}(R) = -\frac{2V_0^2 L^6 \pi m}{R} \times \int_0^\infty \frac{\sin(qR) n_0 q}{q^2 + 2/\tilde{\xi}^2} \exp\left(-q^2 L^2/2\right) \mathrm{d}q\,. \tag{5.11}$$

Note that with this potential, $V_{\mathrm{BP}}^{\mathrm{Gauss}}$ stays finite for all R. This can be understood by noting that the exponential cut-off is an effective UV-regulator, which is absent in the case of a delta function potential. However, the bound state problem will persist even if one uses this scattering potential for the extended Fröhlich model. Additionally, the model loses the appeal of being analytically tractable when including higher-order phonon terms.

5.3 Failure of the extended Fröhlich model

In the previous section, we have seen how a linearised theory, which only tracks one phonon interaction terms, can be used to derive an effective interaction potential. For the single impurity case, the extended Fröhlich model, which also includes two phonon interaction terms, has been successfully applied to improve upon the simpler Fröhlich model [37, 38, 63, 66]. However, we show that the extended Fröhlich model will yield unphysical results for the bipolaron problem. This occurs because the emerging bound state is populated by an infinite number of excitations, which leads to a diverging energy. Within the BO approximation it is indeed possible to predict the position of this resonance fully analytically. It is instructive to perform the calculation explicitly and see where the breakdown of the model happens. Our starting point is the extended Fröhlich model $\hat{\mathcal{H}} = \hat{\mathcal{H}}_{\mathrm{F}} + \hat{\mathcal{H}}_{\mathrm{2ph}}$ (see section 2.1) for two impurities, in the $M \to \infty$ limit[3]

$$\begin{aligned}\hat{\mathcal{H}} = \sum_{\mathbf{k}} \mathcal{E}_k \hat{a}_{\mathbf{k}}^\dagger \hat{a}_{\mathbf{k}} + 2g_{\mathrm{IB}}\sqrt{\frac{n_0}{L^d}} \sum_{\mathbf{k}} W_k \cos\left(\frac{\mathbf{k}\cdot\mathbf{R}}{2}\right)\left(\hat{a}_{\mathbf{k}}^\dagger + \hat{a}_{-\mathbf{k}}\right) + \frac{g_{\mathrm{IB}}}{L^d}\sum_{\mathbf{k},\mathbf{k}'} \cos\left(\frac{(\mathbf{k}'-\mathbf{k})\cdot\mathbf{R}}{2}\right) \\ \left[\left(W_k W_{k'} + W_k^{-1}W_{k'}^{-1}\right)\hat{a}_{\mathbf{k}}^\dagger \hat{a}_{\mathbf{k}'} + \frac{1}{2}\left(W_k W_{k'} - W_k^{-1}W_{k'}^{-1}\right)\left(\hat{a}_{\mathbf{k}}^\dagger \hat{a}_{-\mathbf{k}'}^\dagger + \hat{a}_{-\mathbf{k}}\hat{a}_{\mathbf{k}'}\right)\right].\end{aligned} \tag{5.12}$$

[3] which corresponds to applying the BO approximation

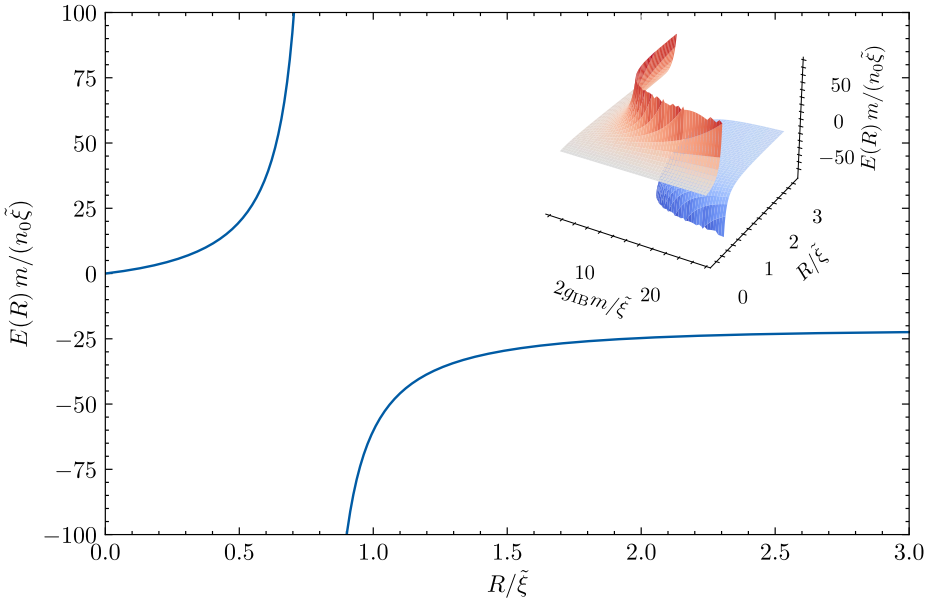

Figure 5.3: The effective potential as predicted by the (regularised) extended Fröhlich model for $\frac{2g_{\mathrm{IB}}m}{\tilde{\xi}} = 15$. The resonance is clearly nonsensical. The reason for the resonance is that the extended Fröhlich model does not account accurately for boson-boson interaction. We note that similar divergencies are observed in the single impurity case (see section 2.1). Still, as demonstrated by the inset, in contrast to a single impurity, where the divergence only occurs at a specific scattering length, for two impurities a resonance can always be found as long as the interaction strength is negative or $\frac{1}{2g_{\mathrm{IB}}} < \frac{\sqrt{2}\pi m}{(2\pi)^2\tilde{\xi}}$.

In the BO approximation, the Hamiltonian is quadratic and can therefore be solved by a coherent state Ansatz $|\{\alpha_k\}\rangle$; see section 2.1 for a detailed discussion in the case of a mobile single impurity. Applying the coherent state ansatz one obtains after some algebra, that the $\{\alpha_k\}$ can be chosen to be real, symmetric in $\mathbf{k}$ and are determined by the self-consistent equation

$$\alpha_k = -2g_{\mathrm{IB}}\sqrt{n_0}\frac{W_k\cos(\mathbf{k}\cdot\mathbf{R}/2)}{\mathcal{E}_k} - 2g_{\mathrm{IB}}\frac{W_k\cos(\mathbf{k}\cdot\mathbf{R}/2)}{\mathcal{E}_k}\frac{1}{L^d}\sum_{\mathbf{k}'}W_{k'}\cos(\mathbf{k}'\cdot\mathbf{R}/2)\alpha_{k'}\,, \quad (5.13)$$

which can be easily resummed as a geometric series. This leads to the following R-dependent part of the ground state energy in the thermodynamic limit

$$E(R) = \frac{n_0}{\frac{1}{2g_{\mathrm{IB}}} + \frac{1}{(2\pi)^d}\int d^d\mathbf{k}\,\frac{W_k^2}{\mathcal{E}_k}\cos^2(\mathbf{k}\cdot\mathbf{R}/2)}\,. \quad (5.14)$$

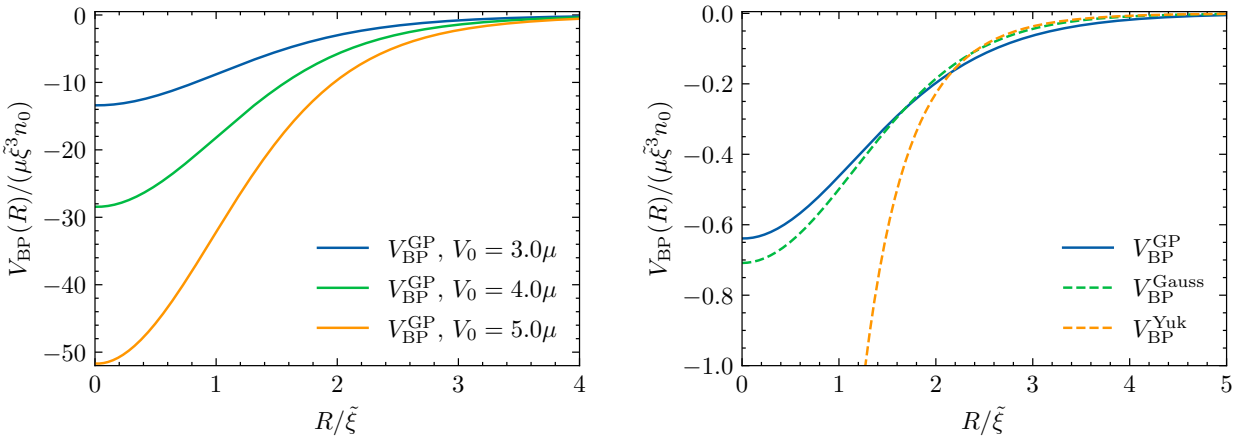

Figure 5.4: a) The effective potential between the two impurities for different V_0 and $L = \tilde{\xi}$ obtained from minimising the GP-functional in the BO approximation. b) Comparing the GP-based results with the Yukawa potential and the results obtained from the linearised model with a Gaussian interaction potential for small interactions $V_0 = 0.9\mu$, which corresponds to $a_{\mathrm{IB}} = -0.6\tilde{\xi}$. For weak couplings, we find good agreement between the results obtained from solving the full GP-equation and the Fröhlich model.

The integral $\int d^d\mathbf{k}\, \frac{W_k^2}{\mathcal{E}_k} \cos^2(\mathbf{k}\cdot\mathbf{R}/2)$ can be solved analytically in 3D using dimensional regularisation and yields

$$\frac{1}{(2\pi)^3}\int d^3\mathbf{k}\, \frac{W_k^2}{\mathcal{E}_k}\cos^2(\mathbf{k}\cdot\mathbf{R}/2) = \frac{m}{(2\pi)^2}\left(\frac{-\sqrt{2}\pi}{\tilde{\xi}} + \pi\frac{\exp\left(-\sqrt{2}R/\tilde{\xi}\right)}{R}\right). \tag{5.15}$$

As can be seen in Figure 5.3 the energy diverges when the denominator in (5.14) is zero, which does not only depend on the coupling g_{IB} but also the separation R. This is due to the accumulation of an infinite number of phonons in the bound state. In a realistic system this effect is balanced by the here neglected phonon-phonon interaction. A similar effect is known from the quantum mechanical setting, see [121] and Appendix C. We note that other approaches that rely on trial wave function that do not re-sum the whole scattering series will not encounter this divergence.

5.4 Main methodology and results

In this section, we describe an approach which eliminates the difficulties encountered in the previous section. The Hamiltonian (5.5) will serve as the starting point for the mean-field treatment. The GP

energy functional in the BO approximation, which needs to be minimised to find the ground state, can now be simply read off from (5.5)

$$E(\varphi, \mathbf{R}) = \int \mathrm{d}^3\mathbf{r} \left\{ \frac{|\nabla\varphi|^2}{2m_\mathrm{r}} + \frac{g_\mathrm{BB}}{2}(|\varphi|^2 - n_0)^2 + \left(V(\mathbf{r}+\mathbf{R}/\mathbf{2}) + V(\mathbf{r}-\mathbf{R}/\mathbf{2})\right)|\varphi|^2 \right\}. \quad (5.16)$$

This energy functional can be minimised using a split-step Fourier algorithm in imaginary time.[4] This, in turn, allows us to calculate the mediated interaction through

$$V_{BP}^{GP}(R) = E(R) - E_0 - E(\infty)\,, \quad (5.17)$$

where E_0 is the energy of the Bose gas without impurities and $E(\infty)$ is the energy of the two polarons at infinite separation and is subtracted to obtain the purely attractive part attributed to the bipolaron.

In Figure 5.2, we show the scattering length for different microscopic interaction amplitudes V_0 while keeping the potential range $L = \tilde{\xi}$ fixed throughout all of our calculations. We focus on (microscopically attractive) $V_0 > 0$ on either side of the first resonance. We can accordingly identify two relevant regimes, which are depicted in Figure 5.2 a). On the left (right) side of the scattering resonance indicated by the dotted line, we find a negative (positive) scattering length for the impurity-boson interaction. For comparison in Figure 5.2 b), we show the s-wave scattering length for the mediated impurity-impurity interaction. In Figure 5.4 a), we show the shape of the mediated potential between two impurities for different V_0. Figure 5.4 b) shows the comparison with the linearised model for weak coupling; here, we chose the s-wave scattering length of the Yukawa potential to match the scattering length of the Gaussian potential. There is good quantitative agreement for weak coupling between the linearised model using a Gaussian pseudopotential and the result obtained using the GP functional. We also observe that the Yukawa potential, which is obtained by employing a zero-range interaction, matches the behaviour of the interaction potential with a finite range for larger separations, indicating that the exact effective range of the potential is

[4] All calculations were performed in Cartesian coordinates, and to speed up the calculations, they were performed on GPUs using `CUDA.jl` [127].

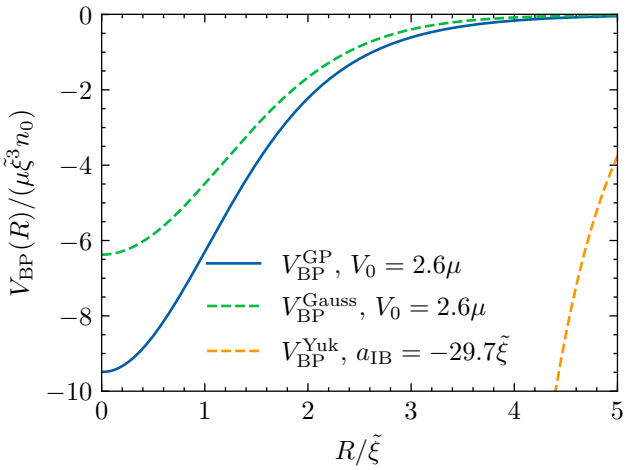

Figure 5.5: The effective potential for the two impurities near the Feshbach resonance. We can see that for a more realistic pseudopotential the transition is smooth across the resonance. In contrast, the diverging scattering length leads to a breakdown of the Yukawa predictions. It also becomes clear that for larger V_0, the Fröhlich model, even with a UV regulated pseudopotential, becomes inadequate.

not highly relevant for the range of the mediated potential. One main difference between a zero range interaction and a more realistic Gaussian interaction is that the mediated potential stays finite for $R = 0$. A similar discrepancy between the Yukawa potential and the mediated potential was reported in [60] using a scattering matrix approach.

In Figure 5.5, we show the mediated interaction close to the Feshbach resonance. Here another shortcoming of the zero range scattering potential is revealed, namely, close to the scattering resonance a_{IB} diverges, leading to infinite attraction, which is unphysical. The results obtained from the GP energy functional and the result obtained employing a Gaussian potential give a more realistic picture. Here, the mediated interaction changes less drastically across the Feshbach resonance. We also observe that for larger V_0, the linearisation approach becomes inadequate and significant deviation from the GP result can be observed. While the Fröhlich model with Gaussian potential underestimates the interaction here, we note that it is a priori not clear whether the Fröhlich model over or underestimates the mediated potential. The two competing effects that the Fröhlich model does not account for are (i) two and higher-order phonon impurity scattering processes, which lead to enhanced mediated impurity-impurity interaction and (ii) the boson-boson interaction, which damps the phonon exchange.

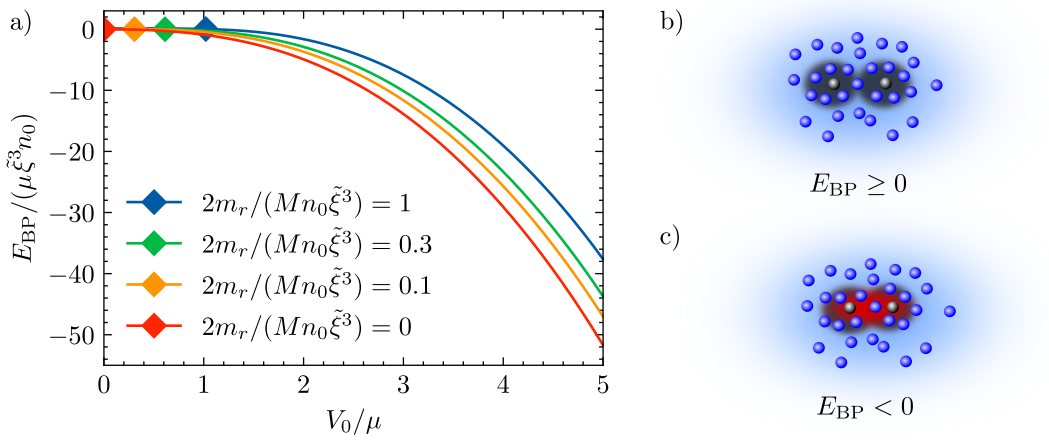

Figure 5.6: a) The binding energy of the bipolaron for different mass ratios. Strictly speaking, our approach is only valid for $m/M \ll 1$. The diamonds indicate the threshold after which a bound state is formed. This threshold decreases with $\frac{m_{\mathrm{r}}}{Mn_0\tilde{\xi}^3}$ and in-fact becomes 0 for $\frac{m_{\mathrm{r}}}{Mn_0\tilde{\xi}^3} = 0$. b) If the interaction strength is weak or the impurities are very light, no bound state is formed, and only two polarons coexist. c) For strong enough interactions, a bound state called the bipolaron emerges.

The bipolaron energy can be calculated by finding the ground state of the resulting stationary Schrödinger equation. Within the mean-field approximation for $p = 0$, the condensate wave function φ can always be chosen to be real. Therefore we do not have to consider the vector potential typically arising within the Born-Oppenheimer approximation [128]. Moreover, we observe that the equation is radially symmetric, and consequently, the ground state will have zero angular momentum. Thus, we have to solve the radial Schrödinger equation

$$\left(-\frac{1}{M}\frac{\mathrm{d}^2}{\mathrm{dR}^2} + V_{\mathrm{BP}}(R)\right) u(R) = E_{\mathrm{BP}} u(R)\,, \tag{5.18}$$

with the boundary condition $u(0) = 0$ to obtain the bipolaron energy. In Appendix D, we discuss the details of how this equation was solved numerically. The results obtained are shown in Figure 5.6. Notably, the dependence on the mass ratio is weak compared to the linearised case,[5] which can be explained by realising that the effective potential stays finite. If the mass ratio becomes small, the kinetic energy becomes less critical, and the solution of (5.18) will be localised around the minimum of the potential. Furthermore, we observe a critical V_0 after which a bound state ($E_{\mathrm{BP}} < 0$), the bipolaron, is formed. In Figure 5.6, we have indicated this value by diamonds.

[5] compare with (5.10) where the energy scales linearly in the impurity mass

As mentioned earlier, it is essential to compare the localisation of this bound state to the range of the impurity-impurity interaction. On average, the separation of the impurities is much greater than the range of the impurity-impurity interaction, which in this case is actually the vital length scale since after integrating out the bosonic degrees of freedom, we have reduced the problem effectively to a single particle scattering problem, with two competing length scales. To make this statement more quantitative, we compare some characteristic effective ranges. Considering a microscopic van-der-Waals interaction the effective range is given by $r_0 \sim (C_6 m/m_e)^{1/4} a_0$ [18], where a_0 is the Bohr radius and typical values are $C_6 \sim 10^3$ and $m/m_e \sim 10^4 - 10^5$, which gives the estimate $r_0 \sim 100 a_0$. To put this into context, one can estimate the healing length in terms of the Bohr radius for typical experimental values (see for example [31]), which leads to $\tilde{\xi} \sim 10^7 - 10^{10} a_0$. Accordingly, the effective range of the impurity-impurity interaction typically is a fraction of the range of the effective interaction potential mediated by the condensate. Nevertheless, in the case of large V_0, the impurity-impurity interaction can no longer be neglected, and few-body physics, like the bound state between the two impurities due to direct impurity-impurity interaction, can become relevant.

5.5 Conclusion

In this chapter, we have presented an approach to address the ground-state interaction of two impurities immersed into a three dimensional Bose gas capable of taking the boson-boson interaction into account. We started by showing that linearisation efforts and the resulting Fröhlich Hamiltonian are inadequate to fully describe the polaron interaction in a Bose gas. We also discussed how naive extensions of the Fröhlich model are inadequate. We then outlined how these issues can be addressed using a mean-field treatment paired with the Born-Oppenheimer approximation, which is valid for heavy impurities. While, strictly speaking, the mean-field approximation completely neglects quantum corrections in the form of deformed phonons, it is important to note that short-scale physics determine the bipolaron properties. Therefore, we do not expect phonons to play a significant role in this regime. We first minimised the mean-field energy functional, from which

we extracted the interaction potential. Here, we compared our results to the Yukawa potential and the results obtained from the linearised model with a Gaussian potential. Next, we calculated the bipolaron energy using the effective potential by solving the resulting radial Schrödinger equation.

To summarise, this chapter highlighted the fundamental problems like diverging mediated interactions associated with approaches based on linearisation when studying the interplay of two impurities and presented a simple way of dealing with these shortcomings. A detailed comparison of the results presented here with other methods, especially with the quasi-exact quantum Monte Carlo method, would be an intriguing direction for future work. In addition to that, we hope that the methods presented will serve as fertile ground to explore the bipolaron in and out of equilibrium in greater detail.

CHAPTER 6

Effective action approach to the non-equilibrium dynamics of a Newtonian impurity coupled to a fluctuating field

The following chapter is based on preliminary results [JJ4].

Introduction

In the previous chapters, we have seen how semi-classical techniques, which can loosely be characterised as c-field treatments, constitute highly effective methods for describing quantum impurities in ultracold gases. Interestingly, classical colloids interacting with fluctuating fields have also attracted significant interest in the area of statistical field theory [129–135]. In the stochastic description employed here, one usually looks at the damped motion of a classical Langevin particle coupled to an external field. Here, temperature is incorporated naturally and an integral part of the system. However, in many classical considerations, the impurity follows a first-order differential equation, and the coupling to the field is linear. Newtonian impurities that naturally arise by taking the classical limit of the quantum theory have been underappreciated in the stochastic field theory community. At first glance, one might conclude that the two flavours mentioned above only show weak similarities. Still, they can be described on an equal footing in the limiting case of a classical impurity. In fact, in chapter 4, we have demonstrated how a heavy quantum impurity is well approximated by a classical impurity following Newtonian equations of motion. In this chapter, we show how one can derive a general effective stochastic description for an impurity that couples quadratically to an arbitrary stochastic field. The effective description, accurate up to second order

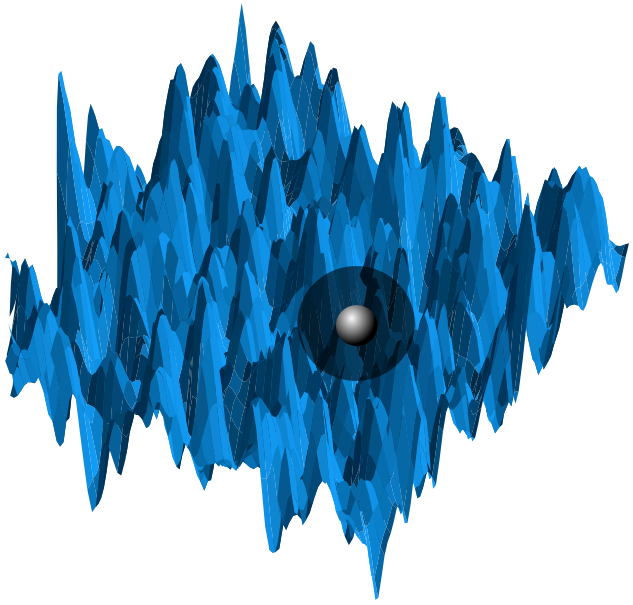

Figure 6.1: Caricature of the impurity interacting with the fluctuating field.

in the impurity-field coupling, can then be used to calculate correlators, their scaling and study the steady state in a true out of equilibrium setting.

Additionally, we benchmark our results against exact simulations, where we find good agreement in the perturbative regime. We have made the package developed to perform the simulations publicly available [136]. At this point, we want to stress that, in stark contrast to the previous chapters, all (semi-) analytical results presented here are only valid in the perturbative limit.

The work is structured as follows. We start by introducing the model in its most general form. From there, we derive a perturbative effective Langevin equation for the impurity, which is valid for a broad class of field theories. Here we focus on two different settings in particular. Namely, by integrating out the field, we first derive the effective action above the mean-field critical point $\mu > 0$, where the expectation value of the order parameter itself vanishes. We refer to this setting as the symmetric case, for which we focus on free theories. This is valid for weakly interacting field theories. Additionally, we sketch how one could include interactions in Appendix F and note that the numerical package can also deal with interacting theories of arbitrary coupling strength. Subsequently, we focus on the degenerate regime ($\mu < 0$), where the field acquires a finite expectation value on the mean-field level. Here, it is crucial to include the field's self-interaction such that the order parameter acquires a finite expectation value. For the degenerate case, we

linearise around the mean-field value of the order parameter. This ultimately leads to a free theory with linear coupling of the field's fluctuations to the impurity degrees of freedom. We then again marginalise the field and arrive at an effective Langevin equation for the impurity. To demonstrate our so far general findings, we apply the formalism to model A, which is an archetypal stochastic field theory [137] and also compare our results with numerical simulations in one dimension. We conclude by summarising the preliminary results and discussing the open questions and further directions.

6.1 The model

In the following we will outline the model in its most general form. We characterise the joint system comprising an impurity, represented via its time-dependent position $\mathbf{y}(t)$, and the field $\varphi(\mathbf{r}, t)$ via a (semi-) classical Hamiltonian

$$\mathcal{H}[\mathbf{y}, \varphi] = \mathcal{H}_\varphi[\varphi] + \mathcal{H}_{\text{int}}[\mathbf{y}, \varphi] \,, \tag{6.1}$$

which is composed of the field's Hamiltonian $\mathcal{H}_\varphi$ and the interaction Hamiltonian $\mathcal{H}_{\text{int}}$. We keep the discussion intentionally general for the field Hamiltonian. In particular, we allow for both real and complex fields. In the case of a complex field we think of φ as (φ, φ^*). For example the field theory could describe a driven dissipative condensate [73, 138–143] after taking the semi-classical limit, which is structurally similar to a Bose-Einstein condensate described by a stochastic Gross-Pitaevskii equation [144–146] or general statistical field theories like model A or model B [137, 147].

For the interaction Hamiltonian, however, we choose a specific form where the impurity couples to the energy density of the field,

$$\mathcal{H}_{\text{int}}[\mathbf{y}, \varphi] = \lambda \int \mathrm{d}^d\mathbf{r}\, V(\mathbf{y}(t) - \mathbf{r}) |\varphi(\mathbf{r}, t)|^2 \,. \tag{6.2}$$

Here, we have introduced the coupling constant λ. In terms of an arbitrary length scale L, the units

of λ are given as

$$[\lambda] = L^{d-2}\,, \tag{6.3}$$

where d denotes the dimension of the system. Ergo, $\lambda\mu^{d/2-1}$, will serve as the (dimensionless) perturbative parameter and hence is supposed to be small. Further, the coupling is locally smoothed by an interaction kernel, which describes the spatial extent of the impurity. In the following, and as is usual in the literature [52, 59, 131, 148] we choose a Gaussian interaction potential with effective range $R^{1/2}$

$$V(r) = \frac{\exp\left(-\frac{r^2}{2R}\right)}{\sqrt{(2\pi R)^d}}\,. \tag{6.4}$$

As discussed in section 2.1 for most applications within the field of ultra-cold atoms, we are in the low energy regime, and the exact shape of the potential does not play a crucial role. Instead, the s-wave scattering length and the effective range of the potential determine the properties of the impurity interaction. For a discussion on s-wave scattering, we refer to the corresponding discussion in the previous chapter and [18]. For the Gaussian potential, in particular, we refer to [75]. While the quadratic coupling might seem odd compared to a statistical field theory setting, the choice of interaction (6.2) is motivated by its quantum pendant. In quantum mechanics, it is well known that the particle couples quadratically to the field theory [10, 71], and it has routinely been utilised in the context of Bose polarons [52, 53, 59, 97].

Setting out from the Hamiltonian description of the coupled system, we assume the dynamical evolution of the impurity to be Newtonian,[1] while the field evolves dissipatively and couples to a thermal bath at temperature T, hence

$$M\ddot{\mathbf{y}}(t) = -\frac{\partial\mathcal{H}_{\text{int}}[\mathbf{y},\varphi]}{\partial\mathbf{y}} = \lambda\int \mathrm{d}^d\mathbf{r}\,(\nabla V)(\mathbf{r}-\mathbf{y}(t))|\varphi(\mathbf{r},t)|^2\,, \tag{6.5}$$

$$\nu\dot{\varphi}(\mathbf{r},t) = -\frac{\delta}{\delta\varphi(\mathbf{r},t)}\left(\mathcal{H}_\varphi[\varphi]+\mathcal{H}_{\text{int}}[\mathbf{y},\varphi]\right)+\eta(\mathbf{r},t)\,, \tag{6.6}$$

where M is the impurity's mass and ν the fields mobility, In the following we choose units such

[1] In the quantum context this can be see as a saddle point approximation of the path integral; see chapter 4.

that $\nu = 1$. The additive noise is denoted by $\eta(\mathbf{r}, t)$ and takes the form of an uncorrelated Gaussian noise sheet defined via

$$\langle \eta(\mathbf{r}, t)\eta(\mathbf{r}', t')\rangle = 2T\delta^d(\mathbf{r} - \mathbf{r}')\delta(t - t') \,. \tag{6.7}$$

These equations serve as the starting point. All numerical results presented in the chapter are calculated by directly solving this set of coupled equations.[2] In the next chapter, we develop a general perturbative framework to derive an effective Langevin equation for the impurity. The Langevin equation can then be used to obtain perturbative expressions for the force-force correlator and the response function. Throughout this chapter we use the following convention for the Fourier transform

$$\varphi(\mathbf{q}, t) = \int \mathrm{d}^d\mathbf{r}\, e^{-i\mathbf{q}\mathbf{r}}\varphi(\mathbf{r}, t) \,, \tag{6.8}$$

$$\varphi(\mathbf{r}, t) = \frac{1}{(2\pi)^d}\int \mathrm{d}^d\mathbf{q}\, e^{i\mathbf{q}\mathbf{r}}\varphi(\mathbf{q}, t) = \int \mathrm{đ}^d\mathbf{q} e^{i\mathbf{q}\mathbf{r}}\varphi(\mathbf{q}, t) \,. \tag{6.9}$$

6.2 Effective action & Langevin equation

This section presents a general perturbative framework for the impurity-field interaction that allows for deriving an effective Langevin equation for the impurity. For the symmetric case, it is possible to obtain the effective stochastic equations of motion to fixed perturbative order in λ by tracing out the field. In the degenerate case, we first linearise and then trace out the field. In either case we accomplish this by using the Martin-Siggia-Rose (MSR) formalism [149], which also naturally arises when taking the semi-classical limit in the Keldysh path integral [73, 150]. The joint stochastic weight of the impurity $\mathbf{y}(t)$ and the field $\varphi(\mathbf{q}, t)$ can be expressed in terms of path integrals over auxiliary ("ghost") fields $\tilde{\mathbf{y}}(t)$, $\widetilde{\varphi}(\mathbf{q}, t)$, by writing

$$\mathcal{P}\left(\mathbf{y}, \varphi\right) = \iint \mathcal{D}[\tilde{\mathbf{y}}]\mathcal{D}[\widetilde{\varphi}] \exp\left(-\mathcal{A}_y[\mathbf{y}, \tilde{\mathbf{y}}] - \mathcal{A}_\varphi[\varphi, \widetilde{\varphi}] + \mathcal{A}_{\mathrm{int}}[\mathbf{y}, \tilde{\mathbf{y}}, \varphi, \widetilde{\varphi}]\right) \,, \tag{6.10}$$

[2] See [136] for the implementation.

with

$$\mathcal{A}_y[\mathbf{y},\tilde{\mathbf{y}}] = \int \mathrm{d}t\, \tilde{\mathbf{y}} \left(M\partial_t^2\right) \mathbf{y}\ , \tag{6.11}$$

$$\mathcal{A}_\varphi[\varphi,\widetilde{\varphi}] = \iint \mathrm{đ}^d\mathbf{q}\mathrm{d}t\, \widetilde{\varphi}(-\mathbf{q},t)\left[\partial_t\varphi(\mathbf{q},t) + \delta_\varphi\mathcal{H}[\varphi(\mathbf{q},t)] + 2T\widetilde{\varphi}(\mathbf{q},t)\right]\ , \tag{6.12}$$

$$\mathcal{A}_{\mathrm{int}}[\mathbf{y},\tilde{\mathbf{y}},\varphi,\widetilde{\varphi}] = \lambda\left[\int \mathrm{d}t\, \tilde{\mathbf{y}}(t) \iint \mathrm{đ}^d\mathbf{q}\mathrm{đ}^d\mathbf{p}\,(-i\mathbf{q})V(\mathbf{q})e^{-i\mathbf{q}\mathbf{y}(t)}\varphi(\mathbf{p},t)\varphi(\mathbf{q}-\mathbf{p},t)\right. \tag{6.13}$$

$$\left. - \int \mathrm{d}t \iint \mathrm{đ}^d\mathbf{q}\mathrm{đ}^d\mathbf{p}V(\mathbf{q})e^{i\mathbf{q}\mathbf{y}(t)}\widetilde{\varphi}(\mathbf{p},t)\varphi(\mathbf{p}-\mathbf{q},t)\right]\ . \tag{6.14}$$

In the next step, we take the marginal density in $\mathbf{y}$ by integrating over the field φ and $\widetilde{\varphi}$. We thus describe the marginal density by an effective action $\mathcal{A}_{y;\mathrm{eff}}[\mathbf{y},\tilde{\mathbf{y}}]$, i.e.

$$\mathcal{P}[\mathbf{y},\tilde{\mathbf{y}}] = \int \mathcal{D}[\varphi,\widetilde{\varphi}]e^{-\mathcal{A}_y[\mathbf{y},\tilde{\mathbf{y}}]-\mathcal{A}_\varphi[\varphi,\widetilde{\varphi}]+\mathcal{A}_{\mathrm{int}}[\mathbf{y},\tilde{\mathbf{y}},\varphi,\widetilde{\varphi}]} = e^{-\mathcal{A}_{\mathbf{y};\mathrm{eff}}[\mathbf{y},\tilde{\mathbf{y}}]}\,. \tag{6.15}$$

Marginalising φ can be achieved in a straightforward way and perturbatively in λ, as long as φ enters the action at most quadratically. However, this requirement is not nearly as restrictive as it appears to be. Below the critical mean-field value and for non-zero self-interaction, the field has a finite mean-field expectation value, and we thus expand the field around said value, in line with standard treatments [7, 46, 73, 147]. Subsequently, we only keep terms up to second order in the fluctuating fields and focus on the coupling terms which are linear in the field.[3] Thus the resulting Hamiltonian is quadratic in the fields by construction.

For the symmetric case, the interaction can be included perturbatively. While in this chapter, we restrict ourselves to free theories in the symmetric regime, we sketch the idea in Appendix F. Furthermore, we believe that the effect of the field's self-interaction is an exciting direction for further studies. We note that for an effective description of the impurity, this is valid up to second order in λ since the back action only enters the expansion for higher orders in λ. For either case this results in the approximate effective marginal density

$$\mathcal{P}_{\mathrm{eff}} = \int \mathcal{D}[\tilde{\mathbf{y}}]\exp\left(-\mathcal{A}_y[\mathbf{y},\tilde{\mathbf{y}}] - \lambda^2\mathcal{A}_y^{(2)}[\mathbf{y},\tilde{\mathbf{y}}]\right)\ , \tag{6.16}$$

[3] This is actually closely related to the idea of the Fröhlich Hamiltonian.

where

$$\mathcal{A}_y^{(2)}[\mathbf{y},\tilde{\mathbf{y}}] = \int_\infty^\infty \mathrm{d}t\, \tilde{\mathbf{y}}(t) \int_{-\infty}^t \mathrm{d}s\, \nabla H(\mathbf{y}(t)-\mathbf{y}(s), t-s) + \frac{1}{2}\int_\infty^\infty \mathrm{d}t\, \tilde{\mathbf{y}}(t) \int_{-\infty}^t \mathrm{d}s\, \tilde{\mathbf{y}}(s) G(\mathbf{y}(t)-\mathbf{y}(s), t-s)\,. \quad (6.17)$$

We find two different expressions for H and G depending depending on the sign of μ. We roughly sketch the derivation for either case and state the results in the following. For the details of the lengthy but otherwise straightforward calculation, we refer to Appendix E.

Symmetric case $\mu > 0$

Assuming the Hamiltonian to be bilinear in the fields,[4] its functional derivative is a linear differential operator

$$\frac{\delta \mathcal{H}[\mathbf{y},\varphi]}{\delta\varphi(\mathbf{q},t)} = \mathcal{L}_\varphi(\mathbf{q})\varphi(\mathbf{q},t)\,. \quad (6.18)$$

The integral over the fields φ and $\widetilde{\varphi}$, ignoring for now the field independent pre-factor $e^{-\mathcal{A}_y[\mathbf{y},\tilde{\mathbf{y}}]}$, can be brought into a Gaussian form since the Hamiltonian is bilinear by assumption and can be written as

$$\int \mathcal{D}[\varphi,\widetilde{\varphi}] e^{-\mathcal{A}_\varphi[\varphi,\widetilde{\varphi}]+\mathcal{A}_{\mathrm{int}}[\mathbf{y},\tilde{\mathbf{y}},\varphi,\widetilde{\varphi}]}\,. \quad (6.19)$$

We can now perform the Gaussian integral over the fields and use the well know relationship

$$\det A = e^{\mathrm{Tr}\ln A}\,, \quad (6.20)$$

to re-exponentiate the resulting expression. The $\mathrm{Tr}\ln$ term is then expanded perturbatively in λ. The details of the calculation can be found in Appendix E and above criticality the following expressions

[4] As described earlier; otherwise the non-bilinearity is treated perturbatively.

for the two terms in (6.17) are obtained

$$H_{\rm sym}(\mathbf{r},t) = 2\iint \mathrm{đ}^d\mathbf{q}\mathrm{đ}^d\mathbf{p}\, e^{i\mathbf{q}\mathbf{r}}|V(\mathbf{q})|^2\,\mathrm{Re}\left[\mathcal{C}^*_\varphi(\mathbf{p},t)\chi_\varphi(\mathbf{p}-\mathbf{q},t))\right]\,, \tag{6.21}$$

$$G_{\rm sym}(\mathbf{r},t) = \iint \mathrm{đ}^d\mathbf{q}\mathrm{đ}^d\mathbf{p}\,\mathbf{q}^2 e^{i\mathbf{q}\mathbf{r}}|V(\mathbf{q})|^2\,\mathrm{Re}\left[\mathcal{C}_\varphi(\mathbf{p},t)\mathcal{C}^*_\varphi(\mathbf{p}-\mathbf{q},t)\right]\,, \tag{6.22}$$

where we introduced response and correlation function of the fields in Gaussian approximation

$$\chi_\varphi(\mathbf{r}-\mathbf{r}',t) = \langle\widetilde{\varphi}^*(\mathbf{r},t)\varphi(\mathbf{r}',t)\rangle_0\,, \tag{6.23}$$

$$\mathcal{C}_\varphi(\mathbf{r}-\mathbf{r}',t) = \langle\varphi^*(\mathbf{r},t)\varphi(\mathbf{r}',t)\rangle_0\,. \tag{6.24}$$

By $\langle ...\rangle_0$ we denote the average taken with any self-interaction of the field set to 0 and $\lambda = 0$. For field theories that obey detailed balance the dissipation-fluctuation relation $-\theta(t)\partial_t\mathcal{C}_\varphi(\mathbf{r},t) = T\chi_\varphi(\mathbf{r},t)$ holds and thus we can verify the following fluctuation dissipation relation for the effective theory

$$-\theta(t)\partial_t G_{\rm sym}(\mathbf{r},t) = TH_{\rm sym}(\mathbf{r},t)\,. \tag{6.25}$$

Degenerate case $\mu < 0$

As mentioned before, for $\mu < 0$ the field acquires a finite expectation value and we can expand the fields around their mean-field values. In particular we write

$$\varphi(\mathbf{r},t) = \sqrt{n_0} + \delta\varphi(\mathbf{r},t)\,, \tag{6.26}$$

$$\widetilde{\varphi}(\mathbf{r},t) = \delta\widetilde{\varphi}(\mathbf{r},t)\,, \tag{6.27}$$

where $\langle\varphi(\mathbf{r},t)\rangle = \sqrt{n_0}$. Performing the expansion we find

$$\mathcal{H}_\varphi[\varphi] + \mathcal{H}_{\rm int}[\mathbf{y},\varphi] \to \mathcal{H}^{(2)}_{\delta\varphi}[\delta\varphi] + \lambda\sqrt{n_0}\int \mathrm{d}^d\mathbf{r}\, V(\mathbf{r}-\mathbf{y}(t))\left[\delta\varphi(\mathbf{r}) + \delta\varphi^*(\mathbf{r})\right]\,, \tag{6.28}$$

where $\mathcal{H}^{(2)}_{\delta\varphi}$ denotes the linearised bilinear part of the Hamiltonian and we have dropped terms of order three and higher in $\delta\varphi$. After dropping the higher order terms we can write the response and correlation functions for the degenerate case as

$$\chi_{\delta\varphi}(\mathbf{r}-\mathbf{r}',t) = \langle \delta\widetilde{\varphi}^*(\mathbf{r},t)\delta\varphi(\mathbf{r}',t)\rangle_0 \tag{6.29}$$

$$\mathcal{C}_{\delta\varphi}(\mathbf{r}-\mathbf{r}',t) = \langle \delta\varphi^*(\mathbf{r},t)\delta\varphi(\mathbf{r}',t)\rangle_0 \ . \tag{6.30}$$

Additionally, we also neglect the quadratic interaction term since it will be dominated by the linear term, as long as the mean-field expectation value is large enough or the fluctuations around it remain small. Again we can marginalise the fields. Due to the linear term in $\delta\varphi$, this is somewhat simpler for the $\mu < 0$ case and does not involve the perturbative expansion of a $\mathrm{Tr}\ln$ term. For the degenerate case we obtain

$$H_d(\mathbf{r},t) = 4n_0 \int \mathrm{đ}^d\mathbf{q}\, e^{i\mathbf{q}\mathbf{r}} |V(\mathbf{q})|^2 \,\mathrm{Re}\left[\chi_{\delta\varphi}(\mathbf{q},t)\right] \ , \tag{6.31}$$

$$G_d(\mathbf{r},t) = 4n_0 \int \mathrm{đ}^d\mathbf{q}\, \mathbf{q}^2 e^{i\mathbf{q}\mathbf{r}} |V(\mathbf{q})|^2 \,\mathrm{Re}\left[\mathcal{C}_{\delta\varphi}(\mathbf{q},t)\right] \ . \tag{6.32}$$

For the details of the calculation we refer to Appendix E. We observe that also for the degenerate case we can verify the fluctuation dissipation relation.

Langevin equation

By performing the "Inverse MSR", which is equivalent to introducing the Hubbard-Stratonovich [151, 152] noise field $\zeta(\mathbf{r},t)$ we can write

$$e^{\int_\infty^\infty \mathrm{d}t\, \tilde{\mathbf{y}}(t)\int_{-\infty}^t \mathrm{d}s\, \tilde{\mathbf{y}}(s) G(\mathbf{y}(t)-\mathbf{y}(s),t-s)} = \int \mathcal{D}[\zeta(t)] e^{-\int \mathrm{d}t\, \tilde{y}(t)\zeta(\mathbf{y}(t),t)} \mathcal{P}_\zeta[\zeta] \,, \tag{6.33}$$

with the (Gaussian) weight for the ζ field

$$\mathcal{P}_\zeta[\zeta] \propto \exp\Big(-\frac{1}{4}\iint \mathrm{d}t\,\mathrm{d}s\, \zeta(\mathbf{y}(s),s) G^{-1}(\mathbf{y}(t)-\mathbf{y}(s),t-s)\zeta(\mathbf{y}(t),t)\Big) \ . \tag{6.34}$$

Here $G^{-1}(r,t)$ is the functional inverse of $G(r,t)$ satisfying $\int \mathrm{d}u\, G^{-1}(r,u-t)G(r,s-u) = \delta(t-s)$. Then, by performing the integral over $\tilde{\mathbf{y}}$ to obtain a δ-functional over paths and interpreting the result as an effective Langevin equation

$$M\ddot{\mathbf{y}}(t) = -\lambda^2 \int_0^t \mathrm{d}s\, \nabla H(\mathbf{y}(t) - \mathbf{y}(s), t-s) + \lambda\zeta(\mathbf{y}(t), t)\ , \tag{6.35}$$

with

$$\langle \zeta(\mathbf{r},t)\zeta(\mathbf{r}',s)\rangle = G(\mathbf{r}-\mathbf{r}', t-s) \tag{6.36}$$

we can recast the problem into a general stochastic differential equation, only containing the impurity coordinate $\mathbf{y}$. From the effective Langevin equation it is now straightforward to read off for example the force-force correlator (FFC) of the impurity

$$M^2 \langle \ddot{\mathbf{y}}(s)\ddot{\mathbf{y}}(t)\rangle = \lambda^2 G(0, t-s) + \mathcal{O}(\lambda^3)\ . \tag{6.37}$$

The FFC can be integrated to yield other correlation functions, and additionally, is a quantity that is also accessible numerically and can therefore serve as a diagnostic tool to assess the validity of the effective Langevin equation. We are now in the position to apply the developed formalism to specific field theories. In the following we focus on the relatively simple case of a real field, where the order parameter is not conserved.

6.3 Model A

In this section we we apply the developed methods to the Landau–Ginzburg–Wilson Hamiltonian

$$\mathcal{H}_\varphi[\varphi] = \int \mathrm{d}^d\mathbf{r}\, \left(|\nabla\varphi(\mathbf{r})|^2 + \frac{\mu}{2}|\varphi(\mathbf{r})|^2 + \frac{u}{4}|\varphi(\mathbf{r})|^4 \right)\ , \tag{6.38}$$

where μ determines the mean-field expectation value of the condensate and u is the self interaction strength of the field. In the remainder, we focus on model A, where the field's dynamics are

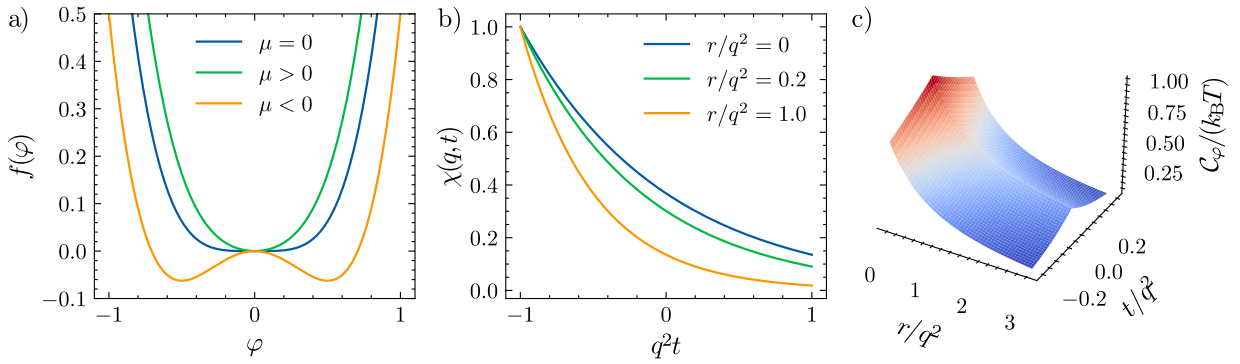

Figure 6.2: a) The non-derivative part $f(\varphi) = \mu\varphi^2 + \frac{u}{4}\varphi^4$ of the Landau–Ginzburg–Wilson Hamiltonian. We can see how for $\mu < 0$ a degenerate minimum emerges. The b) response and c) correlation function for model A in the Gaussian approximation ($u = 0$).

determined by the functional derivative of $\mathcal{H}_\varphi[\varphi]$. Model A is related to the field theory used to describe the ultracold Bose gas in the rest of this thesis by taking the fields to be real and performing a Wick rotation in time, which results in a non-conserved order parameter. We show the non-gradient part of the Hamiltonian density and the free propagators ($u = 0$) for model A in Figure 6.2. Here we can see that in this case, the model possesses a discrete Ising Z_2 symmetry. Before delving into the results, we think, given our slightly unconventional unit-system[5] it is beneficial to explicitly state the units of the parameters and fields at play. The units can be found by noting that the expression in the exponential of (6.10) has to be dimensionless. In terms of an arbitrary length scale L, we then find

$$[\mu] = L^{-2} \quad [x] = L^1, \quad [t] = L^2, \quad [T] = r^0, \quad [R] = L^2, \quad [\widetilde{\varphi}(\mathbf{r}, t)] = L^{-d/2-1}, \tag{6.39}$$
$$[\varphi(\mathbf{r}, t)] = L^{1-d/2}, \quad [\lambda] = L^{d-2}, \quad [u] = L^{4-d}, \quad [y] = L^1, \quad [\tilde{y}] = L^{-1} \quad [M] = L^2 .$$

Symmetric case $\mu > 0$

For model A we find the response and correlation function in Gaussian approximation $u = 0$ and $\lambda = 0$ to be

$$\chi_\varphi(\mathbf{q}, t) = e^{-(\mathbf{q}^2+\mu)t}\Theta(t) , \tag{6.40}$$

[5]It should be noted that we did not set $T = 1$ as is usual in, for example, renormalisation group treatments [138, 147].

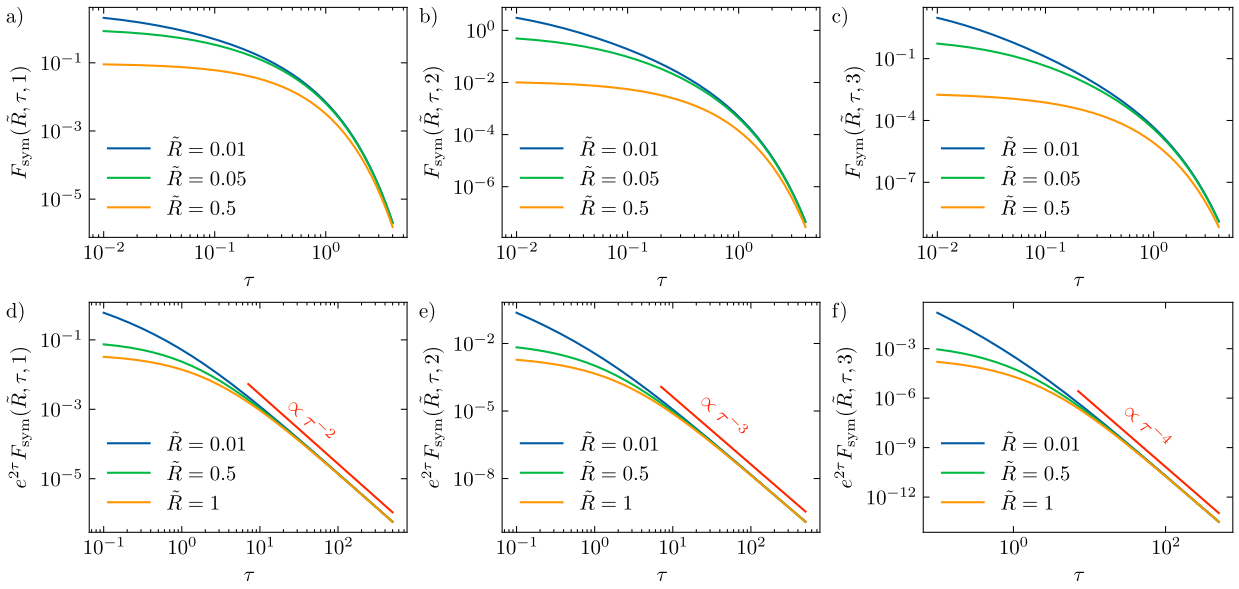

Figure 6.3: a)-c) The FFC scaling function (6.43) for model A and $d = 1, 2, 3$ in the symmetric regime for short time scales . We see that for a large effective potential range R the scaling function remains almost constant for early times. d)-f) The symmetric scaling function for longer times and $d = 1, 2, 3$. Here we multiplied by $e^{2\tau} = e^{2\mu t}$ to show the power-law decay τ^{-1-d}, which depends on the dimension of the system. While for early times, the behaviour is non-universal, for later times, the curves collapse, because the exact shape of the potential no longer plays a role.

$$\mathcal{C}_\varphi(\mathbf{q}, t) = T\frac{e^{-(\mathbf{q}^2+\mu)|t|}}{\mathbf{q}^2+\mu}\,. \tag{6.41}$$

We note that, in general, the approximation $u = 0$ is quite restrictive, especially for the case $\mu \approx 0$ or $\mu < 0$. Nevertheless, in the case where μ is positive and non-zero, it is less restrictive and can be used to approximate weakly interacting fields. This is because, in the symmetric case, the expectation value of the field is zero. Therefore, in first approximation, u only weakly modifies the impurity-field interaction. We are now in the position to calculate the force-force correlator (6.37)

$$M^2\left\langle \ddot{\mathbf{y}}(0)\ddot{\mathbf{y}}(t)\right\rangle = \lambda^2 T^2 \mu^{d-1} F_{\mathrm{sym}}(R\mu, t\mu)\,, \tag{6.42}$$

with the (dimensionless) scaling function

$$F_{\mathrm{sym}}(\tilde{R},\tau) = \frac{\pi^2}{(2\pi)^{2d}\Gamma(d/2+1)^2}e^{-2\tau}\iint \mathrm{d}x\,\mathrm{d}y\, x^{d-1}y^{d+1}\frac{e^{-y^2\tilde{R}-\tau((x-y)^2+x^2)}}{(1+x^2)(1+(y-x)^2)}\,, \tag{6.43}$$

where we have defined the dimensionless quantities $\tau = |\mu|t$ and $\tilde{R} = R|\mu|$. The double integral can be performed numerically. In one dimension, one can simplify this expression and arrive at the semi-analytical function

$$F_{\mathrm{sym}}(\tilde{R},\tau,1) = \frac{1}{2\sqrt{\pi}} e^{-2\tau}\partial_{\tilde{R}} \int_0^\infty \mathrm{d}m \frac{e^{\frac{\tau(\tau+m+2\tilde{R})+\tilde{R}m}{\tau+m+\tilde{R}}} \operatorname{erfc}\left(\sqrt{\frac{\tau(\tau+m+2\tilde{R})+\tilde{R}m}{\tau+m+\tilde{R}}}\right)}{\sqrt{\tau+m+\tilde{R}}} e^{-m} \,. \tag{6.44}$$

In Figure 6.3 we show the scaling function for short and long times. Here we can identify two regimes, namely, for short times, the behaviour is determined by $\tilde{R}+\tau$ and thus is almost constant for large $\tilde{R}$ at short times. For long times we can extract the decay as

$$F_{\mathrm{sym}}(\tilde{R},\tau,1) \propto e^{-2\tau}\tau^{-(d+1)}, \quad \tau \gg 1 \,. \tag{6.45}$$

While the power-law part of the decay is hard to observe for model A as the exponential decay overshadows it, we note that there are other field theories, like model B in the symmetric regime, where the exponential decay is absent. For model B, the dynamics of the field is governed by $-\nabla^2\delta_\varphi \mathcal{H}^A[\varphi]$ and in the symmetric regime the FFC shows the same algebraic decay without the exponential part as Model A. By integrating the FFC, one can obtain other correlators like the velocity correlator or the position correlator. We want to demonstrate this by discussing the velocity correlator. Here, we find that the scaling function $\mathcal{V}(\tau_1,\tau_2) = \int^{\tau_1}\int^{\tau_2} \mathrm{d}\tau\,\mathrm{d}\tau'\, F(\tau,\tau')$ is given by

$$\begin{aligned}\mathcal{V}(\tau_1,\tau_2) \propto \iint \mathrm{d}x\,\mathrm{d}y\, &\frac{x^{d-1}y^{d+1}e^{-y^2\tilde{R}}}{(1+x^2)(1+(y-x)^2)} \\ &\times \frac{e^{-\alpha(x,y)\tau_1} + e^{-\alpha(x,y)\tau_2} - 1 - e^{-\alpha(x,y)|\tau_1-\tau_2|} + 2\alpha(x,y)\min\{\tau_1,\tau_2\}}{\alpha(x,y)} \,,\end{aligned} \tag{6.46}$$

with $\alpha(x,y) = 2 + (x-y)^2 + x^2$. Even though this expression looks quite cumbersome at first, we can make an important observation at this point already, namely that the mean square velocity ($\tau_1 = \tau_2$) grows linearly in time. The linearly increasing kinetic energy, which is directly linked to the root mean square velocity, might look odd at first but is easily explained by noting that we have not assumed any confinement or friction for the impurity.

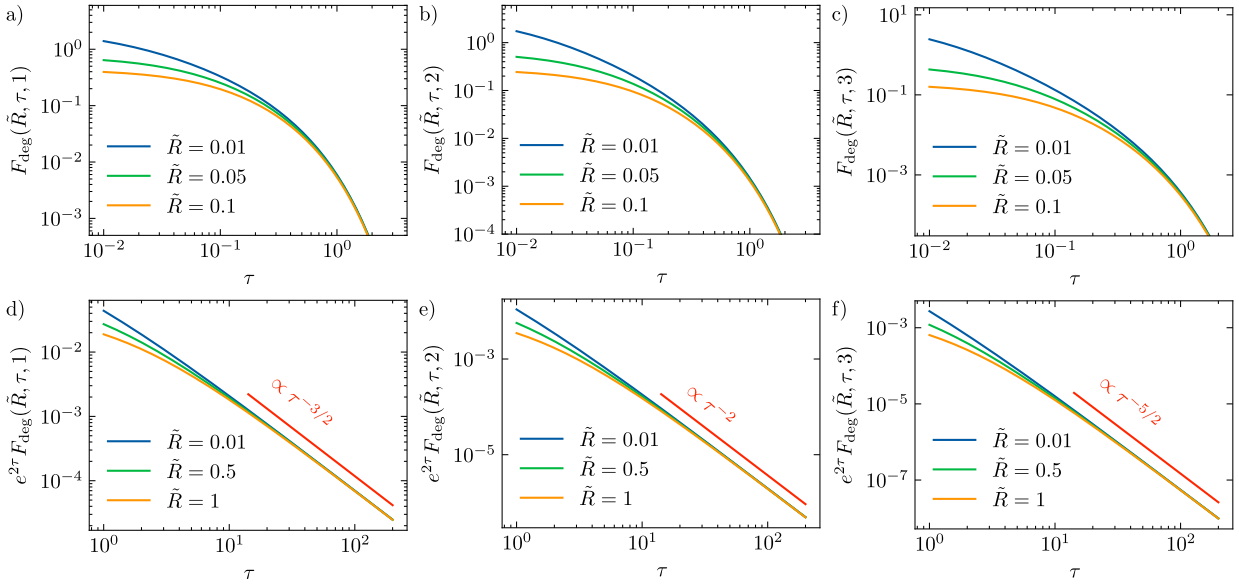

Figure 6.4: a)-c) The scaling function of the FFC (6.51) for model A in the degenerate regime and $d = 1, 2, 3$. The incomplete gamma function does not have a closed form expression for the asymptotic behaviour as $t \to 0$. d)-f) The degenerate scaling function for longer times. We multiplied the scaling function by $e^{2\tau} = e^{2\mu t}$ to show the additional power-law decay, which depends on the dimension of the system.

Degenerate case $\mu < 0$

We now turn our attention to the degenerate case $\mu < 0$. As can be seen in Figure 6.2 for $\mu < 0$ the field's potential has minima at

$$\varphi_0 = \sqrt{n_0} = \pm\sqrt{\frac{|\mu|}{u}}\,. \tag{6.47}$$

As described in the previous section, we expand the field around the finite mean-field expectation value and drop terms of order three and higher. At the same time, we only keep the linear terms in the impurity-field interaction since those are the most dominant. Doing so ultimately results in the (approximate) Hamiltonian

$$\mathcal{H}_\varphi[\delta\varphi] = \int \mathrm{d}^d\mathbf{r}\, \left(|\nabla\delta\varphi(\mathbf{r})|^2 + \mu|\delta\varphi(\mathbf{r})|^2\right) \tag{6.48}$$

and

$$\mathcal{H}_{\mathrm{int}} = \lambda\sqrt{n_0}\int \mathrm{d}^d\mathbf{r}\, V(\mathbf{r}-\mathbf{y}(t))\delta\varphi(x)\,. \tag{6.49}$$

Again, we can use the MSR formalism to rewrite the problem as a path integral and perform the

same steps as before. The only difference is that we can integrate the fields out exactly, and no further approximations have to be made. Thus, we directly arrive at an effective action for the impurity. The simplicity of performing the integration is, of course, only due to the approximation of dropping higher-order terms in $\delta\varphi$ done earlier. We can also see that the response (correlation) function for the fluctuating field in the $\lambda = 0$ case is almost identical to the $\mu > 0$ case, with the only difference that $\mu \to 2|\mu|$. Using (6.31) and (6.37) one can now calculate the FFC fully analytically and find

$$M^2 \langle \ddot{\mathbf{y}}(0)\ddot{\mathbf{y}}(\tau)\rangle = 4\lambda^2 T n_0 |\mu|^{d/2} F_{\mathrm{deg}}(R|\mu|, t|\mu|, d) \,, \tag{6.50}$$

with

$$F_{\mathrm{deg}}(\tilde{R}, \tau) = \frac{\pi^{d/2}}{(2\pi)^d} 2^{\frac{d-2}{2}} e^{2\tilde{R}} \Gamma\left(-\frac{d}{2}, 2(\tilde{R}+\tau)\right) \,, \tag{6.51}$$

where $\Gamma(\cdot\,,\cdot)$ is the incomplete gamma function [153]. From here we can again extract the asymptotic scaling of the FFC

$$F_{\mathrm{deg}} \propto e^{-2\tau} \tau^{-d/2-1} \quad \tau \gg 1 \,, \tag{6.52}$$

which differs from the symmetric case. We show the scaling function and its asymptotic behaviour in Figure 6.4, where we can again observe the two different regimes for short and long times.

Numerical considerations

This section will briefly discuss the numerical results and compare them to the perturbative calculations. For simplicity, we focus on the one-dimensional setting for now. However, with the the numerical package developed within the framework of this chapter it is also possible to study higher dimensional systems. For all numerical calculations we have set $M = 1$. It should be mentioned that while for many one dimensional theories, there are problems with divergencies, especially at

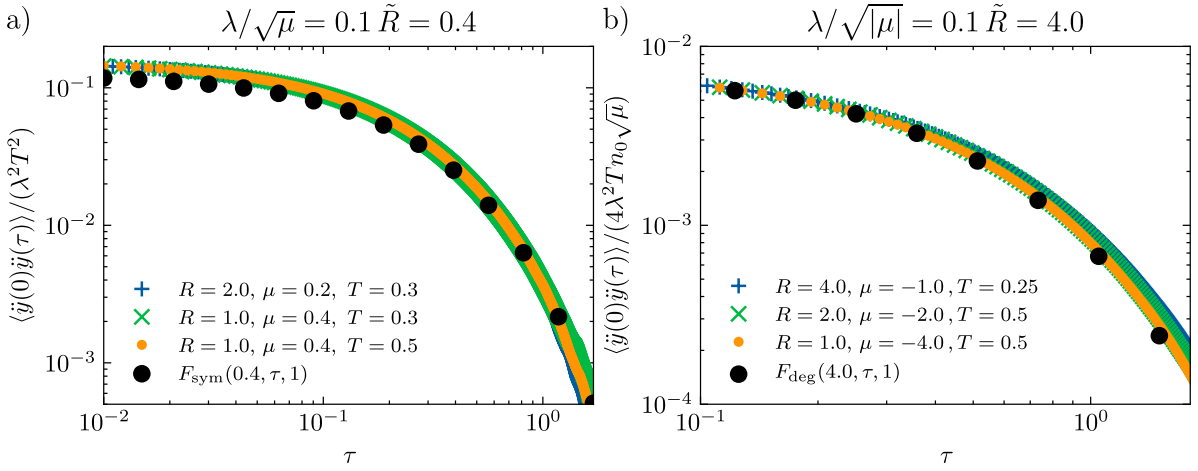

Figure 6.5: The FFC for model A for a) the symmetric and b) the degenerate case within the perturbative regime. The coloured markers are the numerically obtained values, which are calculated by solving the stochastic equations without any approximations. The system size is $N = 1024$ and $M = 1$. The solid black dots represents the theoretical values, which are accurate up to second order in λ. All values in the legend are in units of the lattice spacing and are only provided to demonstrate the scaling collapse.

the critical point[6] [137, 147, 154, 155], in the following the case, $\mu = 0$ is not considered, and thus, all our analytical results are finite. For all numerical considerations, the system has a natural UV (IR) cutoff given by the (inverse) system size. We also note that all numerical results presented here do not depend on the system size within the time scales needed to "measure" the force-force correlator. The numerical results are obtained by initialising a field according to the action with $\lambda = 0$ and then letting the field evolve until a steady state with the impurity is reached. Only then we start measuring the correlator. For the time propagation of the field, a pseudo-spectral Fourier Galerkin method [156] was used, while the time propagation for the impurity was performed using the leap-frog method [157]. Denoting the discretised version of $\varphi(\mathbf{r}, t)$ and $\mathbf{y}(t)$ as $\varphi_{\mathbf{n},i}$ and $\mathbf{y}_i$ respectively each propagation step takes the form

$$\mathbf{y}_{i+1} = \mathbf{y}_i + \Delta t \dot{\mathbf{y}}_i + \frac{\Delta t^2}{2} \lambda \Delta x \sum_{\mathbf{n}} (\nabla V)(\mathbf{n}\Delta x - \mathbf{y}_i) |\varphi_{\mathbf{n},i}|^2 \tag{6.53}$$

$$\varphi_{\mathbf{n},i+1} = \mathcal{F}^{-1}\left(\frac{1}{1 + \Delta t \mathbf{k}^2} \mathcal{F}\left[\varphi_{\mathbf{n},i} - \Delta t \left(\varphi_{\mathbf{n},i}^2 + \mu + 2\lambda V(\mathbf{n}\Delta x - \mathbf{y}_i) \right) \varphi_{\mathbf{n},i} + \sqrt{\frac{2T\Delta t}{\Delta x}} \xi_{\mathbf{n},i} \right] \right) \tag{6.54}$$

[6] In particular for $u = 0$ where the growth of the zero-mode is unbounded.

$$\dot{\mathbf{y}}_{i+1} = \dot{\mathbf{y}}_i \frac{\Delta t}{2} \Delta x \lambda \left(\sum_{\mathbf{n}} (\nabla V)(\mathbf{n}\Delta x - \mathbf{y}_i) |\varphi_{\mathbf{n},i}|^2 + \sum_{\mathbf{n}} (\nabla V)(\mathbf{n}\Delta x - \mathbf{y}_{i+1}) |\varphi_{\mathbf{n},i+1}|^2 \right) \tag{6.55}$$

where $\xi_{\mathbf{n},i} \sim \mathcal{N}(0, \mathbf{1})$, Δt is the time stepping and Δx the grid spacing. For more details on the implementation we refer to [136]. While it is difficult to numerically verify the long time behaviour due to the exponential decay observed for model A, we can see in Figure 6.5 that for the perturbative regime, our analytical expressions agree well with the numerical results. We also note that all analytical results are obtained in the continuum limit for infinite systems.

6.4 Summary & outlook

In this chapter, we have considered a (classical) impurity coupled to a fluctuating field. We have derived a perturbative effective action only containing the impurity degrees of freedom, applicable to a wide range of field theories. Here, we found that it is essential to distinguish between the symmetric ($\mu > 0$) and degenerate ($\mu < 0$) case. Subsequently, we applied our results to model A, where we focused on the FFC and found that the scaling is determined by a dimensionless scaling function F. With the help of the obtained scaling function, we found that the long-time behaviour of the FFC is distinct for the symmetric and degenerate regime. Additionally, we investigated the effects of the size of the impurity and found that for large $\tilde{R}$, the decay of the FFC on short time scales is slowed down. In contrast, the long-time behaviour is universally independent of $\tilde{R}$. Lastly, we tested our perturbative method against numerical results obtained by simulating the complete system. For simplicity, we focused on one-dimensional systems and found good agreement with the effective theory in the perturbative regime.

While the results presented so far are promising, there are many exciting avenues for future studies. A natural next step is to apply our results to a driven dissipative condensate [73, 138–143] and, for example, also compare the predictions with those made in [158], where a treatment using more conventional tools based on the Fröhlich paradigm was developed. We also note that the analysis done for model A in the symmetric case straightforwardly carries over to model B, where the order parameter is conserved. For model B, one does not find an exponential decay for the

FFC at long times but rather only an algebraic decay. Lastly, we would like to note that while the numerical results presented here focused on the perturbative regime, the applicability is, in principle, not limited to specific couplings. It would certainly be worthwhile to study the behaviour of the impurity in the strong coupling regime and for different fields numerically or even investigate the influence of a trapping potential on the impurity.

CHAPTER 7

Conclusion & outlook

This work demonstrated how semi-classical approaches are well suited to model the interaction between impurities and ultracold bosons. In particular, we introduced treatments based on c-field methods to describe the system in and out of equilibrium. We used these methods to study the properties of a single impurity immersed in an ultracold Bose gas and also addressed the medium mediated interaction between two impurities. This section highlights the main results, their impact and suggests further work in the area. We will proceed in the order that the results appear throughout the thesis.

Our first result pertains to the equilibrium properties of the one-dimensional Bose polaron. Using the analytical solution to the mean-field equations and a generalised Bogoliubov transformation to include first-order quantum corrections, we developed a simple and highly accurate description of the one-dimensional Bose polaron valid for typical experimental parameters. Besides the high predictive power and accuracy of the treatment, it also provides powerful insights into the importance of taking the condensate deformation into account. Furthermore, we were able to show that, when starting with the correct mean-field solution, quantum corrections remain small within the parameter space explored; this important realisation paves the way to applying similar approximations to other polaron problems. Beyond the cases considered in this work, the presented methodology has since been applied to other problems, such as bipolarons in one dimension [88, 159]. Additionally, similar approximations based on the GPE have also been used in higher dimensions [52, 53, 59]. Another interesting question arising from the equilibrium treatment is how the presented technique can be amended to the out of equilibrium setting or finite temperatures.

Our second result addresses this question, and here again, we considered an impurity interacting with an ultracold Bose gas and explored the temporal dynamics of the impurity after a sudden impurity-boson interaction quench. Motivated by the previous findings, we adapted the truncated Wigner approximation to develop a mean-field plus first-order quantum correction approach. An essential contrast to earlier works is that for dynamical problems and at finite temperature, the often employed LLP transformation, which eliminates the impurity from the problem, is not suitable without further approximations. We overcame this challenge by describing the impurity degrees of freedom using the position and momentum representation in the path integral. We found that the main advantage of this method compared to, for example, the coherent state representation is that it emphasises the particle nature of the impurity. Furthermore, it enables the straightforward inclusion of first-order quantum corrections. This, in turn, permits the description of the temporal evolution of heavy impurities, and our treatment also includes finite temperatures. We identified different regimes for strong and weak impurity-Bose gas couplings, which may serve as experimental guidance. Additionally, we developed an approximate scheme to calculate the absorption spectrum. We believe that the methodology to calculate the quench dynamics of the impurity presented here is a powerful tool which could be used to study the interplay between several impurities and study their induced correlations in a dynamical setting. The presented treatment could also be adapted to explore the influence of a trap on the impurity delocalisation. Additionally, we envision that similar techniques could be used for higher-dimensional systems, especially when paired with efficient modifications of the truncated Wigner approximation.

After the extensive treatment of the one-dimensional problem, we looked at three-dimensional systems, where we studied the medium-mediated exchange interaction between two impurities using the Born-Oppenheimer approximation paired with a mean-field treatment. The main finding here is that, in contrast to the single impurity case, the Fröhlich model can not be easily extended to go beyond the weak coupling limit and how this can be remedied using semi-classical approximations. In the regime we considered, the mediated interaction is mainly attributed to the density deformation; thus, quantum corrections due to the modified phonons can be neglected. Using the c-field based formalism, we calculated the mediated impurity-impurity interaction and the bipolaron binding

energy. We conjecture that the strategy presented here could serve as the starting point for studying a (bi)polaron gas and identifying the different regimes, ranging from pair formation to multi-particle bound states. We also believe that similar approximations could be used to study the temporal evolution of the bipolaron formation.

In the last chapter, we highlighted the similarities between the polaron problem after applying semi-classical approximations considered so far and standard settings within the area of classical statistical field theory. Here, we developed a general perturbative framework to address the dynamics of an impurity interacting with a fluctuating field. We found that the demarcation of the two cases $\mu > 0$ and $\mu < 0$ should be made. We benchmarked our results against numerical calculations for model A and found excellent agreement in the perturbative limit. While most findings in this chapter are preliminary, we believe that the presented results are an exciting step towards bridging the two fields. We furthermore think that applying our formalism to other field theories, like a driven dissipative condensate in the semi-classical limit, could be another promising avenue.

Appendix A

Experimental realisation of the Bose polaron

This Appendix discusses exemplary experimental realisations of the Bose polaron and, in particular, focuses on the parameter regime accessible by current experiments. We first consider the one-dimensional case, that was considered in chapter 3 and chapter 4. In fact the parameters in chapter 3 were chosen to match the Catani experiment [22]. Next, we turn our attention to the three-dimensional case, where a larger number of experiments have been performed. While to this date, there have been no experiments on bipolarons directly, we use the polaron experiments to contextualise the findings from chapter 5.

1D

In chapter 3 and chapter 4 the one-dimensional Bose polaron was studied. In particular, in chapter 3, we developed a general approach to the one-dimensional Bose polaron and used the parameters of the Catani experiment [22] to demonstrate our findings. In this subsection, we briefly summarise the parameters and discuss why the experimental results deviate from our results and quasi-exact DMC results. For an in-depth discussion, we refer to [37]. In the experiment reported in [22] ^{41}K impurities are initially localised in the surrounding ultracold ^{87}Rb bath, and their subsequent expansion is measured, which can be used to calculate the effective mass of the polaron. The mass ratio here is given by $m/M = 41/87 \approx 0.47$. In the following, we briefly summarise their experimental procedure. The initial system is brought into the ultracold regime through microwave evaporation and subsequent optical evaporation. After tuning the system to vanishing interspecies interaction

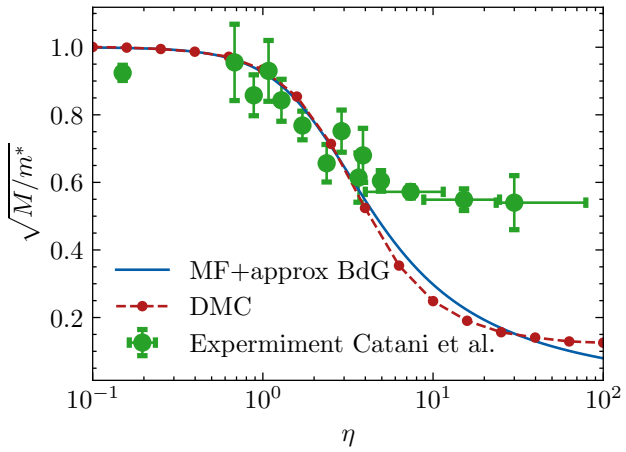

Figure A.1: Comparison between the effective mass as predicted by DMC calculations in [37] and the theoretical results obtained in chapter 3 with the experimentally values from [22]. It can be seen that for weak coupling the agreement between theory and experiment is good. We attribute the deviation for large coupling to the inhomogeneity of the condensate and the breakdown of the strict one-dimensional treatment.

and controlling for the gravitational sag, the system is brought into a quasi-1D state through a 2D lattice. The lattice transverse harmonic oscillator frequency far exceeds both species' chemical potential and temperature, and thus an array of 1D systems is created. Afterwards, the interaction strength g_{IB} is tuned to the desired value by slowly and linearly ramping up the magnetic field.[1] Lastly by turning off the light blades that localise the impurity the axial size $\sigma(t) = \sqrt{\left\langle \hat{\mathbf{X}}(t)^2 \right\rangle}$, from which the effective mass can be calculated, is measured through in situ absorption imaging. To obtain the effective mass, one uses that $\sigma(t) \propto 1/\sqrt{m^*}$. After normalising this relationship to the $g_{\mathrm{IB}} = 0$ value, the effective mass can be calculated from the experimental values. They estimate the Rb peak filling and density to be 180 atoms per tube, translating to $n_{\mathrm{Rb}} = 7\mu\mathrm{m}^{-1}$ and the peak K filling to be 1.4, which justifies focusing on a single impurity. In Figure A.1, we show the comparison between the experimental values and the theory. It becomes apparent that the experiment and the theory only agree for weak to moderate couplings. The discrepancy can be explained by noting that even though the confinement is strong for large coupling, even small deviations from a strictly one-dimensional system can greatly influence the effective mass, as it allows for a current flow past the impurity. Additionally, it should be noted that the condensate is not homogeneous, which has a sizable influence for large couplings. For a more detailed discussion

[1] The interaction strength $g_{\mathrm{BB}} = 2.36 \times 10^{-37}\mathrm{Jm}$ is independent of this magnetic field

Experiment	Mass-ratio m/M	Concentration
MIT-experiment [31]	$40/23 \approx 1.74$	0.3%
Aarhaus-experiment I [5]	1	not exactly reported ($< 10\%$)
JILA-experiment [30]	$40/87 \approx 0.46$	$\approx 1\%$ (from peak density)
Aarhaus-experiment II [32]	1	$\approx 5\%$

Table A.1: The mass ration of the boson-impurity mass m/M realised in different experiments.

on the comparison between the experiment and the theory, we refer to [37].

3D

In this subsection, we look at the experimental realisation of the three-dimensional Bose polaron. We note that in this work, we have only studied three-dimensional bipolarons, where no experimental realisation exists as of now. We thus only briefly summarise the experimentally achievable regime and emphasise the aspects important for possible realisations of the bipolaron in light of the results of chapter 5, i.e. the concentration and the mass ratio, which are summarised in Table A.1. Here, we note that the experiments performed so far are in a regime where mediated impurity-impurity interaction is largely negligible. This has been explicitly tested, for example, in [5], which has the highest impurity density of all experiments. Nevertheless, as noted in [32] higher concentrations are achievable. A major challenge here would be to distinguish between mediated impurity-impurity interactions and single polaron physics. Additionally, we note that mass ratios of at least 0.5 are achievable, and we thus believe that the treatment presented in chapter 5 based on the Born-Oppenheimer approximation is applicable in this regime.

Generally, there are two different approaches to creating the impurity. On the one hand, as done in [30, 31], one can create a mixture with two different species, where one is very dilute; on the other hand, it is possible to work with only one species and use an rf-pulse to transfer a small portion of the atoms into a different spin-state. The spin polarised atoms serve as the impurities in the system. One usually starts with very weak boson-impurity interaction or in the one-species case without impurities and uses evaporation cooling to bring the system into the ultracold regime. Typical temperatures here are $T = 0.1 - 0.8\,T_{\mathrm{C}}$, where T_{C} is the critical temperature of the Bose gas. Most quantities of the impurity can then be extracted by performing rf-spectroscopy. There

are two distinct ways this can be done. Either by injection spectroscopy, performed in [5, 30, 32], where the impurity is suddenly quenched into the Bose gas or through ejection spectroscopy, used in [31], where the impurity is ejected from the condensate. The injection is usually realised through an rf-pulse which transfers the impurity into an interacting state. For the ejection spectrum, a broad Feshbach resonance is used to slowly ramp up the interaction to the desired value. Then the impurity is transferred to a non-interacting state by an rf-pulse. We note that, as pointed out in [31], that the ejection and injection spectrum are distinct, and the former probes the excitation spectrum of the polaron. In contrast, the latter explores the equilibrium properties of the impurity.

Appendix B

Numerical error of the quench dynamics

In this Appendix, we discuss the exact numerical parameters and the associated errors for the results presented in chapter 4. Some error bounds can be straightforwardly estimated, but others, such as finite-size effects, require further investigation. For the time propagation of the bosonic field, the symmetric split-step Fourier algorithm outlined in section 2.2 was used. The propagation error for each trajectory associated with the time discretisation is thus $\mathcal{O}(\Delta t^2)$, where Δt is the time spacing. For all results presented in the main part and the appendix, a time-spacing of $\Delta t = 0.001$ was chosen, which leads to an error or order 10^{-6}. For the propagation of the impurity position, a second-order Runge-Kutta scheme was used, resulting in a local time error of $\mathcal{O}(\Delta t^3)$. We note that for the symmetric split-step Fourier algorithm, we always used the most recent version of the

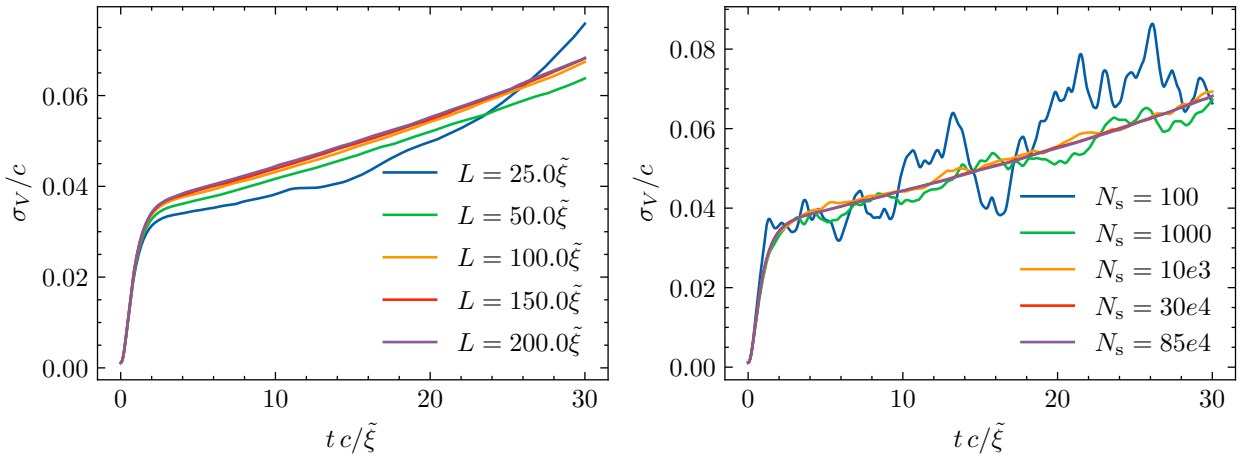

Figure B.1: The velocity variance of the impurity over time for a) different system sizes with $N_s = 850 \times 10^3$ and b) different number of realisations with $L = 200\tilde{\xi}$. All other parameters are $\eta = 3.0$, $\alpha = 0.2$, $\gamma = 0.04$, $n_0 = 5\tilde{\xi}$, $a_0 = 3/\tilde{\xi}$ and $T = 0.5\tilde{\xi}/c$.

impurity position, i.e. after performing half a time step for the second step in real space to guarantee an error of order Δt^2. We can therefore conclude that the error from time stepping is negligible in all presented results.

Another critical error source comes from finite-size corrections. This error can not be estimated from first principles. However, we note that the polaron is a local quantity. Therefore, we do not expect finite-size corrections to be dominant as long as the system is larger than the position variance. In all our simulations, we chose the system size to be $L = 200\tilde{\xi}$, unless otherwise stated and note that the impurity position variance did not exceed $20\tilde{\xi}$ in any of the results presented. As noted in the main text the space discretisation has to be chosen such that $n_0 l \gg 1$ and $l < \xi(\lambda)$ and we thus fix $l = \frac{\xi}{2}$ in the presented results and note that they are independent of the exact lattice spacing as long as the mentioned conditions are met. Additionally, we exemplary show the dependence of the variance of the impurity velocity in Figure B.1 for $\eta = 3$ and note that the results converge quickly with increasing system size.

Lastly, we want to discuss the error arising from sampling over finitely many trajectories. In general it is know that the error for an observable Ω Monte-Carlo simulations scales like $\sim \sigma_\Omega/\sqrt{N}$ [160]. For all our results we have averaged over $N_\mathrm{s} = 8.5 \times 10^5$ realisations, leading to an error of $\max_t [\sigma_\Omega(t)] \times 10^{-3}$. We note that $\sigma_\Omega(t)$ can be estimated while performing the simulations, and we generally found that it was of the order of the observed quantity itself. Thus, the relative error is of order 10^{-3}. In Figure B.1 we demonstrate the convergence in N_s and find that convergence is generally achieved after averaging 10^5 realisations.

Appendix C

Two stationary impurities in an ideal Bose gas

In this Appendix, we discuss two stationary impurities in an ideal Bose gas. The appeal here is that one can solve this model analytically and study the emergence of the bound state in more detail. We consider N bosons interacting with two static impurities located at $\pm R/2$. The Hamiltonian can now be expressed as the sum of single-particle Hamiltonians

$$\hat{H} = \sum_n \Big(\frac{\hat{P}_n^2}{2m} + \frac{2\pi}{m} a_{\mathrm{IB}} \Big[V(\hat{\mathbf{Q}}_n - \mathbf{R}/2) + V(\hat{\mathbf{Q}}_n + \mathbf{R}/2) \Big] \Big), \tag{C.1}$$

where the interaction potentials are taken to be the pseudo potential $V(r) = \frac{\pi a_{\mathrm{IB}}}{m} \delta^3(r) \partial_r r$. The potential is always attractive and hosts a bound state in the single particle case only on the right side of the Feshbach resonance and is to be understood as a boundary condition on the wave function [21, 121]. This can be seen by integrating over a ball of radius ϵ, integrating the Laplacian arising from the kinetic energy by parts, and noting that we do not allow for simple singularities. Taking $\epsilon \to 0$ then yields the boundary conditions specified below. First we note that for the eigenvalue equation associated with (C.1) the wave function factorises $\Phi(r_1, r_2, ..., r_N) = \varphi(r_1)\varphi(r_2)...\varphi(r_N)$ and $E = N\mathcal{E}$. It is therefore sufficient to solve the following eigenvalue problem

$$\frac{-\nabla^2}{2m} \varphi(r) = \mathcal{E} \varphi(r), \tag{C.2}$$

subject to the boundary condition[1]

$$\lim_{r_\pm \to 0} \left(r_\pm \varphi(r) + a_{\mathrm{IB}} \partial_{r_\pm} (r_\pm \varphi(r)) \right) = 0, \tag{C.3}$$

with $r_\pm = |\mathbf{r} \pm \mathbf{R}/\mathbf{2}|$. The general solution to (C.2) in spherical coordinates is given by $G(r) = \frac{e^{ikr}}{4\pi r}$. It can now be shown [121], that any solution satisfying (C.2) and (C.3) with $\mathrm{Im}\, k = \kappa > 0$ is of the form $\varphi(r) = AG(r_+) + BG(r_-)$. From (C.3) it follows then immediately that

$$\frac{1}{a_{\mathrm{IB}}} R - \kappa R = \pm e^{-\kappa R}\,. \tag{C.4}$$

This equation has at least one solution if $-1 < \frac{1}{a_{\mathrm{IB}}} R$. Hence independent of a_{IB}, there is always at least one bound state as long as the impurities are close enough together. Thus we see that having two impurities serves to enhance the possibility of having a bound state. Indeed, the above treatment suggests that there will always be a bound state if the impurities are sufficiently close together. However, it should be noted that using an approach that involves separate pseudopotentials is only valid when the impurities are sufficiently well separated. We note that this result does not depend on the choice of the pseudopotential and is also recovered if one chooses other regularisation schemes.

[1] See [21, 161] for details on the pseudo potential in the context of ultra cold gases.

Appendix D

Solving the radial Schrödinger equation

This Appendix, will outline the numerical approach taken to solve the radial Schrödinger equation. Usually, the ground state of radial Schrödinger equations is found employing the shooting method [162]. In recent years the field of scientific machine learning has made large improvements, and it has been shown that neural networks can be used to solve differential equations by leveraging their property of being universal function approximators [163, 164]. Another related use employs a neural network as a variational wave function to minimise an energy functional. This has been shown to yield good results for the ground state and also the first excited state of the stationary Schrödinger equation in [165]. Here, we are going to combine these two approaches and minimise the energy functional of the radial Schrödinger equation with an additional penalty term to enforce the boundary condition $u(0) = 0$. In practice this can be written as a minimisation problem with loss L

$$\begin{aligned} u(x) &= \mathrm{net}(x), \\ L[u] &= (u, \hat{H}u)/(u, u) + \alpha(u, u), \end{aligned} \tag{D.1}$$

where $(\cdot\,, \cdot)$, denotes the standard scalar product, $\hat{H} = \frac{-1}{2M}\frac{\mathrm{d}^2}{\mathrm{dR}^2} + V_{\mathrm{BP}}(R)$ is the radial part of the Hamiltonian and α is a hyper-parameter, that will be chosen such that $\alpha \gg E_g$, which ensures, that $u(0) = 0$. In practice this is implemented using PyTorch and we note that the derivatives arising in $(u, \hat{H}u)$ can be calculated exactly using PyTorch's automatic differentiation package. For the presented results we used a shallow network with only one hidden layer and a width of 1000.

Appendix E

Marginalising the field

In this appendix we fill in the details for calculating the effective action. As in the main text we differentiate between $\mu > 0$ and $\mu < 0$.

Symmetric case $\mu > 0$

For $\mu > 0$ the starting point is the bi-linear action in the path integral

$$\begin{aligned} &\int \mathcal{D}[\varphi, \varphi^* \widetilde{\varphi}, \widetilde{\varphi}^*] e^{-\frac{1}{2}\mathcal{A}_\varphi[\varphi,\widetilde{\varphi}]+\frac{1}{2}\mathcal{A}_{\rm int}[\mathbf{y},\tilde{\mathbf{y}},\varphi,\widetilde{\varphi}]} \\ &= \int \mathcal{D}[\varphi, \varphi^* \widetilde{\varphi}, \widetilde{\varphi}^*] \exp\left(- \int \mathrm{d}t\, \mathrm{d}^d\mathbf{p}\, \mathrm{d}^d\mathbf{q}\, \underline{\varphi}^\dagger(\mathbf{p},t) \underline{M}(\mathbf{p},\mathbf{q},t;[\mathbf{y},\tilde{\mathbf{y}}]) \underline{\varphi}(\mathbf{p},t) \right) , \end{aligned} \tag{E.1}$$

where $\underline{M}(\mathbf{p},\mathbf{q};[\mathbf{y},\tilde{\mathbf{y}}])$ is a 4x4 matrix given by

$$\begin{aligned} \underline{M}(\mathbf{p},&\mathbf{q};[\mathbf{y},\tilde{\mathbf{y}}]) = \underline{\Gamma}^{-1}(\mathbf{p},\mathbf{q},t) + (\lambda/2)\underline{V}(\mathbf{p},\mathbf{q},t;[\mathbf{y},\tilde{\mathbf{y}}]) \\ &= \begin{pmatrix} 0 & \Gamma^{-1}(\mathbf{p},t)/2 \\ (\Gamma^{-1})^\dagger(\mathbf{p},t)/2 & \gamma/2 \end{pmatrix} \delta(\mathbf{p}-\mathbf{q}) + \frac{\lambda}{2} \begin{pmatrix} V(\mathbf{p},\mathbf{q},t,\mathbf{y},\tilde{\mathbf{y}}) & \tilde{V}(\mathbf{p},\mathbf{q},t,\mathbf{y}) \\ \tilde{V}(\mathbf{p},\mathbf{q},t,\mathbf{y},\tilde{\mathbf{y}}) & 0 \end{pmatrix} , \end{aligned} \tag{E.2}$$

with

$$\Gamma(\mathbf{p},t) = \partial_t + \mathcal{L}_\varphi(\mathbf{q}) I_{2x2} \,, \tag{E.3}$$

$$\gamma = 2T I_{2x2} \,, \tag{E.4}$$

$$V(\mathbf{q},\tilde{\mathbf{y}}(t),\mathbf{y}(t)) = -i\mathbf{q}\tilde{\mathbf{y}}(t) V(\mathbf{q}) e^{i\mathbf{q}\mathbf{y}} I_{2x2} \,, \tag{E.5}$$

$$\tilde{V}(\mathbf{q}, \mathbf{y}(t)) = V(\mathbf{q}) e^{i\mathbf{q}\mathbf{y}} I_{2x2}\,, \tag{E.6}$$

where I_{2x2} denotes the 2x2 identity matrix and thus the individual entries are the block matrices. Lastly, we have defined

$$\underline{\varphi}(t, \mathbf{q}) = \begin{pmatrix} \varphi(t, \mathbf{q}) \\ \varphi^*(t, \mathbf{q}) \\ \widetilde{\varphi}(t, \mathbf{q}) \\ \widetilde{\varphi}^*(t, \mathbf{q}) \end{pmatrix}. \tag{E.7}$$

It might at first seem odd that we have to consider a 4x4 matrix, but in fact each field as two degrees of freedom, namely its real and imaginary part, thus if we want to integrate out the fields it is necessary to correctly account for these. By using standard results of path integration [166], valid for hermitian matrices, the Gaussian integral (E.1) can be performed and is given by

$$\int \mathcal{D}[\varphi, \widetilde{\varphi}] e^{-\mathcal{A}_\varphi[\varphi,\widetilde{\varphi}] + \mathcal{A}_{\mathrm{int}}[\mathbf{y},\tilde{\mathbf{y}},\varphi,\widetilde{\varphi}]} = N^{-1} \left(\det\left[\underline{M}(\mathbf{p}, \mathbf{q}, t; [\mathbf{y}, \tilde{\mathbf{y}}])\right]\right)^{-1}. \tag{E.8}$$

As of now, this result is exact to all orders in λ, up to a constant N fixed by the normalisation constant on the marginal probability density. For notational convenience we introduce the following convention for the operator matrices of the form $\underline{A}(\mathbf{p}, \mathbf{q}, t_1, t_2)$

$$\underline{AB} \equiv \iint \mathrm{d}^d\mathbf{p}_2\, \mathrm{d}t_2\, A(\mathbf{p}_1, \mathbf{p}_2, t_1, t_2) B(\mathbf{p}_2, \mathbf{p}_3, t_2, t_3) \tag{E.9}$$

and suppress indices for the formal manipulations. In order to evaluate the determinant, we make use of the identity

$$\det A = e^{\mathrm{Tr}\ln A}. \tag{E.10}$$

Applied to the determinant in (E.8), one obtains

$$\left(\det\left[\underline{\Gamma}^{-1}+\lambda\underline{V}\right]\right)^{-1}=\exp\left(-\operatorname{Tr}\ln\left[(\underline{\Gamma}^{-1}+\frac{\lambda}{2}\underline{V})\right]\right)\,. \tag{E.11}$$

Factorising the logarithm, one can separate out the $\mathbf{y},\tilde{\mathbf{y}}$-independent parts

$$\operatorname{Tr}\ln\left(\underline{\Gamma}^{-1}+\lambda\underline{V}\right)=\operatorname{Tr}\left(\ln\underline{\Gamma}^{-1}+\ln\left(1+\frac{\lambda}{2}\underline{\Gamma V}\right)\right)\,, \tag{E.12}$$

Reintroducing the prefactor $e^{-\mathcal{A}_y[\mathbf{y},\tilde{\mathbf{y}}]}$, and comparing the resulting expression to the desired form of the effective action, (6.15), one obtains

$$\mathcal{P}[\mathbf{y},\tilde{\mathbf{y}}]=N^{-1}e^{-\mathcal{A}_y[\mathbf{y};\tilde{\mathbf{y}}]}e^{-\operatorname{Tr}\left(\ln\underline{\Gamma}^{-1}+\ln\left(1+\frac{\lambda}{2}\underline{\Gamma V}(\tilde{\mathbf{y}},\mathbf{y})\right)\right)}=e^{-\mathcal{A}_{\mathbf{y};\mathrm{eff}}[\mathbf{y},\tilde{\mathbf{y}}]}\,. \tag{E.13}$$

The first term, $\operatorname{Tr}\ln\underline{\mathbf{\Gamma}}^{-1}$, cancels the λ-independent part of the normalisation constant. Hence, we identify the *exact* expression for the effective action as

$$\mathcal{A}_{y;\mathrm{eff}}[\mathbf{y},\tilde{\mathbf{y}}]=\mathcal{A}_{\mathbf{y}}[\mathbf{y},\tilde{\mathbf{y}}]+\operatorname{Tr}\ln\left(1+\frac{\lambda}{2}(\underline{\Gamma V})\right)\,. \tag{E.14}$$

In order to make analytical progress, we need to expand this expression in powers of λ to obtain the perturbative corrections to the effective action of the form

$$\mathcal{A}_{y;\mathrm{eff}}[\mathbf{y},\tilde{\mathbf{y}}]=\sum_{k=0}^{\infty}\lambda^k\mathcal{A}_y^{(k)}[\mathbf{y},\tilde{\mathbf{y}}]\,, \tag{E.15}$$

with the nonperturbative part being $\mathcal{A}_y^{(0)}=\mathcal{A}_y[\mathbf{y},\tilde{\mathbf{y}}]$ as introduced in (6.11). Expanding the logarithm within (E.14) in powers of λ gives

$$\operatorname{Tr}\ln\left(1+\lambda(\underline{\Gamma V})\right))=\lambda\operatorname{Tr}(\underline{\Gamma V})-\frac{\lambda^2}{2}\operatorname{Tr}\left((\underline{\Gamma V})^2\right)+\dots\,. \tag{E.16}$$

Comparing this expansion to the perturbative ansatz in (E.15), one can identify the individual terms as

$$\mathcal{A}_y^{(k)}[\mathbf{y},\tilde{\mathbf{y}}] = \frac{(-1)^{k-1}}{k2^k}\,\mathrm{Tr}\left[(\underline{\Gamma V})^k\right]\ ,\ k\geq 1\ . \tag{E.17}$$

One can further show that the first term, $\mathcal{A}^{(1)}[\mathbf{y},\tilde{\mathbf{y}}]$, vanishes as is expected from the statistical invariance of the problem under the symmetry transform $\lambda \leftrightarrow -\lambda$. The leading perturbative correction hence is the term proportional to λ^2,

$$\mathcal{A}_y^{(2)}[\mathbf{y},\tilde{\mathbf{y}}] = \frac{1}{8}\,\mathrm{Tr}\left[(\underline{\Gamma V})^2\right]\ . \tag{E.18}$$

In order to evaluate this trace, we need to further clarify the notation. The matrix multiplication follows the convention introduced in (E.9). Likewise, the the trace of a matrix is given by

$$\mathrm{Tr}\,\mathbf{A}(\mathbf{p},\mathbf{q},t_1,t_2) = \sum_i \iint \mathrm{d}t\,\mathrm{đ}^d\mathbf{p} A_{ii}(\mathbf{p},\mathbf{p},t,t)\ . \tag{E.19}$$

Applied to the trace in (E.18), we first present $\underline{\Gamma}$ for the decoupled theory ($\lambda = 0$), by inverting the matrix we find

$$\underline{\Gamma}(t,\mathbf{q}) = \begin{pmatrix} -2\gamma\Gamma^\dagger(t,\mathbf{q})\Gamma(t,\mathbf{q}) & 2\Gamma^\dagger(t,\mathbf{q}) \\ 2\Gamma(t,\mathbf{q}) & 0 \end{pmatrix}\ . \tag{E.20}$$

From the quadratic theory, one straightforwardly identifies the field's response and correlation function

$$\Gamma(t,\mathbf{q}) = \chi_\varphi(\mathbf{q},t) I_{2x2} = \frac{1}{|\Gamma^{-1}(\mathbf{q},t)|^2} I_{2x2} = \left(\partial_t + \mathcal{L}_\varphi(\mathbf{q})\right)^{-1} I_{2x2} \tag{E.21}$$

$$-\gamma\Gamma^\dagger(t,\mathbf{q})\Gamma(t,\mathbf{q}) = \mathcal{C}_\varphi(\mathbf{q},t) I_{2x2} = \frac{-\gamma}{|\Gamma^{-1}(\mathbf{q},t)|^2} I_{2x2} = \frac{2T}{|\left(\partial_t + \mathcal{L}_\varphi(\mathbf{q})\right)|^2} I_{2x2}, \tag{E.22}$$

where the third equality in each line are formal operator inverses. Hence,

$$\underline{\Gamma}(\mathbf{p},\mathbf{q},t_1,t_2) = 2\begin{pmatrix} \mathcal{C}_\varphi(\mathbf{p},t_1-t_2)I_{2x2} & \chi_\varphi(\mathbf{p},t_1-t_2)I_{2x2} \\ \chi_\varphi(\mathbf{p},t_1-t_2)^* I_{2x2} & 0 \end{pmatrix} . \tag{E.23}$$

We can now evaluate the trace term and after realising that $\underline{V}(\mathbf{p},\mathbf{q},t_1,t_2) = \underline{V}(\mathbf{p},\mathbf{q},t_1)\delta(t_1-t_2)$ we find

$$\mathrm{Tr}\left((\underline{\Gamma V})^2\right) = \sum_i \iint \mathrm{d}^d\mathbf{p}_1\,\mathrm{d}^d\mathbf{p}_2\,\mathrm{d}^d t_1\,\mathrm{d}^d t_2\;\left[\underline{\Gamma}(\mathbf{p}_1,t_{12})\underline{V}(\mathbf{p}_{12},t_2)\underline{\Gamma}(\mathbf{p}_2,-t_{12})\underline{V}(-\mathbf{p}_{12},t_1)\right]_{ii} \tag{E.24}$$

where we have introduced $t_{12} = t_1 - t_2$ and $\mathbf{p}_{12} = \mathbf{p}_1 - \mathbf{p}_2$. Performing the matrix multiplication, the sum and shifting the momentum integration variable we find

$$\begin{aligned}\iint \mathrm{d}^d\mathbf{q}\,\mathrm{d}^d\mathbf{p}\,\mathrm{d}^d s\,\mathrm{d}^d t\,\Big[& 2i\mathbf{q}|V(\mathbf{q})|^2 e^{i\mathbf{q}(\mathbf{y}(s)-\tilde{\mathbf{y}}(t)}\mathcal{C}_\varphi(\mathbf{q},s-t)\,\mathrm{Re}\left[\chi_\varphi(\mathbf{p}-\mathbf{q},s-t)\right] \\ & +\frac{1}{2}\mathbf{q}^2|V(\mathbf{q})|^2 e^{i\mathbf{q}(\mathbf{y}(s)-\tilde{\mathbf{y}}(t))}\,\mathrm{Re}\left[\mathcal{C}_\varphi(\mathbf{q},t)\mathcal{C}^*_\varphi(\mathbf{p}-\mathbf{q},t)\right]\Big]\end{aligned} \tag{E.25}$$

where we have used that by causality $\chi(\cdot,t_{12})\chi(\cdot,-t_{12}) = 0$ and $\mathcal{C}_\varphi(\mathbf{p},s-t) = \mathcal{C}^*_\varphi(\mathbf{p},t-s)$. We can now identify the parts with those given in the main text.

Degenerate case $\mu < 0$

In this section we want to show how to marginalise the field in the degenerate case. For notational convenience we suppress the explicit time and momentum dependence. The quadratic part of the Hamiltonian is given by

$$\mathcal{A}^2_{\delta\varphi} = \iint \mathrm{d}t\,\mathrm{d}^d\mathbf{q}\left(\underline{\delta\varphi}(\omega,\mathbf{q})^\dagger \underbrace{\begin{pmatrix} 0 & \Gamma^{-1}(t,\mathbf{q}) \\ (\Gamma^{-1})^\dagger(t,\mathbf{q}) & \gamma \end{pmatrix}}_{\underline{\Gamma}^{-1}} \underline{\delta\varphi}(t,\mathbf{q})\right) . \tag{E.26}$$

$\underline{\Gamma}^{-1}$ is a 4x4 matrix and and the entries of the matrices are 2x2 matrices. We have also defined,

$$\underline{\delta\varphi}(t,\mathbf{q}) = \begin{pmatrix} \delta\varphi(t,\mathbf{q}) \\ \delta\varphi^*(t,-\mathbf{q}) \\ \delta\widetilde{\varphi}(t,\mathbf{q}) \\ \delta\widetilde{\varphi}^*(t,-\mathbf{q}) \end{pmatrix} . \tag{E.27}$$

In contrast to the symmetric case, the interaction term enters here linearly as

$$\mathcal{A}_{\text{int}} = \iint \mathrm{d}\omega\, \mathrm{d}^d\mathbf{q}\, \underline{\delta\varphi}^\dagger(t,\mathbf{q})\underline{V}(t,\mathbf{q}) \tag{E.28}$$

with the interaction vector

$$\underline{V}(t,\mathbf{q}) = \begin{pmatrix} V(\mathbf{q},\tilde{\mathbf{y}}(t),\mathbf{y}(t)) \\ V(\mathbf{q},t,\tilde{\mathbf{y}}(t),\mathbf{y}(t)) \\ \tilde{V}(\mathbf{q},t,\mathbf{y}(t)) \\ \tilde{V}(\mathbf{q},t,\mathbf{y}(t)) \end{pmatrix} , \tag{E.29}$$

where $V(\mathbf{q},\tilde{\mathbf{y}}(t),\mathbf{y}(t)) = -i\mathbf{q}\tilde{\mathbf{y}}(t)V(\mathbf{q})e^{i\mathbf{q}\mathbf{y}}$ and $\tilde{V}(\mathbf{q},\mathbf{y}(t)) = V(\mathbf{q})e^{i\mathbf{q}\mathbf{y}}$. The linear term means that it is now straight-forward to integrate out the field and we directly obtain the effective action as

$$\mathcal{A}^{\text{eff}} = \iiint \mathrm{d}t\, \mathrm{d}s\, \mathrm{d}^d\mathbf{q}\, \underline{V}(s,-\mathbf{q})^T\underline{\Gamma}(\mathbf{q},s-t)\,\underline{V}(t,\mathbf{q}) , \tag{E.30}$$

where we have used that $\underline{V}(x)$ is real and we can thus use that complex conjugation is equivalent to $\mathbf{q} \to -\mathbf{q}$. We note that here we do not have to expand a trace-log term and the approximation was made by dropping higher order terms in $\delta\varphi\,(\delta\widetilde{\varphi})$. We are now left with finding the inverse of the 4x4 matrix $\underline{\Gamma}$. In fact since γ is diagonal and for complex fields one typically finds after linearisation that Γ symbolically takes the following form [73]

$$\Gamma(\mathbf{q},t) = \frac{1}{|K^*(\mathbf{q},\partial_t)|^2 - |\Delta|^2} \begin{pmatrix} K(\mathbf{q},\partial_t) & -\Delta \\ -\Delta^* & K^*(\mathbf{q},\partial_t) , \end{pmatrix} = \begin{pmatrix} \alpha(\mathbf{q},t) & -\beta(\mathbf{q},t) \\ -\beta^*(\mathbf{q},t) & \alpha^*(\mathbf{q},t) \end{pmatrix} . \tag{E.31}$$

We then find

$$\underline{\Gamma}(t,\mathbf{q}) = \begin{pmatrix} -\gamma\Gamma^\dagger(t,\mathbf{q})\Gamma(t,\mathbf{q}) & \Gamma^\dagger(t,\mathbf{q}) \\ \Gamma(t,\mathbf{q}) & 0 \end{pmatrix} , \tag{E.32}$$

and we thus arrive at

$$\begin{aligned} G_{\mathrm{deg}} =& 4\gamma V(-\mathbf{q},\tilde{\mathbf{y}}(s),\mathbf{y}(s))V(\mathbf{q},\tilde{\mathbf{y}}(t),\mathbf{y}(t)) \\ & \times \mathrm{Re}\left[|\alpha(s-t,\mathbf{q})|^2 + |\beta(s-t,\mathbf{q})|^2 - 2\alpha^*(s-t,\mathbf{q})\beta(s-t,\mathbf{q})\right] \\ =& 4\gamma\tilde{\mathbf{y}}(s)\tilde{\mathbf{y}}(t)\left(\mathbf{q}^2|V(\mathbf{q})|^2 e^{i\mathbf{q}(\mathbf{y}(t)-\mathbf{y}(s))}\,\mathrm{Re}\left[\mathcal{C}_{\delta\varphi}(\mathbf{q},s-t)\right]\right) , \end{aligned} \tag{E.33}$$

we note that $\int \mathrm{d}^d\mathbf{q}\, G_{\mathrm{deg}}(\mathbf{q})$ is real, and

$$\begin{aligned} H_{\mathrm{deg}} =& 2V(-\mathbf{q},\mathbf{y}(s))\tilde{V}(\mathbf{q},\tilde{\mathbf{y}}(t),\mathbf{y}(t))\,\mathrm{Re}\left(\alpha(\mathbf{q},t-s) - \beta^*(\mathbf{q},t-s)\right) \\ & + 2\tilde{V}(-\mathbf{q},\tilde{\mathbf{y}}(s),\mathbf{y}(s))V(\mathbf{q},\mathbf{y}(t))\,\mathrm{Re}\left(\alpha^*(\mathbf{q},t-s) - \beta(\mathbf{q},t-s)\right) \\ =& \mathbf{q}\tilde{\mathbf{y}}(t)e^{i\mathbf{q}(\mathbf{y}(t)-\mathbf{y}(s))}2\,\mathrm{Im}\left[\alpha^*(\mathbf{q},t-s) - \beta(\mathbf{q},t-s)\right] \\ & + q\tilde{\mathbf{y}}(s)e^{i\mathbf{q}(\mathbf{y}(s)-\mathbf{y}(t))}2\,\mathrm{Im}\left[\alpha(\mathbf{q},s-t) - \beta^*(\mathbf{q},s-t)\right] \\ =& \mathbf{q}\tilde{\mathbf{y}}(t)e^{i\mathbf{q}(\mathbf{y}(t)-\mathbf{y}(s))}2\,\mathrm{Im}[\chi_{\delta\varphi}(\mathbf{q},t-s)] + \mathbf{q}\tilde{\mathbf{y}}(s)e^{i\mathbf{q}(\mathbf{y}(s)-\mathbf{y}(t))}2\,\mathrm{Im}[\chi_{\delta\varphi}(\mathbf{q},s-t)] . \end{aligned} \tag{E.34}$$

If we now use this expression in the action we can relabel s and t and find the form given in the main text. For the limiting case of real fields one obtains the same result and usually $\alpha = \beta = 0$. We find that $C_{\delta\varphi}$ and χ_δ have the form of the well known correlation and response function of a free field.

Appendix F

Interacting field in the symmetric regime

The goal of this Appendix is to outline the rationale for how to include the self-interaction of the field above criticality. Here we want to expand on the comments in the main text and discuss one possible way how to include the self-interaction perturbatively using a typical quartic interaction.[1] We also note that while this derivation is somewhat cumbersome, the conclusion is that one can replace the bare propagator with its dressed counterpart. In the MSR functional the interaction term takes the following form

$$\mathcal{A}_u = u \int \mathrm{d}^d\mathbf{r}\, \mathrm{d}t\, \widetilde{\varphi}(x,t)\varphi^3(\mathbf{r},t) \tag{F.1}$$

In order to treat this additional term perturbatively we introduce the Hubbard Stratonovich fields κ and $\tilde{\kappa}$. With the help of those, we write

$$e^{\mathcal{A}_u} = \int \mathcal{D}[\kappa,\tilde{\kappa}] e^{\int \mathrm{d}^d\mathbf{r}\, \tilde{\kappa}(\mathbf{r},t)\varphi(\mathbf{r},t)^2 + \widetilde{\varphi}(\mathbf{r},t)\varphi(\mathbf{r},t)\kappa(\mathbf{r},t) + \frac{1}{u}\tilde{\kappa}(\mathbf{r},t)\kappa(\mathbf{r},t)}\,. \tag{F.2}$$

The field now enters the action bi-linearly again and we can now proceed as before and integrate out the original field. With the modification, that we now do not only have the free action anymore, but

$$\underline{\Gamma}^{-1} \to \underline{\Gamma}_{\Sigma}^{-1} = \underline{\Gamma}^{-1} + \underline{\Sigma}\,, \tag{F.3}$$

[1] Here, we focus on real fields for ease of notation; the complex case is analogous.

with

$$\Sigma = \begin{pmatrix} \tilde{\kappa}(\mathbf{p},t) I_{2x2} & \kappa(\mathbf{p},t)/2 I_{2x2} \\ \kappa(\mathbf{p},t)/2 I_{2x2} & 0 \end{pmatrix} \delta(\mathbf{p},\mathbf{q}) \, . \tag{F.4}$$

After performing the integration we arrive at

$$e^{\mathcal{A}_{y;\mathrm{eff}}[\mathbf{y},\tilde{\mathbf{y}}]} = \int \mathcal{D}[\kappa,\tilde{\kappa}] e^{\frac{1}{u}\tilde{\kappa}(\mathbf{r},t)\kappa(\mathbf{r},t) - \mathrm{Tr}\left(\ln \underline{\Gamma}_{\Sigma}^{-1} + \ln(1+\lambda \underline{\Gamma}_{\Sigma} \underline{V}(\tilde{\mathbf{y}},\mathbf{y}))\right)} \, . \tag{F.5}$$

The second trace-log term is structurally, as in the free case and can be expanded in the same way. Here we can also observe that written formally

$$\underline{\Gamma}_{\Sigma} = \frac{1}{\underline{\Gamma}^{-1} + \underline{\Sigma}} \, , \tag{F.6}$$

and we can thus identify $\underline{\Sigma}$ as the self-energy-like contribution to the propagator. As before, expanding the $\ln$ will now yield the different contributions in λ. So far, the calculations have been exact in u and λ. To proceed, we are now introducing further approximations to calculate the modification of the propagator.

If we neglect the back-action of the impurity on the condensate we can replace $\underline{\Sigma}$ in the second trace term by it's expected value, which can be calculated from the effective action for $\underline{\Gamma}_{\Sigma}$. To be more concrete, using

$$\int \mathcal{D}[\kappa,\tilde{\kappa}] e^{\frac{1}{u}\tilde{\kappa}(\mathbf{r},t)\kappa(\mathbf{r},t) + \frac{1}{2}\,\mathrm{Tr}\ln(\underline{\Gamma}_{\Sigma})} \tag{F.7}$$

we calculate the expectation value of $\underline{\Gamma}_{\Sigma}$ to given accuracy and then insert this expectation value into $\mathrm{Tr}\ln(1+\lambda\underline{\Gamma}_{\Sigma}\underline{V})$. In this way we can include the self-interaction of the field. We once again stress that this does not account for the back action of the field onto the impurity. The main advantage of using this approach is that all results obtained for the free field carry over in a natural way by simply replacing $\underline{\Gamma}$ with its dressed counterpart $\underline{\Gamma}_{\Sigma}$

Bibliography

[1] M. E. Peskin and D. V. Schroeder, *An Introduction to quantum field theory* (Addison-Wesley, Reading, USA, 1995).

[2] L. Landau, Phys. Z. Sowjetunion **3**, 644 (1933).

[3] S. Pekar, Zh. Eksp. Teor. Fiz. **16** (1946).

[4] A. Schirotzek, C. H. Wu, A. Sommer, and M. W. Zwierlein, Phys. Rev. Lett. **102**, 230402 (2009).

[5] N. B. Jørgensen, L. Wacker, K. T. Skalmstang, M. M. Parish, J. Levinsen, R. S. Christensen, G. M. Bruun, and J. J. Arlt, Phys. Rev. Lett. **117**, 055302 (2016).

[6] L. D. Landau and S. I. Pekar, Eksp. Teor. Fiz **18**, 419 (1948).

[7] H. Fröhlich, Adv. Phys. **3**, 325 (1954).

[8] T. D. Lee, F. E. Low, and D. Pines, Phys. Rev. **90**, 297 (1953).

[9] H. Spohn, Ann. Phys. (N. Y). **175**, 278 (1987).

[10] G. D. Mahan, *Many-Particle Physics* (Berlin: Springer, 2000).

[11] R. P. Feynman, Phys. Rev. **97**, 660 (1955).

[12] J. L. Bredas and G. B. Street, Acc. Chem. Res. **18**, 309 (1985).

[13] S. Glenis, M. Benz, E. LeGoff, M. G. Kanatzidis, J. L. Schindler, and C. R. Kannewurf, J. Am. Chem. Soc. **115**, 12519 (1993).

[14] N. Mott, Phys. C Supercond. **205**, 191 (1993).

[15] A. S. Alexandrov and J. T. Devreese, *Advances in Polaron Physics*, Vol. 159 (Springer-Verlag, Berlin, 2010).

[16] W. D. Phillips, Rev. Mod. Phys. **70**, 721 (1998).

[17] M. H. Anderson, J. R. Ensher, M. R. Matthews, C. E. Wieman, and E. A. Cornell, Science **269**, 198 (1995).

[18] C. J. Pethick and H. Smith, *Bose-Einstein Condensation in Dilute Gases*, Vol. 9780521846 (Cambridge University Press, 2008).

[19] L. Pitaevskii and S. Stringari, *Bose-Einstein Condensation and Superfluidity* (Oxford University Press, 2016).

[20] I. Bloch, J. Dalibard, and S. Nascimbène, Nat. Phys. **8**, 267 (2012).

[21] C. Chin, R. Grimm, P. Julienne, and E. Tiesinga, Rev. Mod. Phys. **82**, 1225 (2010).

[22] J. Catani, G. Lamporesi, D. Naik, M. Gring, M. Inguscio, F. Minardi, A. Kantian, and T. Giamarchi, Phys. Rev. A **85**, 023623 (2012).

[23] Y. Zhang, W. Ong, I. Arakelyan, and J. E. Thomas, Phys. Rev. Lett. **108**, 235302 (2012).

[24] C. Kohstall, M. Zaccanti, M. Jag, A. Trenkwalder, P. Massignan, G. M. Bruun, F. Schreck, and R. Grimm, Nature **485**, 615 (2012).

[25] M. Koschorreck, D. Pertot, E. Vogt, B. Fröhlich, M. Feld, and M. Köhl, Nature **485**, 619 (2012).

[26] F. Scazza, G. Valtolina, P. Massignan, A. Recati, A. Amico, A. Burchianti, C. Fort, M. Inguscio, M. Zaccanti, and G. Roati, Phys. Rev. Lett. **118**, 083602 (2017).

[27] M. Cetina, M. Jag, R. S. Lous, J. T. Walraven, R. Grimm, R. S. Christensen, and G. M. Bruun, Phys. Rev. Lett. **115**, 135302 (2015).

[28] M. Cetina, M. Jag, R. S. Lous, I. Fritsche, J. T. Walraven, R. Grimm, J. Levinsen, M. M. Parish, R. Schmidt, M. Knap, and E. Demler, Science **354**, 96 (2016).

[29] P. Massignan, M. Zaccanti, and G. M. Bruun, Reports Prog. Phys. **77**, 034401 (2014).

[30] M. G. Hu, M. J. Van De Graaff, D. Kedar, J. P. Corson, E. A. Cornell, and D. S. Jin, Phys. Rev. Lett. **117**, 055301 (2016).

[31] Z. Z. Yan, Y. Ni, C. Robens, and M. W. Zwierlein, Science **368**, 190 (2020).

[32] M. G. Skou, T. G. Skov, N. B. Jørgensen, K. K. Nielsen, A. Camacho-Guardian, T. Pohl, G. M. Bruun, and J. J. Arlt, Nat. Phys. **17**, 731 (2021).

[33] S. P. Rath and R. Schmidt, Phys. Rev. A **88**, 053632 (2013).

[34] G. E. Astrakharchik and L. P. Pitaevskii, Phys. Rev. A **70**, 013608 (2004).

[35] J. Tempere, W. Casteels, M. K. Oberthaler, S. Knoop, E. Timmermans, and J. T. Devreese, Phys. Rev. B **80**, 184504 (2009).

[36] W. Casteels, T. Cauteren, J. Tempere, and J. T. Devreese, Laser Phys. **21**, 1480 (2011).

[37] F. Grusdt, G. E. Astrakharchik, and E. Demler, New J. Phys. **19**, 103035 (2017).

[38] Y. E. Shchadilova, R. Schmidt, F. Grusdt, and E. Demler, Phys. Rev. Lett. **117**, 113002 (2016).

[39] J. Vlietinck, W. Casteels, K. Van Houcke, J. Tempere, J. Ryckebusch, and J. T. Devreese, New J. Phys. **17**, 033023 (2015).

[40] W. Li and S. Das Sarma, Phys. Rev. A **90**, 013618 (2014).

[41] J. Levinsen, M. M. Parish, and G. M. Bruun, Phys. Rev. Lett. **115**, 125302 (2015).

[42] Y. E. Shchadilova, F. Grusdt, A. N. Rubtsov, and E. Demler, Phys. Rev. A **93**, 043606 (2016).

[43] W. Casteels and M. Wouters, Phys. Rev. A **90**, 043602 (2014).

[44] R. S. Christensen, J. Levinsen, and G. M. Bruun, Phys. Rev. Lett. **115**, 160401 (2015).

[45] T. Ichmoukhamedov and J. Tempere, Phys. Rev. A **100**, 043605 (2019).

[46] F. Grusdt and E. Demler, arXiv:1510.04934 (2015).

[47] F. Isaule, I. Morera, P. Massignan, and B. Juliá-Díaz, Phys. Rev. A **104**, 023317 (2021).

[48] A. Lampo, C. Charalambous, M. Á. García-March, and M. Lewenstein, Phys. Rev. A **98**, 063630 (2018).

[49] L. A. Ardila and S. Giorgini, Phys. Rev. A **92**, 33612 (2015).

[50] L. Parisi and S. Giorgini, Phys. Rev. A **95**, 023619 (2017).

[51] L. A. P. Ardila, Nat. Rev. Phys. **4**, 214 (2022).

[52] N. E. Guenther, R. Schmidt, G. M. Bruun, V. Gurarie, and P. Massignan, Phys. Rev. A **103**, 013317 (2021).

[53] M. Drescher, M. Salmhofer, and T. Enss, Phys. Rev. Res. **2**, 032011 (2020).

[54] H. T. C. Stoof, D. B. M. Dickerscheid, and K. Gubbels, *Ultracold Quantum Fields*, 1st ed. (Springer Netherlands, 2009).

[55] L. Salasnich and F. Toigo, Phys. Rep. **640**, 1 (2016).

[56] A. G. Volosniev and H. W. Hammer, Phys. Rev. A **96**, 031601 (2017).

[57] S. I. Mistakidis, A. G. Volosniev, N. T. Zinner, and P. Schmelcher, Phys. Rev. A **100**, 013619 (2019).

[58] G. Panochko and V. Pastukhov, Ann. Phys. (N. Y). **409**, 167933 (2019).

[59] R. Schmidt and T. Enss, (2021), arXiv:2102.13616v1 .

[60] A. Camacho-Guardian, L. A. Peña Ardila, T. Pohl, and G. M. Bruun, Phys. Rev. Lett. **121**, 013401 (2018).

[61] J. T. Devreese, "Polarons," in *Digit. Encycl. Appl. Phys.* (Wiley VHC Verlag, 2003).

[62] N. N. Bogolyubov, J. Phys. **11**, 23 (1947).

[63] T. Lausch, A. Widera, and M. Fleischhauer, Phys. Rev. A **97**, 33620 (2018).

[64] J. Jager, *Strongly interacting Bose-polarons*, Master thesis, Imperial College London (2018).

[65] R. Shankar, *Principles of quantum mechanics* (Plenum, New York, NY, 1980).

[66] D. Dzsotjan, R. Schmidt, and M. Fleischhauer, Phys. Rev. Lett. **124**, 223401 (2020).

[67] F. Grusdt, K. Seetharam, Y. Shchadilova, and E. Demler, Phys. Rev. A **97**, 033612 (2018).

[68] L. A. P. Ardila, G. E. Astrakharchik, and S. Giorgini, Phys. Rev. Res. **2**, 23405 (2020).

[69] B. Kain and H. Y. Ling, Phys. Rev. A **98**, 033610 (2018).

[70] A. Polkovnikov, Ann. Phys. (N. Y). **325**, 1790 (2010).

[71] A. Altland and B. D. Simons, *Condensed Matter Field Theory* (Cambridge University Press, 2010).

[72] A. Polkovnikov, Phys. Rev. A **68**, 053604 (2003).

[73] L. M. Sieberer, M. Buchhold, and S. Diehl, Reports Prog. Phys. **79**, 096001 (2016).

[74] L. V. Keldysh, Sov. Phys. JETP **20**, 1018 (1965).

[75] J. Javanainen and J. Ruostekoski, J. Phys. A. Math. Gen. **39**, L179 (2006).

[76] F. Casas, A. Murua, and M. Nadinic, Comput. Phys. Commun. **183**, 2386 (2012).

[77] C. F. Barenghi and N. G. Parker, *A primer on quantum fluids* (SpringerBriefs in Physics, 2016).

[78] T. Giamarchi, *Quantum Physics in One Dimension* (Oxford University Press, 2007).

[79] E. H. Lieb and W. Liniger, Phys. Rev. **130**, 1605 (1963).

[80] G. Lang, *Correlations in low-dimensional quantum gases*, Springer Theses (Springer International Publishing, Cham, 2017).

[81] F. M. Cucchietti and E. Timmermans, Phys. Rev. Lett. **96**, 210401 (2006).

[82] A. A. Blinova, M. G. Boshier, and E. Timmermans, Phys. Rev. A **88**, 053610 (2013).

[83] M. Bruderer, W. Bao, and D. Jaksch, Epl **82**, 30004 (2008).

[84] N. D. Mermin and H. Wagner, Phys. Rev. Lett. **17**, 1133 (1966).

[85] A. Kantian, U. Schollwöck, and T. Giamarchi, Phys. Rev. Lett. **113**, 070601 (2014).

[86] V. Hakim, Phys. Rev. E **55**, 2835 (1997).

[87] T. Tsuzuki, J. Low Temp. Phys. **4**, 441 (1971).

[88] M. Will, G. E. Astrakharchik, and M. Fleischhauer, Phys. Rev. Lett. **127**, 103401 (2021).

[89] M. Girardeau, J. Math. Phys. **1**, 516 (1960).

[90] I. M. Uzunov and V. S. Gerdjikov, Phys. Rev. A **47**, 1582 (1993).

[91] I. V. Barashenkov and E. Y. Panova, Phys. D **69**, 114 (1993).

[92] R. P. Feynman, Phys. Rev. **56**, 340 (1939).

[93] M.-w. Xiao, (2009), arXiv:0908.0787 .

[94] M. Drescher, M. Salmhofer, and T. Enss, Phys. Rev. A **99**, 023601 (2019).

[95] A. G. Volosniev, H. W. Hammer, and N. T. Zinner, Phys. Rev. A **92**, 023623 (2015).

[96] K. K. Nielsen, L. A. Ardila, G. M. Bruun, and T. Pohl, New J. Phys. **21**, 043014 (2019).

[97] S. I. Mistakidis, G. C. Katsimiga, G. M. Koutentakis, T. Busch, and P. Schmelcher, Phys. Rev. Lett. **122**, 183001 (2019).

[98] D. Boyanovsky, D. Jasnow, X. L. Wu, and R. C. Coalson, Phys. Rev. A **100**, 043617 (2019).

[99] L. A. P. Ardila, Phys. Rev. A **103**, 033323 (2021).

[100] N. E. Guenther, P. Massignan, M. Lewenstein, and G. M. Bruun, Phys. Rev. Lett. **120**, 050405 (2018).

[101] C. Charalambous, M. A. Garcia-March, A. Lampo, M. Mehboud, and M. Lewenstein, SciPost Phys. **6**, 10 (2019).

[102] S. I. Mistakidis, A. G. Volosniev, and P. Schmelcher, Phys. Rev. Res. **2**, 023154 (2020).

[103] O. Gamayun, O. Lychkovskiy, E. Burovski, M. Malcomson, V. V. Cheianov, and M. B. Zvonarev, Phys. Rev. Lett. **120**, 220605 (2018).

[104] V. Pastukhov, J. Phys. A Math. Theor. **51**, 195003 (2018).

[105] F. Tonielli, N. Chakraborty, F. Grusdt, and J. Marino, Phys. Rev. Res. **2**, 032003 (2020).

[106] A. D. Martin and J. Ruostekoski, New J. Phys. **12**, 055018 (2010).

[107] Y. Castin, in *J. Phys. IV JP*, Vol. 116 (2004) pp. 89–132.

[108] S. I. Mistakidis, F. Grusdt, G. M. Koutentakis, and P. Schmelcher, New J. Phys. **21**, 103026 (2019).

[109] J. Vaníček and D. Cohen, Philos. Trans. R. Soc. A Math. Phys. Eng. Sci. **374**, 20150164 (2016).

[110] B. Kain and H. Y. Ling, Phys. Rev. A **89**, 23612 (2014).

[111] T. Fogarty, S. Deffner, T. Busch, and S. Campbell, Phys. Rev. Lett. **124**, 110601 (2020).

[112] S. Campbell, M. Á. García-March, T. Fogarty, and T. Busch, Phys. Rev. A **90**, 013617 (2014).

[113] M. M. Khan, H. Terças, J. T. Mendonça, J. Wehr, C. Charalambous, M. Lewenstein, and M. A. Garcia-March, Phys. Rev. A **103**, 023303 (2021).

[114] F. Lingua, L. Lepori, F. Minardi, V. Penna, and L. Salasnich, New J. Phys. **20**, 045001 (2018).

[115] C. D. Mink, A. Pelster, J. Benary, H. Ott, and M. Fleischhauer, SciPost Phys. **12**, 051 (2022).

[116] L. N. Cooper, Phys. Rev. **104**, 1189 (1956).

[117] A. S. Alexandrov and A. B. Krebs, Sov. Phys. - Uspekhi **35**, 345 (1992).

[118] A. Klein and M. Fleischhauer, Phys. Rev. A **71**, 033605 (2005).

[119] P. Naidon, J. Phys. Soc. Japan **87**, 043002 (2018).

[120] G. Panochko and V. Pastukhov, Atoms **10**, 19 (2022).

[121] S. Albeverio, F. Gesztesy, R. Høegh-Krohn, and H. Holden, *Solvable Models in Quantum Mechanics* (American Mathematical Society, Providence, Rhode Island, 2004).

[122] A. S. Dehkharghani, A. G. Volosniev, and N. T. Zinner, Phys. Rev. Lett. **121**, 080405 (2018).

[123] F. Brauneis, H. W. Hammer, M. Lemeshko, and A. G. Volosniev, SciPost Phys. **11**, 8 (2021).

[124] G. M. Koutentakis, S. I. Mistakidis, and P. Schmelcher, Atoms **10**, 3 (2022).

[125] P. Jeszenszki, A. Y. Cherny, and J. Brand, Phys. Rev. A **97**, 042708 (2018).

[126] M. Hamzavi, M. Movahedi, K. E. Thylwe, and A. A. Rajabi, Chinese Phys. Lett. **29**, 080302 (2012).

[127] T. Besard, C. Foket, and B. De Sutter, IEEE Trans. Parallel Distrib. Syst. **30**, 827 (2019).

[128] F. Wilczek and A. Shapere, *Geometric Phases in Physics* (WORLD SCIENTIFIC, 1989).

[129] A. Furukawa, A. Gambassi, S. Dietrich, and H. Tanaka, Phys. Rev. Lett. **111**, 055701 (2013).

[130] M. Krüger, A. Solon, V. Démery, C. M. Rohwer, and D. S. Dean, J. Chem. Phys **148**, 84503 (2018).

[131] V. Démery and D. S. Dean, Phys. Rev. Lett. **104**, 080601 (2010).

[132] B. G. Van Ravensteijn and I. K. Voets, Phys. Today **74**, 38 (2021).

[133] U. Basu, V. Démery, and A. Gambassi, (2022), arXiv:2203.13702 .

[134] D. Venturelli, F. Ferraro, and A. Gambassi, (2022), arXiv:2203.06001 .

[135] S. Pigeon, K. Fogelmark, B. Söderberg, A. , V. Khane, M. H. Al-Dahhan -, and M. Gross, J. Stat. Mech. Theory Exp. **2021**, 063209 (2021).

[136] J. Jager, "ColloidFluctuatingField.jl," https://github.com/phyjonas/ColloidFluctuatingField.jl (2022).

[137] P. C. Hohenberg and B. I. Halperin, Rev. Mod. Phys. **49**, 435 (1977).

[138] U. C. Täuber and S. Diehl, Phys. Rev. X **4**, 021010 (2014).

[139] M. H. Szymańska, J. Keeling, and P. B. Littlewood, Phys. Rev. Lett. **96**, 230602 (2006).

[140] J. Kasprzak, M. Richard, S. Kundermann, A. Baas, P. Jeambrun, J. M. Keeling, F. M. Marchetti, M. H. Szymánska, R. André, J. L. Staehli, V. Savona, P. B. Littlewood, B. Deveaud, and L. S. Dang, Nature **443**, 409 (2006).

[141] I. Carusotto and C. Ciuti, Rev. Mod. Phys. **85**, 299 (2013).

[142] M. Wouters and I. Carusotto, Phys. Rev. Lett. **99**, 140402 (2007).

[143] K. Dunnett and M. H. Szymańska, Phys. Rev. B **93**, 195306 (2016).

[144] C. W. Gardiner, J. R. Anglin, and T. I. Fudge, J. Phys. B At. Mol. Opt. Phys. **35**, 1555 (2002).

[145] M. Bijlsma and H. T. Stoof, Phys. Rev. A **55**, 498 (1997).

[146] S. P. Cockburn and N. P. Proukakis, Laser Phys. **19**, 558 (2009).

[147] U. C. Täuber, *Critical Dynamics: A Field Theory Approach to Equilibrium and Non-Equilibrium Scaling Behavior* (Cambridge University Press, 2012) pp. 1–511.

[148] J. Jager and R. Barnett, Phys. Rev. Res. **3**, 033212 (2021).

[149] P. C. Martin, E. D. Siggia, and H. A. Rose, Phys. Rev. A **8**, 423 (1973).

[150] A. Kamenev, *Field Theory of Non-Equilibrium Systems* (Cambridge University Press, 2011) pp. 1–341.

[151] J. Hubbard, Phys. Rev. Lett. **3**, 77 (1959).

[152] R. Stratonovich, Sov. Phys. Dokl. **2**, 416 (1957).

[153] G. J. O. Jameson, Math. Gaz. **100**, 298 (2016).

[154] C. De Dominicis, E. Brézin, and J. Zinn-Justin, Phys. Rev. B **12**, 4945 (1975).

[155] J. Zinn-Justin, *Quantum Field Theory and Critical Phenomena* (Oxford University Press, 2010).

[156] C. K. Birdsall and A. B. Langdon, *Plasma Physics via Computer Simulation* (CRC Press, 2004) pp. 1–465.

[157] G. J. Lord, C. E. Powell, and T. Shardlow, *An Introduction To Computational Stochastic PDEs* (Cambridge University Press, 2014) pp. 1–503.

[158] A. Vashisht, M. Richard, and A. Minguzzi, SciPost Phys. **12**, 8 (2022).

[159] A. Petković and Z. Ristivojevic, Phys. Rev. A **105**, L021303 (2022).

[160] N. T. Thomopoulos, *Essentials Monte Carlo Simul. Stat. Methods Build. Simul. Model.*, Vol. 9781461460 (Springer New York, 2013) pp. 1–171.

[161] K. Huang and C. N. Yang, Phys. Rev. **105**, 767 (1957).

[162] J. Killingbeck, J. Phys. A. Math. Gen. **20**, 1411 (1987).

[163] I. E. Lagaris, A. Likas, and D. I. Fotiadis, IEEE Trans. Neural Networks **9**, 987 (1998).

[164] I. E. Lagaris, A. C. Likas, and D. G. Papageorgiou, IEEE Trans. Neural Networks **11**, 1041 (2000).

[165] H. Li, Q. Zhai, and J. Z. Chen, Phys. Rev. A **103**, 32405 (2021).

[166] H. Kleinert, *Path Integrals in Quantum Mechanics, Statistics, Polymer Physics, and Financial Markets*, 5th ed. (WORLD SCIENTIFIC, 2009) pp. 1–1581.